

VILNIUS GEDIMINAS TECHNICAL UNIVERSITY

Urtė RADVILAITĖ

SPHERICAL HARMONICS MODELS AND THEIR APPLICATION TO NON-SPHERICAL SHAPE PARTICLES

DOCTORAL DISSERTATION

TECHNOLOGICAL SCIENCES,
MECHANICAL ENGINEERING (09T)



LEIDYKLA

Vilnius TECHNIKA 2016

Doctoral dissertation was prepared at Vilnius Gediminas Technical University in 2012–2016.

Supervisor

Prof. Dr Habil. Rimantas KAČIANAUSKAS (Vilnius Gediminas Technical University, Mechanical Engineering – 09T).

The Dissertation Defense Council of Scientific Field of Mechanical Engineering of Vilnius Gediminas Technical University:

Chairman

Prof. Dr Dalius MAŽEIKAS (Vilnius Gediminas Technical University, Mechanical Engineering – 09T).

Members:

Prof. Dr Habil. Gintautas DZEMYDA (Vilnius University, Informatics Engineering – 07T),

Assoc. Prof. Dr Artūras KILIKEVIČIUS (Vilnius Gediminas Technical University, Mechanical Engineering – 09T),

Prof. Dr Habil. Marek MOLENDAS (Institute of Agrophysics of Polish Academy of Sciences, Mechanical Engineering – 09T),

Prof. Dr Vytautas TURLA (Vilnius Gediminas Technical University, Mechanical Engineering – 09T).

The dissertation will be defended at the public meeting of the Dissertation Defense Council of Mechanical Engineering in the Senate Hall of Vilnius Gediminas Technical University at **2 p. m. on 12 January 2017**.

Address: Saulėtekio al. 11, LT-10223 Vilnius, Lithuania.

Tel.: +370 5 274 4956; fax +370 5 270 0112; e-mail: doktor@vgtu.lt

A notification on the intend defending of the dissertation was send on 9 December 2016.

A copy of the doctoral dissertation is available for review at VGTU repository <http://dspace.vgtu.lt> and at the Library of Vilnius Gediminas Technical University (Saulėtekio al. 14, LT-10223 Vilnius, Lithuania).

VGTU leidyklos TECHNIKA 2399-M mokslo literatūros knyga

ISBN 978-609-457-980-6

© VGTU leidykla TECHNIKA, 2016

© Urtė Radvilaitė, 2016

urte.radvilaite@vgtu.lt

VILNIAUS GEDIMINO TECHNIKOS UNIVERSITETAS

Urtė RADVILAITĖ

SFERINIŲ HARMONIKŲ MODELIAI IR JŲ TAIKYMAS NESFERINĖS FORMOS DALELĖMS

DAKTARO DISERTACIJA

TECHNOLOGIJOS MOKSLAI,
MECHANIKOS INŽINERIJA (09T)



LEIDYKLA
Vilnius TECHNIKA 2016

Disertacija rengta 2012–2016 metais Vilniaus Gedimino technikos universitete.

Vadovas

prof. habil. dr. Rimantas KAČIANAUSKAS (Vilniaus Gedimino technikos universitetas, mechanikos inžinerija – 09T).

Vilniaus Gedimino technikos universiteto Mechanikos inžinerijos mokslo krypties disertacijos gynimo taryba:

Pirmininkas

prof. dr. Dalius MAŽEIKAS (Vilniaus Gedimino technikos universitetas, mechanikos inžinerija – 09T).

Nariai:

prof. habil. dr. Gintautas DZEMYDA (Vilniaus universitetas, informatikos inžinerija – 07T),

doc. dr. Artūras KILIKEVIČIUS (Vilniaus Gedimino technikos universitetas, mechanikos inžinerija – 09T),

prof. habil. dr. Marek MOLENDAS (Lenkijos mokslų akademijos agrofizikos institutas, mechanikos inžinerija – 09T),

prof. dr. Vytautas TURLA (Vilniaus Gedimino technikos universitetas, mechanikos inžinerija – 09T).

Disertacija bus ginama viešame Mechanikos inžinerijos mokslo krypties disertacijos gynimo tarybos posėdyje **2017 m. sausio 12 d. 14 val.** Vilniaus Gedimino technikos universiteto senato posėdžių salėje.

Adresas: Saulėtekio al. 11, LT-10223 Vilnius, Lietuva.

Tel.: (8 5) 274 4956; faksas (8 5) 270 0112; el. paštas doktor@vgtu.lt

Pranešimai apie numatomą ginti disertaciją išsiusti 2016 m. gruodžio 9 d.

Disertaciją galima peržiūrėti VGTU talpykloje <http://dspace.vgtu.lt> ir Vilniaus Gedimino technikos universiteto bibliotekoje (Saulėtekio al. 14, LT-10223 Vilnius, Lietuva).

Abstract

The dissertation investigates spherical harmonics method for describing a particle shape. The main object of research is the non-spherical shape particles. The purpose of this dissertation is to create spherical harmonics model for a non-spherical particle. The dissertation also focuses on determining the suitability of the low-resolution spherical harmonics for describing various non-spherical particles.

The work approaches a few tasks such as testing the suitability of a spherical harmonics model for simple symmetric particles and applying it to complex shape particles. The first task is formulated aiming to test the modelling concept and strategy using simple shapes. The second task is related to the practical applications, when complex shape particles are considered.

The dissertation consists of introduction, 4 chapters, general conclusions, references, a list of publications by the author on the topic of the dissertation, a summary in Lithuanian and 5 annexes.

The introduction reveals the investigated problem, importance of the thesis and the object of research, describes the purpose and tasks of the thesis, research methodology, scientific novelty, the practical significance of results and defended statements. The introduction ends in presenting the author's publications on the topic of the dissertation, offering the material of made presentations in conferences and defining the structure of the dissertation.

Chapter 1 revises the literature: the particulate systems and their processes, shapes of the particles and methods for describing the shape, shape indicators. At the end of the chapter, conclusions are drawn and the tasks for the dissertation are reconsidered.

Chapter 2 presents the modelling approach and strategies for the points of the particle surface, spherical harmonics, the calculation of the expansion coefficients, integral parameters and curvature and also the conclusions.

Chapters 3 and 4 analyze the modelling results of the simple and complex particles. At the end of the both chapters conclusions are drawn.

5 articles focusing on the topic of the dissertation have been published: two articles – in the Thomson ISI register, one article – in conference material and scientific papers in Thomson ISI Proceedings data base, one article – in the journal quoted by other international data base, one article – in material reviewed during international conference. 8 presentations on the subject of the dissertation have been given in conferences at national and international levels.

Reziumė

Disertacijoje nagrinėjamas sferinių harmonikų dalelių formos modelis. Pagrindinis tyrimo objektas yra nesferinės formos dalelės. Disertacijos tikslas – sukurti sferinių harmonikų modelį nesferinės formos dalelėms. Disertacijoje siekiama ištirti žemo laipsnio sferinių harmonikų tinkamumą įvairių nesferinių dalelių formų aprašymui.

Darbe sprendžiami uždaviniai: sferinių harmonikų modelio tinkamumo paprastoms simetrinėms dalelėms tyrimas bei sferinių harmonikų modelio taikymas sudėtingos formos dalelių aprašymui. Pirmasis uždavinys suformuluotas siekiant patikrinti modeliavimo teoriją ir skaičiavimo strategiją naudojant paprastas simetrines formas. Antrasis uždavinys siejasi su praktiniais taikymais, kai modeliuojamos sudėtingos formos dalelės.

Disertaciją sudaro įvadas, keturi skyriai, rezultatų apibendrinimas, naudotos literatūros ir autoriaus publikacijų disertacijos tema sąrašai, santrauka lietuvių kalba ir 5 priedai.

Įvadiniame skyriuje aptariama tiriamoji problema, darbo aktualumas, pristatomas tyrimų objektas, formuluojamas darbo tikslas bei uždaviniai, aprašoma tyrimų metodika, darbo mokslinis naujumas, darbo rezultatų praktinė reikšmė, ginamieji teiginiai. Įvado pabaigoje pristatomos disertacijos tema autoriaus paskelbtos publikacijos ir pranešimai konferencijose bei disertacijos struktūra.

Pirmasis skyrius skirtas literatūros analizei. Pateikiama trumpa apžvalga apie dalelių sistemose vykstančius procesus, dalelių formas ir taikomus metodus formos aprašymui, literatūroje dažniausiai sutinkamus formos rodiklius. Skyriaus pabaigoje formuluojamos išvados ir tikslinami disertacijos uždaviniai.

Antrajame skyriuje pateiktas matematinis modelis dalelių formai aprašyti: modeliavimo idėja, dalelės paviršiaus taškų strategijos, sferinių harmonikų teorija, koeficientų, integralinių rodiklių ir kreivių skaičiavimas, skyriaus išvados.

Trečiajame ir ketvirtajame skyriuose pateikiami modeliavimo rezultatai paprastoms ir sudėtingoms dalelėms. Abiejų skyrių pabaigoje pateikiamos išvados.

Disertacijos tema paskelbti 5 straipsniai: du – mokslo žurnaluose, įtrauktuose į Thomson ISI sąrašą, vienas – konferencijų medžiagoje, referuotoje Thomson ISI Proceedings duomenų bazėje, vienas – kitų tarptautinių duomenų bazių cituojamame žurnale, vienas – recenzuojamoje tarptautinių konferencijų medžiagoje. Disertacijos tema perskaityti 8 pranešimai Lietuvos bei kitų šalių konferencijose.

Notations

Symbols

$A(\varphi, \theta)$ – an actual surface and spherical harmonics expansion;

A_φ – derivative with respect to angle φ ;

A_θ – derivative with respect to angle θ ;

$A_i(\theta, \phi)$ – spherical harmonics expansion in certain segment;

\mathbf{a} – a vector of unknown coefficients;

a_l^m – spherical harmonics expansion coefficient;

a, b, c – dimensions of a particle;

c_{cor} – correction factor;

D – discrete descriptor;

E_{eff} – effective elastic modulus;

$E_j(\varphi, \theta)$ – an approximation error;

E, F, G – first fundamental constants;

F_{Hn} – normal Hertzian contact force;

$\mathbf{f}(\varphi, \theta)$ – a vector of polynomial functions;

H – mean curvature;

h – altitude of pyramid;

I – moment of inertia;

i – index for a polar line, index of the i^{th} part of the surface;

j – a subscript of a model with a different complexity, index for an azimuthal line;

k – a subscript used for a reference model;
 L – spherical harmonics expansion degree;
 L, M, N – second fundamental constants;
 l – degree of spherical harmonics;
 M – total number of terms in expansion;
 m – order of spherical harmonics;
 N – a number of sampling points;
 N_l^m – normalization constant;
 n – normal to the surface;
 P – a point of a surface;
 $P_l^m(\cos \varphi)$ – associated Legendre polynomials;
 q – a subscript used for a strategy;
 R – discrete value of radius;
 R_A – radius of an average point;
 r – a polar radius;
 $r(\varphi, \theta)$ – a polar radius function;
 $r_{qk}(\varphi_{qk}, \theta_{qk})$ – discrete values of polar radius;
 S – surface area;
 $S(\mathbf{x})$ – an original surface in Cartesian coordinates;
 $S_i - i^{th}$ element of a surface area;
 S_{tr} – area of a triangle;
 $S_R(\varphi, \theta)$ – an original surface in spherical coordinates;
 $S_R(\varphi_{qk}, \theta_{qk})$ – discrete values of original surface;
 S_w – area of a whole surface;
 thr – a subscript for a threshold model;
 u – displacement;
 V – volume;
 W_i – particular segment of the surface;
 \mathbf{X} – vector of parametric functions of the surface;
 \mathbf{x} – a vector of Cartesian coordinates;
 x, y, z – Cartesian coordinates;
 $[Y_j(\varphi_{qk}, \theta_{qk})]$ – transformation matrix;
 $Y_l^m(\theta, \varphi)$ – spherical harmonics;
 δ – Kronecker symbol
 $\theta_{.,ed}$ – singular azimuthal angle;
 ν – Poisson's ratio;
 ρ_{eff} – effective radius of curvature;
 φ, θ – spherical angles;
 $(\varphi_{qk}, \theta_{qk})$ – discrete values of spherical angles.

Operators and Functions

\overline{Y} – conjugate of a complex number;

d – derivative;

$\det(.)$ – determinant of a matrix;

$||.||^2$ – an Euclidean norm;

\int – integral;

$[.]^{-1}$ – inverse matrix;

$|.|$ – length of a vector;

$[.]^T$ – a matrix transpose;

$||.||^\infty$ – a maximum norm;

∂ – partial derivative;

$[.]^+$ – pseudo-inverse matrix;

\times – vector product.

Contents

INTRODUCTION	1
Problem Formulation	1
Relevance of the Thesis	2
The Object of Research	3
The Aim of the Thesis	3
The Tasks of the Thesis	3
Research Methodology	3
Scientific Novelty of the Thesis	4
Practical Value of the Research Findings	4
The Defended Statements	4
Approval of the Research Findings	5
Structure of the Dissertation	6
 1. REVIEW OF LITERATURE ON PARTICLES AND THEIR SHAPES ...	7
1.1. Particulate Systems and Processes	7
1.2. Mathematical Methods for Shape Representation	9
1.3. Shape Descriptors	11
1.4. Shapes of the Particles	13
1.5. Conclusions of Chapter 1 and Formulation of the Tasks of the Thesis .	17

2. MATHEMATICAL MODEL OF THE PARTICLE SHAPE	19
2.1. Modelling Approach	19
2.2. Modelling Strategies for the Particle Surface	23
2.3. Spherical Harmonics	24
2.4. Calculation of Coefficients	27
2.5. Calculation of Integral Parameters	28
2.6. Calculation of Curvature	33
2.7. Conclusions of Chapter 2	36
3. SPHERICAL HARMONICS APPLICATION TO SIMPLE PARTICLES .	37
3.1. Modelling of Ellipsoid Particle	37
3.1.1. Description of the Ellipsoidal Surface	37
3.1.2. Modelling of the Ellipsoid	38
3.1.3. Analysis of the Ellipsoid Results	39
3.2. Modelling of Cylinder Particle	42
3.2.1. Description of the Cylinder Surface	42
3.2.2. Modelling of Cylinder	43
3.2.3. Analysis of the Cylinder Results	48
3.3. Modelling of Rectangular Parallelepiped	49
3.3.1. Description of the Parallelepiped Surface	49
3.3.2. Modelling of Rectangular Parallelepiped	51
3.4. The Curvature and Other Factors for Contact Calculation	56
3.5. Comparison Study of Low-Resolution Harmonics for Various Shapes	63
3.6. Conclusions of Chapter 3	70
4. SPHERICAL HARMONICS APPLICATION TO COMPLEX PARTICLES	73
4.1. Modification of the Modelling Technique	73
4.2. Modelling of Bean Particle	75
4.3. Modelling of Chickpea Particle	77
4.4. Modelling of Maize Particle	79
4.5. Comparative Analysis of the Results	80
4.6. Conclusions of Chapter 4	82
GENERAL CONCLUSIONS	83
REFERENCES	87
LIST OF PUBLICATIONS BY THE AUTHOR ON THE TOPIC OF THE DISSERTATION	95

SUMMARY IN LITHUANIAN	97
ANNEXES ¹	111
Annex A. Low-Resolution Spherical Harmonics	112
Annex B. Analytical Descriptors of Particle Shape	113
Annex C. Various Characteristics of Modelled Shapes	114
Annex D. The Co-authors Agreements to Present Publications for the Dissertation Defence	118
Annex E. The Copies of Scientific Publications by the Author on the topic of the Dissertation	122

¹The annexes are supplied in the enclosed compact disc

Introduction

Problem Formulation

Mathematical modelling and information technologies plays an important role in many areas of sciences and engineering. Among many specific applications, particulate solids, especially granular materials, could be distinguished. They present a huge class of materials widely used in chemical, pharmaceutical, food and other industries. It is obvious that transportation of particulates and their treatment in technological processes are heavily influenced by the microscopic properties of individual particles. Various problem-oriented computer-based technologies and data systems are used to control the behaviour of particulates containing huge number of particles.

An important property of particulate solid is the shape of particle. The research addressing characterisation and mathematical description of particle shape concerns basically non-spherical shapes. In the earlier stage, empirical indirect relationships between the mechanical properties and the shape characteristics prevailed. Recently, many different mathematical models that constitute particle shapes have been systematically formulated and utilized by applying computational and information technologies.

Identification methods for variety classification or quality inspection (i. e., crushed, damaged, diseased, immature, or overmature) require an accurate de-

scription of the grain geometry. Characterization methods used to describe the behaviour of particulate systems during handling may also benefit from an accurate description of the geometry of grains, as it has been experimentally proven that properties such as flowability, dilatancy, crushability, and segregation are highly influenced by the particle shape.

The main issue in the investigation of granular systems is related to contact mechanics during collisions between products or machinery parts. The shape and volume of the particle is important in packing problems while local angularities has the impact on the contact calculation. In general, a good approximation of the particle shape results in the high accuracy of the mechanical problem.

Since there is a lack of universal tool for shape approximation as well as the contact calculation, the spherical harmonics technique presented in this work allows to develop the method suitable for the description of the arbitrary shaped particle.

Relevance of the Thesis

The understanding the behaviour of particulate materials is of major importance. Although it could seem to be a rather simple task, the granular materials consist of large number of particles, thus, the experiments are quite expensive and difficult to carry out. Furthermore, there is a lack of computational methods for modelling the granular materials. Recently, the discrete element method has become the dominant computational tool for investigating the behaviour of granular matter. Discrete element method allows for a microscopic insight into granular material behaviour with tracing in time all dynamical parameters of particles. The most important parameter for discrete element method is particle shape, that strongly effect the simulation results.

In reality, the majority of granular particles are non-spherical, and there exists not so many methods for the description of such shapes. Both monomeric and composite approach have their own disadvantages. The use of smooth continuous shapes (ellipsoids, generalised super-ellipsoids or super-quadratics) is inconvenient because the detection of contact can only be achieved by iteratively solving sets of nonlinear equations. It is clear that shape models created using a single function are applicable for only a limited number of shapes. The composite approach can be used to represent arbitrarily shaped, irregular, complex geometrical entities fairly well, but a different technique is required to describe the contact of particles.

Because of the lack of universal tools for describing the shape and calculating the contact, the semi-analytical method using spherical harmonics is considered.

Spherical harmonics is suitable for arbitrary shaped particles and the modelling concept is the same despite of the shape (spherical, non-spherical, symmetric or not, etc.). Such versatile technique can simplify the modelling of particle shapes.

The Object of Research

The object of research is non-spherical particles and their description using spherical harmonics.

The Aim of the Thesis

The main aim of the thesis is to develop spherical harmonics model to describe non-spherical particles and investigate the suitability of low resolution spherical harmonics for non-spherical particle shape description.

The Tasks of the Thesis

In order to achieve the aim of the thesis, the following problems had to be solved:

1. To review the existing methods for describing the particle shape and applications of spherical harmonics.
2. To develop the method for describing a particle shape using low-resolution ($L \leq 3$) spherical harmonics.
3. To analyze the suitability of the low-resolution spherical harmonics model by applying it to simple symmetric particles (ellipsoidal, cylindrical and parallelepiped shapes).
4. To apply the developed spherical harmonics model to non-spherical complex particles.

Research Methodology

To investigate the object, the following research methods are chosen:

- mathematical modelling such as spherical harmonics expansion and least square method;

- numerical simulation for testing the modelling technique with samples.

Scientific Novelty of the Thesis

The aspects of scientific novelty on non-spherical particle shape description are as follows:

1. The presented modelling concept is to model the particle shape using spherical harmonics. The spherical harmonic expansion uses discrete points of the surface and transforms them into expansion coefficients. For the calculation of the expansion coefficients the least squares method and the pseudo-inverse matrix computational procedure is used.
2. Various strategies for positioning the sampling points is considered calculating the expansion coefficients. Furthermore, the analysis of the results shows that each strategy has the different impact on the modelling results.
3. The suitability for the use of spherical harmonics is tested with simple symmetric particles evaluating some descriptors such as surface area and volume. The presented results show that low-resolution spherical harmonics expansion (up to $L = 3$) approximates such particles with high accuracy.
4. The model is applied for the complex particles. Considering these shapes, the modelling technique is modified by introducing the surface division into smaller parts.

Practical Value of the Research Findings

Spherical harmonics method presented here can be applied for arbitrary shaped particles. Such method allows to approximate the shape with analytical function which later can be used in calculation of various descriptors (integrate for surface area, volume or moments of inertia, differentiate for normal vector and radius of curvature) or contact forces.

The Defended Statements

The following statements based on the results of present investigation may serve as the official hypotheses to be defended:

1. The low-resolution spherical harmonics are proper approximation tool to describe the shape of rounded and angular equal-sized particles, the accuracy of the method drops, however, with extension or flattening of particle.
2. Application of least square approximation combined with adaptive positioning strategies increases accuracy of spherical harmonics approximation.
3. For description of complex non star-shaped particles, the spherical harmonics have to be combined with the regional sub-division.

Approval of the Research Findings

The main results of the doctoral dissertation were published in 5 scientific papers: 2 papers in journals indexed in Thomson ISI Web of Science (Radvilaitė *et al.* 2016, 2017), 1 paper in conference proceedings indexed in Thomson ISI Proceedings (Kačianauskas *et al.* 2015), 1 paper indexed in other international databases (Radvilaitė *et al.* 2014) and 1 paper in conference proceedings (Radvilaitė *et al.* 2015).

The author has made eight presentations at eight scientific conferences at national and international levels:

- Young scientists conference “Interdisciplinary research of physical sciences and technology”, held on 11 February 2014 in Vilnius;
- XXIInd seminar of Association of Lithuania Computational Mechanics, held on 25 April, 2014 in Vilnius;
- International conference “Numerical Analysis and Applied Mathematics (ICNAAM)”, held on 22–28 September, 2014 in Rhodes, Greece;
- XXIIIrd seminar of Association of Lithuania Computational Mechanics, held on 24 April, 2015 in Vilnius;
- International conference “Optimization and Analysis of Structures (OAS 2015)”, held on 23–25 August, 2015 in Tartu, Estonia;
- International conference “Polish Congress of Mechanics and Computer Methods in Mechanics (PCM-CMM 2015)”, held on 8–11 September, 2015 in Gdansk, Poland;
- XXIVth seminar of Association of Lithuania Computational Mechanics, held on 20 April, 2016 in Vilnius;

- International conference “Modern Building Materials, Structures and Techniques (MBMST 2016)”, held on 26–27 May, 2016 in Vilnius.

Structure of the Dissertation

The dissertation consists of introduction, four main chapters, general conclusions, references, a list of publications by the author on the topic of the dissertation and a summary in Lithuanian. The total scope of the dissertation is 126 pages, 62 equations, 31 figure and 11 tables. For the purpose of the present dissertation, references were made to 94 source papers.

Review of Literature on Particles and Their Shapes

This chapter provides the overview of the literature on particulate systems and processes, shapes of the particles, methods for describing the shape, both mathematical and applied in discrete element method, and indicators for characterizing the shape.

Parts of this chapter are published in Radvilaitė (2014), Kačianauskas *et al.* (2015), Radvilaitė *et al.* (2015), Radvilaitė *et al.* (2016) and Radvilaitė *et al.* (2017).

1.1. Particulate Systems and Processes

Granular materials are important in almost all areas of science and technology. They present a huge class of materials widely used in chemical, pharmaceutical, food and other industries. Despite the form they are used, whether as fillers in composite materials, as packings with their own mechanical properties, or whether designed to be dissolved as a supply of chemicals, their size and shape often determines their effectiveness in each particular application. Thus, proper understanding of mechanical behaviour of granular materials is of major importance for both fundamental developments and industrial applications (Garboczi 2011; Markauskas *et al.* 2010).

Identification methods for variety classification or quality inspection (i. e., crushed, damaged, diseased, immature, or overmature) require an accurate description of the grain geometry. Characterization methods used to describe the behaviour of particulate systems during handling may also benefit from an accurate description of the geometry of grains, as it has been experimentally proven that properties such as flowability, dilatancy, crushability (González-Montellano *et al.* 2012; Horabik *et al.* 2016; Markauskas *et al.* 2015; Mellmann *et al.* 2014; Parafiniuk *et al.* 2013), and segregation (Jha *et al.* 2008) are highly influenced by the particle shape. The role of the shape in particular problems is considered by Cleary (2008); Kock and Huhn (2007); Santamarina and Cho (2004). Basic concepts and different measures used to classify particle shapes are given in review papers by Blott and Pye (2008); Bullard and Garboczi (2013); Nouguié-Lehon *et al.* (2003); Parafiniuk *et al.* (2014).

As granular materials are simple systems of a large number of particles of various size, shape, and material, several phenomena in nature as well as many industrial applications involve static or dynamic granular assemblies. Depending on the physical background the number of particles being involved in these assemblies differs largely. While laboratory scale experiments usually involve small numbers of particles, industrial applications like silos may contain several cubic meters of granular material in which the particle number may easily exceed the order of 10^9 per cubic meter. In nature some phenomena like avalanches or earthquakes often incorporate hundreds of tons of granular material therefore involving even larger quantities of particles (Džiugys and Peters 2001; Krugger-Emdem *et al.* 2007; Peña *et al.* 2009).

Granular materials present a complex mechanical response when subjected to an external load. The shape, angularity and size distribution of the grains, the evolution of the granular skeleton (spatial arrangement of particles, void ratio, fabric, force chains), and some phenomena occurring at the grain scale (like rolling or sliding) are determinant factors for the overall macroscopic response (Peña *et al.* 2007).

Grains not only slide and roll in granular materials, they also are being compressed and sheared. Sliding is an irreversible, plastic process that only heats up the system. Rolling is not itself irreversible, but it does eventually lead to sliding, crushing and heat. These processes are discussed in works by Jiang and Liu (2007, 2008). In addition, grains in granular materials interact at contact points, where forces arise to oppose the relative displacement between contacting particles. Such behaviour and the focus on the stress-strain relationship for dense assemblies in the linear elastic regime is analysed by Agnolin and Roux (2008).

Different theories of granular materials, like elasticity or hydrodynamics, is presented by Bräuer *et al.* (2006); Jiang and Liu (2009); Krimer *et al.* (2006); Møller and Bonn (2007).

To investigate the behaviour of the granular materials are very important, but the properties and processes of such materials are not fully understandable. Because of large number of particles involved in granular matters, the experiments are quite expensive and difficult to carry out. Furthermore, there is a lack of computational methods for modelling the granular materials. Recently, the discrete element method has become the dominant computational tool for investigating the behaviour of granular matter. Discrete element method allows for a microscopic insight into granular material behaviour with tracing in time all dynamical parameters of particles, such as position of individual grains, their velocity, acceleration and acting inter-particle forces (Balevičius *et al.* 2011; Kačianauskas *et al.* 2014).

Thus, the particle shape is the most important factor determining the accuracy of the simulation results. However, there exist many different methods for describing a particle shape.

1.2. Mathematical Methods for Shape Representation

Particle shapes can be described mathematically using certain functions or even the theory of differential geometry.

The advancement of modelling, digitizing and visualizing techniques for 3D shapes has led to an increasing amount of 3D models. There are many possible representation techniques for both surface and volume models: implicit surfaces, CSG (constructive solid geometry), BSP (binary space partitioning) trees, octrees, B-rep (boundary representation), free form surfaces, etc. The review of all this methods can be found in study by Tangelder and Velthkamp (2008). Furthermore, in review works by Tangelder and Velthkamp (2008); Zhang and Lu (2004); Zhang *et al.* (2007) the classification of 3D surfaces shape representation is discussed. Here, basically two categories of shape representation (contour-based and region-based methods) are distinguished.

The simplest way to represent a particle system is either to use a set of points (point cloud data) or solid objects (volumetric data). Both types of data can be represented by a set of position vectors $\{X\} = \{\mathbf{x}_1, \mathbf{x}_2, \dots, \mathbf{x}_n\}$ and weights $\{f\} = \{f_1, f_2, \dots, f_n\}$ (Keys *et al.* 2011).

Another shape descriptor that is conceptually simple is known as the “shape histogram”. This descriptor is based on a density map of the structure on a polar or spherical grid. The shape histogram is constructed in 2D by first generating n_θ equiangular gridlines on the unit circle. The shape histograms method is an intuitive and discrete representation of complex spatial objects. The shape histogram has the disadvantage that it requires registration to match shapes that are not aligned spatially, unless only radial bins are used (i.e. $n_\theta = n_\varphi = 1$). Shape histograms with only radial bins are typically only applicable for obtaining coarse measures of similarity, since they lose much of their discerning capabilities without an angular component (Keys *et al.* 2011; Novotni and Klein 2004; Zhang *et al.* 2007).

Fractal analysis is quite new mathematical idea to describe irregular shape using fractional numbers instead of integers. The concept of fractals, which has the shape formed in nature, has been usually analyzed using Euclidian geometry. The key parameter for fractal analysis is the fractal dimension, which is a real non-integer number, differing from the more familiar Euclidean or topological dimension. The fractal dimension for a line of any shape varies between one and two, and for a surface – between two and three. In recent years, fractal geometry techniques have found widespread applications in many disciplines, including medicine, biology, geography, meteorology, manufacturing, and material science (Arasan *et al.* 2011).

In molecular dynamics, the concept of spheropolygons, which is the object resulting from dilating a polygon by a sphere, was introduced. In 3D models, the dilation of a polyhedra by a sphere has a precise mathematical meaning using the Minkowski operator (Galindo-Torres *et al.* 2009, 2010; Galindo-Torres and Pedroso 2010).

Another mathematical method applied for the shape description is Zernike moments and polynomials. These moments are computed as a projection of the function defining the object onto a set of orthonormal functions within the unit ball. It is easier to recover 3D shape from Zernike moments and there will be less computationally expensive. However, 3D Zernike moments suffer by the severe instability of geometrical moments and hence always in case of high orders (Novotni and Klein 2004; Zhang and Lu 2004; Zhang *et al.* 2007). Although Zernike moment descriptor has a robust performance, it has several shortcomings. To overcome these shortcomings, a generic Fourier descriptor (GFD) has been proposed. The GFD is acquired by applying a 2D Fourier transform on a polar-raster sampled shape image (Zhang and Lu 2004).

The mostly used approaches, including semi-analytical models, are discussed in Masad *et al.* (2005). In this study, a number of computational methods were

utilized to describe the surface characteristics of granular materials, while the role of Fourier series and spherical harmonic series, wavelet analysis and a gradient method were emphasised.

The gradient method (Masad *et al.* 2005) was applied to model surface angularity. This method was adopted to smooth a highly angular particle that has sharp angular corners. The wavelet transform works by mapping an image onto a low-resolution image and a series of detailed images (Mallat 1989). The wavelet analysis is a powerful method for modelling on the scale of the texture, and a series of detailed images providing quantitative predictions on the real behaviour of granular materials is demonstrated in Amaratunga and Castrillon-Candas (2001); Johnson and Williams (2009); Masad *et al.* (2005).

The standard mathematical tool, Fourier series, has been used recently to quantify the shape of particles (Masad *et al.* 2005). The method, based on the 2D image analysis for particle shape characterization, was introduced in Soga *et al.* (2001). Further, it was modified for 3D shapes and applied to sand characterization (Mollon and Zhao 2013, 2014).

Recently, spherical harmonic functions has received much attention. Spherical harmonic expansions are well-understood tool of applied mathematics and have a well-established standing in the molecular sciences. They are perhaps best known as the orbital shape determining functions as solutions of the angular part of Schrödinger's equation for the hydrogen atom although they occur in a great variety of different physical problems such as electromagnetism, gravity, mechanics or hydrodynamics (Morris *et al.* 2005). The earliest contributions using spherical harmonics have been found in concrete (Garboczi 2002). Successful 3D applications of sophisticated spherical harmonics comprise lunar regolith (Garboczi 2011) or sand (Liu *et al.* 2011; Zhou *et al.* 2015) particles. Spherical harmonics also has been widely applied to some other fields such as medicine for the representation of organs (Abdallah *et al.* 2010; Mofrad *et al.* 2014; Santhanam *et al.* 2010), action recognition (Razzaghi *et al.* 2013) or in biology for the representation of parts of insects (Shen *et al.* 2009). Furthermore, they are encountered, inter alia, in weather and climate modeling, in the representation of gravitational, topographic, and magnetic data in geophysics, in the numerical solution of certain partial differential equations, etc. (Rokhlin and Tygert 2006).

1.3. Shape Descriptors

In reality, the majority of granular particles is non-spherical, and may have irregular, randomly shaped geometries. Consequently, various models of varying com-

plexity have been used to approximate such shapes. The existing discrete element method models for particles may be classified with respect to descriptors comprising the characterization of the global shape compared with a sphere, in terms of the sphericity, aspect ratio, or squareness; the sharpness of edges, in terms of angularity or roundness; and the smoothness (roughness) of the particle surface (Kačianauskas *et al.* 2014). The most used descriptors are given in Table 1.1.

Table 1.1. Descriptors for characterizing the particle shape

Descriptor	Formula	References
Sphericity	$\Psi = \frac{A}{\frac{\pi \times L^2}{4}}$ $\Psi = \frac{A_s}{A}$ $\Psi_{BS} = \frac{\rho_{is}}{\rho_{es}}$ $\Psi = \sqrt{\frac{R_{insc}}{R_{circ}}}$ $\Psi = \frac{\pi^{1/3}(6V)^{2/3}}{S}$	<p>Arasan <i>et al.</i> (2011)</p> <p>Jalaal <i>et al.</i> (2012), Bullard and Garboczi (2013) Bullard and Garboczi (2013)</p> <p>Mollon and Zhao (2012, 2014)</p> <p>Feinauer <i>et al.</i> (2015), Zhou <i>et al.</i> (2015)</p>
Roundness	$R = \frac{4\pi A}{P^2}$ $R_W = \frac{\sum_{i=1}^N \rho_i }{\sum_{i=1}^N \rho_{ic}}$ $R = \frac{\sum R_c}{n_c R_{insc}}$	<p>Arasan <i>et al.</i> (2011)</p> <p>Bullard and Garboczi (2013)</p> <p>Mollon and Zhao (2012, 2014)</p>
Angularity	$K = \frac{P}{P_{elip}}$ $AI = \frac{s^2}{2\pi^2} \sum_{\theta=0}^{\pi/s} \sum_{\varphi=0}^{2\pi/s} \frac{ r_p - r_{EE} }{r_{EE}}$	<p>Arasan <i>et al.</i> (2011)</p> <p>Zhou <i>et al.</i> (2015)</p>
Convexity	$C = \frac{A}{A_{rect}}$	Arasan <i>et al.</i> (2011)
Regularity	$R = \log \left(\frac{P}{P - P_{conv}} \right)$	Mollon and Zhao (2012)

Three useful parameters for characterizing the particle shape are the length L , the width W and the thickness T . These three quantities then define some kind of minimum dimension orthogonal box that just contains the particle (Garboczi 2011; Liu *et al.* 2011). Then three dimension ratios can be defined:

$$\text{Aspect ratio} = \frac{S}{L}, \quad (1.1)$$

$$\text{Elongation} = \frac{I}{L}, \quad (1.2)$$

$$\text{Flatness} = \frac{S}{I}, \quad (1.3)$$

where S is the smallest dimension, I – intermediate dimension, L – the longest dimension of a rectangular box containing exactly the particle (Mollon and Zhao 2012, 2014).

One of most often used parameter to describe the geometry of the particle is sphericity. There is more than one definition in the literature for this descriptor. Sphericity indicates how equiaxed the particle is, and is the opposite of anisometry or ellipticity (Bullard and Garboczi 2013). Sphericity of the sphere is equal to 1.

Another descriptor is roundness. Roundness gives information about how blunt-ed or rounded the corners and edges of the particle are, and is the opposite of angularity (Bullard and Garboczi 2013). This is a shape factor that has a maximum value of 1 for a circle and smaller values for shapes having a lower ratio of area to perimeter, longer or thinner shapes, or objects having rough edges (Arasan *et al.* 2011). According to Mollon and Zhao (2012), it is a measure of the average sharpness of the angles of the particle. However, this definition is not perfectly objective since it is difficult to determine what curve along the contour of a particle is sharp enough to be called a “corner” (Mollon and Zhao 2012).

Besides the already mentioned descriptors, there is angularity. This is a shape factor that has a minimum value of 1 for circle and higher values for shapes having angular edges (Arasan *et al.* 2011).

1.4. Shapes of the Particles

The particle shape is an important property influencing the interaction of separate grains, and, in recent decades, many studies have been dedicated to improving the understanding of the role of the shape in the behaviour of granular materials. Because the solution of the contact problem for arbitrary shaped surfaces in three dimensions is complicated, a smooth sphere has become the most popular particle shape in discrete element method studies, and the explicitly defined Hertz solution for single sphere-sphere and sphere-plane contacts is extensively employed to simulate various particulate solids using the discrete element method (Kačianauskas *et al.* 2014).

The discrete element method is applied to model and analyze the mechanical behavior of assemblies of particulate material, where particles with the shape of discs in two-dimensional (2D) or spheres in three-dimensional (3D) are used for

easy implementation and time-saving advantages. The influence of particle shape on flow and accumulation behaviors of particles is almost not considered in such approaches (Jin *et al.* 2011).

Early discrete element programs modelled the interactions between circular disks or spherical particles. The simple calculation to find the location and overlap of two spheres, together with the well-established theory for their elastic interaction guaranteed their selection for this purpose. This simplicity is appealing from the points of view of both implementation and computational speed, which is important given the demand for very large numbers of particles in some simulations. Although spheres bear only the crudest resemblance to most soil particles, much useful work has used spheres and they are still widely used in research. However, it is clear that spheres cannot reproduce all the aspects of the behaviour of non-spherical particles and this has led to the development of more complex particle models (Harkness 2009).

The advantage of using discs or spheres to represent particle shape is their simplicity especially in terms of inter-particle contact detection. Moreover the contact force models for contacting spheres and spheres contacting flat walls are well known. Since discrete element simulations usually involve large numbers of discrete elements, minimizing computing time is a very important aspect (Höhner *et al.* 2011). It is well known that an important fraction of the computation time in a discrete element method calculation may be devoted to contact detection and calculation of the overlap distance between particles. For circular particles (in 2D) or spherical particles (in 3D) the calculation is trivial: the overlap is simply the distance between the particle centres, minus the sum of the radii of the two contacting particles (Houlsby 2009).

While spheres are easy to handle in a discrete element method code, they show a different mechanical behaviour on the single grain level as well as in larger assemblies compared to the actual particle behaviour in most application areas. For example interlocking of particles cannot be simulated using spherical shape representation. Therefore the physical meaning of results obtained from these simulations is questionable (Höhner *et al.* 2011).

For almost any other particle shape the calculation is much more complex, and the resulting computation can become sufficiently lengthy that it impacts significantly on overall run time. For most applications real particles are, of course, not spherical. However, the simplicity of the contact detection and overlap calculations is a powerful driver that encourages the use of the spherical idealisation. Particle shape can in some applications have a very important influence on the behaviour of a granular medium, and so means of modelling non-circular (or non-spherical) particles is required (Houlsby 2009).

Majority of particles existing in nature, such as gravel, tablets, and seeds, are non-spherical with non-smooth edges and corners. Particles with different shapes have different properties. Thus, particle shapes have an important influence on the overall characteristics of a single particle or an entire particle system. In order to get more realistic behaviour of the granular materials, simulation in discrete element method should consider non-spherical particles (Jin *et al.* 2011).

Although spheres remain popular in discrete element method because of their computational efficiency in contact detection, particles in real life are largely non-spherical. Granular and powder materials are present in many shapes, most of which are non-spherical. The processing of these materials is important in many engineering applications. Various methods to model non-spherical particles have been proposed in the literature, most of which impose restrictions on the shape of the particles, i. e., either the particle has to be polyhedral or the particle shape is restricted to a particular type of function (Boon *et al.* 2013).

Representation of the particle shape is one of the key challenges of discrete element method simulations. In order to obtain more realistic particle behaviour other particle shape approximations have been introduced into the discrete element method. Basically two different approaches can be recognized: the single-particle approach and the clustered-particle approach. In a single particle approach the particle is a single particle of complicated geometry such as an ellipsoid, superquadric or polyhedron. In the clustered particle approach smaller body elements such as spheres are connected in order to form a clustered particle of complex shape.

Elliptical particles are probably the most widely used nonspherical smooth particle shape in discrete element method simulations. The usage of ellipses (2D) and ellipsoids (3D) decreases the inherent rolling tendency of spherical particles which is considered as one of the major causes of deviation of discrete element method simulations from realistic particle behaviour. Contact detection between elliptical and ellipsoidal particles usually involves a numerical calculation of polynomial roots which can be very time-consuming depending on the applied numerical algorithm and the chosen initial value of the iteration. Thus, the use of such particles includes algorithms for particle intersection computing, stress-strain behaviour, fabric, and particle generation (Höhner *et al.* 2011; Jin *et al.* 2011).

Another interesting approach to implement more complex particles is the usage of polyhedral body shapes. A particular case of the composite approach was introduced by Cundall (1988), and improved by Chen *et al.* (2011), for polyhedral shapes, wherein convex particles were constructed using cutting planes. The advantage of using polyhedral shapes is that a wide variety of complex particle shapes can be simulated, meaning that more realistic results can be obtained from discrete element method simulations. However, the presence of sharp ver-

tices complicates the treatment of particle contacts. Thus, the question of how contact forces between two colliding polyhedral bodies are calculated is still not completely answered. In some algorithms only the vertices of the polyhedral surface are checked for contact with another polyhedra while in others – contacts are differentiated among different contact types. (Höhner *et al.* 2011; Kačianauskas *et al.* 2014).

Recently, a hybrid sphero-polyhedral approach (Alonso-Marroquín *et al.* 2013; Galindo-Torres *et al.* 2010; Galindo-Torres and Pedroso 2012; Mollon and Zhao 2013), where a sphero-polyhedron is considered as a polyhedron with rounded corners and edges, has been developed to simplify the calculation of sharp contacts between polyhedral particles. The composite approach approximates complicated real shapes by combining various regular shapes such as cutting planes, and cylindrical and/or spherical surfaces.

The composite-particle or clustered-particle approach is basically restricted to multi-sphere models (Kodam *et al.* 2009; Kruggel-Emdem *et al.* 2008). In the multi-sphere model the single particle is represented by a composition of connected spheres which may vary in size and even overlap each other. This shape representation algorithm can be easily implemented and shows efficient contact detection because it employs a sphere-sphere contact detection algorithm for irregular shaped objects. Once a model particle is created, the relative distances between the component spheres remain fixed throughout the simulation so that the generated clustered particle remains a rigid body. The most significant advantage of this approach is that it allows an easy and efficient calculation of the contact between complex particles using only spherical contact models (Höhner *et al.* 2011; Kačianauskas *et al.* 2014).

Several studies have attempted to apply the multi-sphere model to approximate regularly shaped smooth surfaces by further increasing the number of subspheres in a systematic fashion. Particular examples validating the use of the multi-sphere model to approximate elongated spherocylindrical particles were given by Abbaspour-Fard (2004) and perfect ellipsoids were considered by Markauskas *et al.* (2010). A discussion of the approximation of non-smooth spherical particles using the multi-sphere model was given Kruggel-Emdem *et al.* (2008); it was shown that the application of the refined multi-sphere model could potentially change the macroscopic response. The authors assumed that the refinement of the particle model, which was achieved by increasing the number of subspheres, itself introduced additional errors. The discussion of this issue was continued in later investigations (Höhner *et al.* 2011, 2012, 2014; Kodam *et al.* 2009; Szarf *et al.* 2011) where the role of local non-convexity and multiple contacts, which lead to increased inter-particle friction and interlocking of particles, was emphasised.

1.5. Conclusions of Chapter 1 and Formulation of the Tasks of the Thesis

1. Granular materials are important in many areas of science and technology. Although they are simple systems of a large number of particles, the proper understanding of their behaviour is of major importance. The review of literature on granular materials shows that there are various processes that are related to granular materials and their behaviour. Due to a large number of particles involved, the experiments are quite expensive to carry out. On the other hand, there is a lack of computational methods that are suitable for simulating such materials.
2. The particle shape is an important property influencing the behaviour of granular materials. Recently, the discrete element method has become the dominant computational tool for investigating such systems. As accurate shape description has an impact on the simulation results, there exist various models for approximating the shape. Each of them introduces some assumptions to simplify the shape. However, the majority of particles in reality is non-spherical and a good approximation tool is still lacking.
3. The performed review on particle shapes and their description methods revealed that there is not yet developed a versatile analytical description method for non-spherical particles. Known semi-analytical method of spherical harmonics is potentially a suitable method for solving this problem. The performance of this approach should be based, however, on research results.

In order to achieve the aim, the following have to be solved:

1. To develop the method for describing a particle shape using low-resolution ($L \leq 3$) spherical harmonics.
2. To analyze the suitability of the low-resolution spherical harmonics model by applying it to simple symmetric particles (ellipsoidal, cylindrical and parallelepiped shapes).
3. To apply the developed spherical harmonics model to non-spherical complex particles.

Mathematical Model of the Particle Shape

This chapter presents the modelling concept using spherical harmonics. Several strategies for the positioning of the sampling points are introduced. Later they are used in modelling the chosen shapes in order to test the sensitivity of the spherical harmonics expansion. As the least squares method and pseudo-inverse matrix procedure is used for the calculation of the expansion coefficients they are discussed in more details. This chapter also introduces the calculation of some integral parameters for the spherical harmonics models and also the calculation of curvature and contact is discussed here.

Parts of this chapter are published in Radvilaitė (2014), Kačianauskas *et al.* (2015), Radvilaitė *et al.* (2015), Radvilaitė *et al.* (2016) and Radvilaitė *et al.* (2017).

2.1. Modelling Approach

The particle is assumed to be continuous star-shaped 3D body obeying plane symmetry, where at least one symmetry plane exist. It is described in the local frame of reference, while two local coordinate systems, Cartesian coordinates $Oxyz$ or spherical coordinates $Or\varphi\theta$, with their origin positioned in the centre of mass, can be simultaneously applied for the description of particle. Conventionally, a continuous body is composed by the infinite number of points in the particle volume. The position of each point within the body is defined by three independent coordinates

building a vector $\mathbf{x} = \{x, y, z\}$. When applying spherical coordinates, position of the point may be defined by the polar radius r and two azimuthal and polar spherical angles, φ and θ , varying within the limits $0 \leq \varphi < 2\pi$ and $0 \leq \theta \leq \pi$, respectively. The coordinate frame and positioning of point p defined by Cartesian coordinates \mathbf{x}_p and spherical coordinates r_p , φ_p and θ_p are shown in Fig. 2.1.

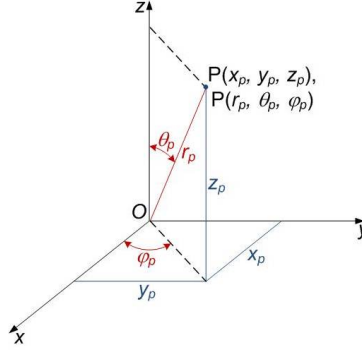


Fig. 2.1. Coordinate frame and positioning of point P

The well-known direct relationship allows a parametric evaluation of Cartesian coordinates

$$x = r \cos \varphi \sin \theta, y = r \sin \varphi \sin \theta, z = r \cos \theta. \quad (2.1)$$

An inverse relationship to spherical coordinates could also be used

$$r = (x^2 + y^2 + z^2)^{1/2}, \varphi = \tan^{-1} \left(\frac{y}{x} \right), \theta = \cos^{-1} \left(\frac{z}{r} \right). \quad (2.2)$$

The modelling concept elaborated and applied hereafter operates systematically with the specified surfaces manifested in terms of three namely, original, reference, and actual, categories. These different categories are characterised by different mathematical models, and they are considered at different modelling stages. The *original* model denoted hereafter by S , presents a surface that exactly matches the particle shape. The term ‘exact’ is used to characterize a perfect shape composed of a set of analytically expressed functions. Explicitly, the original surface in Cartesian coordinates is described as follows:

$$S(\mathbf{x}) = 0. \quad (2.3)$$

Referring to spherical coordinates, the original surface is described by the polar radius r varying as a function of the polar angles φ and θ :

$$r(\varphi, \theta) = S_R(\varphi, \theta). \quad (2.4)$$

Another definition of the surface is referred to as the *reference* surface. The reference surface denoted hereafter by R is assumed to be a discrete model of the original surface S . Since the reference surface is only an approximated surface, therefore it is not unique. The definition of reference surface assumes the existence of the family of k reference surfaces R_k , each of which denoted by subscript k , where $k = 1, 2, \dots, K$. The reference surface R_k is specified as a discrete set $\mathbf{x}_k = \{\mathbf{x}_{k1}, \dots, \mathbf{x}_{kp}, \dots\}$ consisting of the coordinates \mathbf{x}_{kp} of $p = 1, 2, \dots, N_k$ sampling points. In the sampling points, Eq. (2.3) is satisfied, thus $S(\mathbf{x}_{kp}) = 0$. Usually the increase of k means a finer hierarchically constructed cloud of points.

On the other hand, the reference surface can be formed by applying various modelling strategies, denoting each particular strategy by a subscript q ($q = 1, 2, 3, \dots$). As a result, a double indexing of reference surfaces is applied, and each of them is denoted as R_{qk} , but defined by the vector \mathbf{x}_{qk} .

Alternatively, the reference surface R_{qk} can be considered in spherical coordinates and defined by the vector of discrete values of the polar radius $\mathbf{r}_{qk} = \{r_{qk1}, \dots, r_{qkp}, \dots\}$. By using Eq. (2.4), the reference surface R_{qk} can be related to discrete sets of the values of spherical angles φ_{qk} and θ_{qk} characterising sampling points as follows

$$\mathbf{r}_{qk}(\varphi_{qk}, \theta_{qk}) = \mathbf{S}_R(\varphi_{qk}, \theta_{qk}). \quad (2.5)$$

In many situations, the original surface may be not known explicitly, consequently, the coordinates of sampling points \mathbf{x}_{kp} or $r_{qkp}(\varphi_{qkp}, \theta_{qkp})$ of the reference surface are obtained on the basis of the available knowledge about discrete data. They may be extracted from real measurements, using the available computer imaging and data processing techniques for an arbitrary particle shape.

The *actual* surface, denoted hereafter by A , presents semi-analytical approximation of the original surfaces S , restricting to the description in spherical coordinates $A(\varphi, \theta) \approx S_R(\varphi, \theta)$, where the actual model A is presented by a truncated series containing the finite number M of terms. Here, each term $a_i f_i(\varphi, \theta)$ is the product of unknown coefficients a_i and analytically specified polynomials $f_i(\varphi, \theta)$, where $i = 1, 2, \dots, M$. The scalar product can be presented in the vector form:

$$A(\varphi, \theta) = \mathbf{f}(\varphi, \theta)^T \cdot \mathbf{a}. \quad (2.6)$$

Here, unknown coefficients form a vector $\mathbf{a} = \{a_1, \dots, a_2, \dots, a_M\}^T$, while polynomials $\mathbf{f}(\varphi, \theta)$ are formed in the same manner. The complexity level of approximation in Eq. (2.6) is defined by the number M_j of polynomials. Fixing hierarchically different values of M_j , different actual models $A_j(\varphi, \theta)$ with the different complexity, defined by the subscript j ($j = 1, \dots, L$), may be developed. Thus, the approximation error can be expressed in terms of difference between the original and actual surface

$$E_j(\varphi, \theta) = A_j(\varphi, \theta) - S_R(\varphi, \theta). \quad (2.7)$$

It is obvious that an increase of $j \rightarrow \infty$ reduces the approximation error up to zero and guarantees the convergence $E_{j=L, L < \infty}(\varphi, \theta) \rightarrow 0$. Each of the hierarchically developed actual surfaces A_j describes the original surface S on the basis of the discretely defined reference surfaces R_{qk} . A summary of the above discussion yields that each of the actual surfaces $A_{jqk}(\varphi, \theta) \equiv A_{jqk}(\mathbf{a}_{jqk}, \mathbf{f}_j(\varphi_{qk}, \theta_{qk}))$, apart from its complexity level j , involves the properties of reference model R_{qk} reflecting the modelling strategy q and the sampling model k . The evaluation procedure is implemented, however, by approximating the reference surfaces R_{qk} .

The universal semi-analytical modelling concept have been presented here. However, this work uses the spherical harmonics as the analytically specified polynomials $f_i(\varphi, \theta)$ in Eq. (2.6). Thus, the spherical harmonics expansion reads as

$$A(\varphi, \theta) \cong \sum_{l=0}^L \sum_{m=-l}^l a_l^m Y_l^m(\varphi, \theta), \quad (2.8)$$

where a_l^m are the unknown expansion coefficients and $Y_l^m(\varphi, \theta)$ – spherical harmonics.

The maximal order of the spherical harmonic expansion is usually defined by the integer parameter called the expansion degree L . It is obvious that the expansion degree L predefines the number of actual models j ($j = 1, 2, \dots, L$), while the total number of terms is defined as

$$M = \sum_{l=0}^L (2l + 1) = (L + 1)^2. \quad (2.9)$$

2.2. Modelling Strategies for the Particle Surface

In practical situations, the accuracy of a specified shape, described by spherical harmonics, depends not only on the complexity of expansion, but also even more on the suitability of the reference model. The issue on formation of the reference surface R_{qk} involves two steps: 2D positioning of sampling points defined by vectors φ_{qk} and θ_{qk} in the subspace φ - θ and calculation of surface points in the three-dimensional space $\mathbf{r}_{qk}(\theta_{qk}, \varphi_{qk})$ applying Eq. (2.4). The choice of a reference model may be considered as mathematical parameterization of a mesh representing the surface.

The problem, however, is not strictly mathematical, while the practical implementation of positioning comprises heuristic arguments, formulated in terms of an appropriate modelling strategy. Each of the strategies conditionally denoted by a subscript q stands for a heuristic rule how to construct a grid by generating a sequence of sampling points φ_{qk} and θ_{qk} with different sets k ($k = 1, 2, \dots, K$), where each new set of points $k + 1$ is obtained on the basis of the previous set k .

For practical implementation of the positioning, several strategies aimed to describe low-resolution harmonics are elaborated and tested numerically. They are characterised as follows:

- sequential refinement via a regularly sized grid;
- adaptive refinement via a variably sized grid;
- refinement using local correction;
- sampling of the Gauss integration points.

Each of the strategies is based on specified assumptions. The grid-based strategies employ a concept of grid that covers a modelling sub-domain dividing it into cells, while the sampling points are embedded into nodes of the grid. By applying the sequential refinement strategy, a finer grid is formed by a regular sub-division of grid cells. The strategy offers a relatively simple method, however, the discussion presented in Mouse *et al.* (2008) points out the difficulties to predict the size of a cell that satisfies the given tolerance.

An adaptive refinement strategy forms an irregularly shaped family of grids, where the size of cells varies according to the specified rules. The character of surface should be taken into account and the size of the grid cells is adapted to match the variation of the surface.

The Gaussian point strategy is applied to generate a surface using the Gaussian integration points as sampling points. In general, the Gaussian points present a part of the numerical Gaussian quadrature integration method. The practical application

of this technique in the particle shape analysis is reported by Garboczi (2002), however, it is limited to a relatively high order quadrature with a large number up to 120 points.

As four strategies is used for the surface description, they are denoted by subscript q . Using the equiangular refining strategy ($q = 1$), the angular subdomain is covered by the regular polar-shaped grid containing $n_\varphi \times n_\theta$ cells and $(n_\varphi + 1) \times n_\theta + 1$ nodes, where only variation of n_θ is allowed. Four schemes for specification of sampling points were studied within this strategy. The first simplest scheme denoted by subscript k ($k = 1$) contains 4×16 cells, where the grid is specified by 69 nodes. The remaining three schemes ($k = 2, 3, 4$) are generated by splitting cells into azimuthal direction. As a result, 8×16 grid with 137 nodes, 16×16 grid with 273 nodes and 32×16 grid with 545 nodes were generated, respectively. Finally, the size of grid cell is defined by constant value of polar angle, $\Delta\varphi = \pi/2n_\varphi = 0.0985\pi$ and by variable azimuthal angle, $\Delta\theta = \pi/2n_\theta$, respectively.

The second strategy ($q = 2$) is regular equidistance refining strategy supported with four sequential schemes containing the data structure of previous sample. It presumes regular equidistance subdivision with constant cell size $\Delta l = (a+c)/n_\varphi$ yielding, however, variable angular size $\Delta\theta$.

The next strategy $q = 3$ is selected to illustrates technique where the global adaptive refining is combined with the local refinement. The last strategy $q = 4$ presents the Gauss points strategy.

In regard of particular applications, additional simplifications compatible with the above strategies can be introduced. Therefore, positioning of points in two polar and azimuthal directions may be performed independently of each other. For axi-symmetric surfaces, only one-dimensional radially oriented positioning is sufficient.

2.3. Spherical Harmonics

Spherical harmonics are solution of the Laplace's equation forming an orthogonal system. These functions were first introduced in 1782 by P. S. Laplace (Laplace and Bowditch 1829).

The term "spherical harmonics" for these functions first was introduced by Thomson and Tait (1867) in their book "Treatise on Natural Philosophy" in 1867. Here, the definition of spherical harmonics is given as

“A *spherical harmonic function* is defined as a homogeneous function, V , of x, y, z , which satisfies the equation

$$\frac{d^2V}{dx^2} + \frac{d^2V}{dy^2} + \frac{d^2V}{dz^2} = 0. \quad (2.10)$$

Its degree may be any positive or negative integer; or it may be fractional; or it may be imaginary” (Thomson and Tait 1867).

Spherical harmonic expansions are a widely used and well-understood tool of applied mathematics. They are encountered in weather and climate modelling, in the representation of gravitational, topographic, and magnetic data in geophysics, in the numerical solution of certain partial differential equations (Rokhlin and Tygert 2006).

As mentioned above, spherical harmonics are solution of the Laplace’s equation. The Laplace’s equation given in Eq. (2.10) is in Cartesian coordinates. Given relations between Cartesian and spherical coordinates (Eq. (2.1) and Eq.(2.2)) Laplace’s equation is transformed into equation in spherical coordinates as

$$\nabla^2 f = \frac{1}{r^2} \frac{\partial}{\partial r} \left(r^2 \frac{\partial f}{\partial r} \right) + \frac{1}{r^2 \sin \theta} \frac{\partial}{\partial \theta} \left(\sin \theta \frac{\partial f}{\partial \theta} \right) + \frac{1}{r^2 \sin^2 \theta} \frac{\partial^2 f}{\partial \varphi^2} = 0. \quad (2.11)$$

The equation in Eq. (2.11) is solved by separating the variables and the solution is spherical harmonics.

Spherical harmonics $Y_l^m(\theta, \varphi)$ are single-valued, smooth, i. e. infinitely differentiable, complex functions of two variables θ and φ , indexed by two integers l and m (Morris *et al.* 2005).

Spherical harmonic basis functions $Y_l^m(\theta, \varphi)$ are defined as

$$Y_l^m(\theta, \varphi) = N_l^{|m|} P_l^{|m|}(\cos \theta) e^{im\varphi}, \quad (2.12)$$

where $N_l^{|m|}$ is the normalization factor and $P_l^{|m|}(\cos \theta)$ is the associated Legendre polynomial (Razzaghi *et al.* 2013).

Spherical harmonic functions $\{Y_l^m(\theta, \varphi) : |m| \leq l \in N_0\}$ are formed on the unit sphere S^2 with two parameters (θ, φ) in spherical coordinates. Although spherical harmonics are defined as complex functions, most applications use the real valued functions. Using Euler’s formula the exponent $e^{im\varphi}$ in Eq. (2.12) is expanded into sine and cosine. Thus, the real valued spherical harmonics are

$$Y_l^m(\theta, \varphi) = \begin{cases} \sqrt{2} N_l^m \cos(m\phi) P_l^m(\cos \varphi), & \text{when } m > 0, \\ N_l^0 P_l^0(\cos \varphi), & \text{when } m = 0, \\ \sqrt{2} N_l^{|m|} \sin(|m|\varphi) P_l^{|m|}(\cos \varphi), & \text{when } m < 0, \end{cases} \quad (2.13)$$

here: the subscript $l \in N_0$ indicates the expansion degree, the superscript $-l \leq m \leq l$ indicates the order of spherical harmonics, N_l^m and $P_l^m(\cos \varphi)$ – the normalization factor and the associated Legendre polynomial, respectively.

The normalization factor can be derived from the orthonormal feature of spherical harmonics

$$\int_0^{2\pi} \int_0^\pi Y_l^m(\omega) \overline{Y_{l'}^{m'}}(\omega) \sin \theta d\varphi d\theta = \delta_{mm'} \delta_{ll'}, \quad (2.14)$$

and then normalization factor is

$$N_l^m = \sqrt{\frac{2l+1}{4\pi} \frac{(l-m)!}{(l+m)!}}. \quad (2.15)$$

Spherical harmonic definition uses the associated Legendre polynomials $P_l^m(x)$. These functions are real and defined on the interval $[-1, 1]$. The associated Legendre polynomials are given as

$$P_l^m(x) = \frac{(-1)^m}{2^l l!} (1-x^2)^{\frac{m}{2}} \frac{d^{l+m}}{dx^{l+m}} (x^2-1)^l. \quad (2.16)$$

The formula in Eq. (2.16) can be complicated and expensive for calculation, so associated Legendre polynomials can be expressed using some recurrence relations. The algorithm using recurrence relations is given below:

- compute $P_l^0(x) = P_l(x)$ using

$$\begin{aligned} P_0 &= 1, \\ P_1 &= x, \\ (l+1)P_{l+1} &= (2l+1)xP_l - lP_{l-1}; \end{aligned}$$

- then calculate $P_m^m(x) = \frac{(2m)!}{2^m m!} (1-x^2)^{m/2}$;
- for $i = m$ use the formula $P_{m+1}^m(x) = (2m+1)xP_m^m(x)$;
- from $i = m+1$ to $i+1 = k$ calculate using $(i-m+1)P_{i+1}^m(x) = (2i+1)P_i^m(x) - (i+m)P_{i-1}^m(x)$.

The normalization factor is calculated easily, only inserting the values of the indices into Eq. (2.15). The final form of spherical harmonics is derived combining all required terms into Eq. (2.13). The expressions of spherical harmonics till degree $L = 3$ are given in Table A.1 and their 3D views – in Table A.2 in Annex A.

2.4. Calculation of Coefficients

Development of the polynomial expressions in Eq. (2.6) in terms of spherical harmonics is a computational procedure where the calculation of real coefficients a_l^m is required, but different methodologies can be applied. Theoretically, the coefficients of the expansion present integral obtained over the curved shape, and various numerical integrations are used. Calculations using the Gaussian quadrature formula are discussed in Garboczi (2002) and discrete Fourier transformations are considered in Feinauer *et al.* (2015). The above techniques do not depend on particular shapes and local effects are not distinguished. Another approach was used by Mouse *et al.* (2008). Here, the surface integrals were transformed into boundary integrals, and the Monte Carlo integration over the edges was applied. Further, a fast spectral surface reconstruction from point clouds and local surface smoothing was also demonstrated.

The least square method is used for the evaluation of polynomial coefficients, where the error E between the original surface $S_R(\varphi_i, \theta_i)$ and reference surface described by spherical harmonics is being minimized:

$$E = \min_{a_l^m} \left(\sum_{i=1}^n \left(S_R(\varphi_i, \theta_i) - \sum_{l=0}^N \sum_{m=-l}^l a_l^m Y_l^m(\varphi_i, \theta_i) \right)^2 \right). \quad (2.17)$$

Regarding the expression in Eq. (2.8) with respect to Eqs. (2.9), (2.13) and (2.15), Eq. (2.17) may be written as a linear matrix equation. Considering an arbitrarily specified reference model R_{qk} , defined by fixed values of the sampling points φ_{qk} and θ_{qk} , the linear equation reads as follows:

$$[\mathbf{Y}_j(\varphi_{qk}, \theta_{qk})] \mathbf{a}_{jqk} = \mathbf{r}_{qk}(\varphi_{qk}, \theta_{qk}). \quad (2.18)$$

Here, $[\mathbf{Y}_j]$ stands for a rectangular transformation matrix, relating unknown coefficients \mathbf{a}_{jqk} with the discrete values $\mathbf{r}_{qk}(\varphi_{qk}, \theta_{qk})$ of the original surface \mathbf{S}_R , defined at the sampling points of the reference model.

The number of columns M of the transformation matrix is predefined by the expansion degree L , which is obtained according to Eq. (2.9). The number of rows N is equal to the number of sampling points. In general, the number of sampling surface points $N > M$ is large enough to meet the required precision. Generation of this matrix is rather a routine task, because each column i of the matrix, corresponding to the specified harmonic term, is fulfilled by the values of harmonic functions Y_l^m for the whole range of sampling points. This evaluation technique has been recently demonstrated by Zhou *et al.* (2015).

Mathematical aspects of the approximation problem in Eq. (2.18) and solution properties are discussed by Courrieu (2008). Using the matrix algebra, a solution is obtained by rather a standard pseudo-inversion procedure

$$\mathbf{a}_{jqk} = [\mathbf{Y}_{jqk}]^+ S_{R,qk}(\varphi_{qk}, \theta_{qk}). \quad (2.19)$$

Here, a pseudo-inverse matrix is formally defined by the expression

$$[\mathbf{Y}_{jqk}]^+ = [\mathbf{Y}_{jqk}]^T ([\mathbf{Y}_{jqk}][\mathbf{Y}_{jqk}]^T)^{-1}. \quad (2.20)$$

Whenever the rank is lower, the solution of the above problem is non-unique. Consequently, Eq. (2.18) yields a non-unique set of coefficients. In this case, the generalised Moore-Penrose pseudo-inversion approach is applied further in the evaluation of a unique set of coefficients. Application of the Moore-Penrose inverse has another advantage – it avoids catastrophic numerical results that can result from ill-conditioning because of unsuccessful positioning of sampling points in the reference model, and reduces approximation errors itself. It is obvious that a unique solution by inverting the matrix $[\mathbf{Y}_{jqk}] = [\mathbf{Y}_j(\varphi_{qk}, \theta_{qk})]$ is available for the exceptional case, where the rank of matrix $[\mathbf{Y}_{jqk}]$ is equal to M .

It could be mathematically shown, see Courrieu (2008), that the pseudo-inversion in Eq. (2.19) is equivalent to the least-square approximation. The quality of approximation could be estimated by the least-square error norm.

2.5. Calculation of Integral Parameters

Various particle parameters and descriptors can be used for characterizing the particle shape as well as comparing differently approximated models. Deviation of the actual surface from the original shape is a natural descriptor. When applying spherical coordinates, such a descriptor $D(\varphi, \theta)$ is identified with a continuous

error $E(\varphi, \theta)$ between the original and actual surface, evaluated by Eq. (2.7), and varies over the entire particle surface area.

Since a discrete approach prevails in the framework of this approach, the above descriptor also needs to be formulated in a discrete form. Any descriptor strongly depends on the discretisation of the surface, and different reference models with different sampling points are involved in the characterisation of shape. The main weakness of the arbitrarily discrete error descriptor is that minimises errors at sampling points, while the in-between error is not controlled. For increasing robustness of descriptors, the reference threshold model, denoted hereafter by the abbreviation *thr*, is introduced. It is defined by a dense grid the number of sampling points N_{thr} of which is substantially larger as compared to that of reference models used for approximation purposes, and locations of these points are different. Consequently, the discrete descriptors are defined with respect to the reference threshold. As a result, deviation of the actual surface from the original one described in Eq. (2.18), is estimated by deviations at each point P from the reference threshold. An arbitrarily actual surface is characterised by a discrete descriptor calculated with respect to the reference threshold

$$\mathbf{D}_{jqk}(\varphi_{thr}, \theta_{thr}) = [\mathbf{Y}_j(\varphi_{thr}, \theta_{thr})] \mathbf{a}_{jqk} - \mathbf{r}_{qk}(\varphi_{thr}, \theta_{thr}). \quad (2.21)$$

Characterisation of the actual model, obtained using a specified discrete set, is performed further in terms of scalar quantities, Euclidean and maximal, error norms. The Euclidean norm is applied in evaluating the suitability of the model over the entire domain:

$$\|\mathbf{D}_{jqk}\|^2 = \left(\sum_{p=1}^{N_{thr}} D_{jqk}(\varphi_{thr}, \theta_{thr})^2 \right)^{1/2}. \quad (2.22)$$

A more sophisticated normalized least-square error norm of surface weighting was used in (Feinauer *et al.* 2015).

The maximum error norm $\|\mathbf{D}_{jqk}\|^\infty$ characterises the local deviations

$$\|\mathbf{D}_{jqk}\|^\infty = \max_{p=1, N_{qk}} D_{jqk}(\varphi_{thr}, \theta_{thr}). \quad (2.23)$$

In the case of Cartesian coordinates, three separate descriptors, standing for deviations of the coordinates x , y , z , can be explored, see (Zhou *et al.* 2015).

The global quality is evaluated by Euclidian error norm. The expression in Eq. (2.22) is normalised by R as follows

$$\|\bar{E}_{jqk}\|^2 = \frac{1}{R} \left(\sum_{p=1}^{N_{thr}} D_{jqkp}(\varphi_{thr,p}, \theta_{thr,p})^2 \right)^{1/2}, \quad (2.24)$$

$$\|\bar{E}_{jqk}\|_{max} = \max_{p=1, N_{thr}} \frac{1}{R} D_{jqkp}(\varphi_{thr,p}, \theta_{thr,p}), \quad (2.25)$$

$$\|\bar{E}_{jqk}\|_{min} = \min_{p=1, N_{thr}} \frac{1}{R} (-D_{jqkp}(\varphi_{thr,p}, \theta_{thr,p})). \quad (2.26)$$

The choice of two local criteria is motivated later showing that the sign of the local deviation has some physical meaning leading to different particles properties.

Another category of descriptors may have clear physical or geometric interpretation. The surface area S and the volume of particle V are the mostly applied integral quantities. Theoretically, the surface area of the particle is considered in spherical coordinates by integrating the surface over the entire angular subdomain. The projection of differential curved surface element dS in spherical coordinates is expressed as $dS = g_s(\varphi, \theta)d\theta d\varphi$. Here, projection factor g_s contains components of metric tensor. It is explicitly expressed in terms of surface $S_R(\theta, \varphi)$ as modulus of vector product of surface derivatives, see Garboczi (2002); Zhou *et al.* (2015).

The surface area of the particle is given as

$$S = \int_0^{2\pi} \int_0^\pi A (A_\varphi^2 + A_\theta^2 \sin^2 \theta + A^2 \sin^2 \theta)^{1/2} d\theta d\varphi, \quad (2.27)$$

where A is the expansion of spherical harmonics, A_φ and A_θ is the derivatives of function $A(\theta, \varphi)$ according to angles φ or θ , respectively.

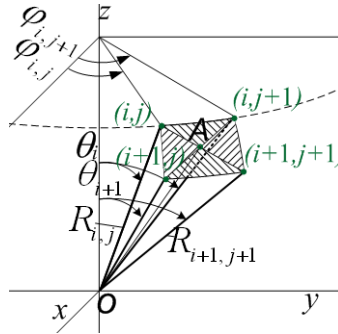


Fig. 2.2. The scheme for the numerical integration

Numerical integration procedure was developed for calculation of the surface integral Eq. (2.27) and it was utilised on the basis of the reference model where polar cells are formed by polar grid. Cell between polar lines i and $i+1$ and azimuthal lines j and $j+1$ is defined by four nodes $\{(i, j), (i+1, j), (i, j+1), (i+1, j+1)\}$. Splitting cell into the patch of four triangles, the surface is replaced by assembly of triangles, while the surface integral by summation of all triangles (Fig. 2.2). It should be remarked, that the first cell closed to pole is naturally triangle.

The patch geometry is defined by the geometry of grid, however, the fifth point as internal point A has to be introduced. It is located in the center of the grid cell, while its radius R_A is calculated as the average of the four radii of main points

$$R_A = \frac{R_{i,j} + R_{i+1,j} + R_{i,j+1} + R_{i+1,j+1}}{4}. \quad (2.28)$$

As the cell is split into the patch of four triangles, the area of each triangle is calculated separately. The area of the whole cell is calculated as the sum of areas of four triangles

$$S_i = \sum_{j=1}^4 S_{trik,j}. \quad (2.29)$$

As a result, each triangle is described by three local nodal points 1, 2 and 3, respectively, and it is defined by three polar radii. Transforming nodal points into Cartesian space, the polar triangle is transformed to arbitrary oriented space triangle, geometry of which is defined by three vectors of three vertices point coordinates, which are given by vectors $\mathbf{x}_1 = \{x_1, y_1, z_1\}^T$, $\mathbf{x}_2 = \{x_2, y_2, z_2\}^T$ and $\mathbf{x}_3 = \{x_3, y_3, z_3\}^T$. The area of this triangle embedded in three-dimensional Cartesian space is expressed as modulus of vector product

$$S_{tr} = \frac{1}{2} \|(\mathbf{x}_3 - \mathbf{x}_1) \times (\mathbf{x}_2 - \mathbf{x}_1)\|, \quad (2.30)$$

which may be interpreted as approximation of Eq. (2.27). Using linear algebra, calculation of the 3D triangle area is transformed to this expression

$$S_{tr} = \frac{1}{2} \sqrt{\det(M_1)^2 + \det(M_2)^2 + \det(M_3)^2}, \quad (2.31)$$

where

$$\begin{aligned} \det(M_1) &= \begin{vmatrix} x_2 & x_3 & 1 \\ y_2 & y_3 & 1 \\ z_2 & z_3 & 1 \end{vmatrix}, \det(M_2) = \begin{vmatrix} x_3 & x_1 & 1 \\ y_3 & y_1 & 1 \\ z_3 & z_1 & 1 \end{vmatrix}, \\ \det(M_3) &= \begin{vmatrix} x_1 & x_2 & 1 \\ y_1 & y_2 & 1 \\ z_1 & z_2 & 1 \end{vmatrix}. \end{aligned} \quad (2.32)$$

The surface area of whole particle is equal to the sum of all area of every cell on the surface

$$S_w = \sum_i S_i. \quad (2.33)$$

Calculation of the volume follows the same path. The equation for the volume in polar coordinates is given by integral taken over elementary surface which is expressed as triple mixed product

$$V = \frac{1}{3} \int_0^{2\pi} \int_0^\pi A^3 \sin \theta d\theta d\varphi. \quad (2.34)$$

As the triangles are already formed, calculation of the entire volume for the whole body is equal to the sum of all volumes of pyramids:

$$V_i = \frac{1}{3} \sum_{j=1}^4 h_j S_{tr,j}. \quad (2.35)$$

As the area of triangles as pyramid base has been already calculated the altitude of the pyramid is needed. It is calculated according to

$$h = \frac{|D|}{\sqrt{A^2 + B^2 + C^2}}, \quad (2.36)$$

where D is the determinant of the matrix formed by coordinates of all triangle vertices, coefficients A , B and C is calculated as

$$A = \det(M_1), B = -\det(M_2), C = \det(M_3). \quad (2.37)$$

The volume of the whole particle is the sum of volumes of all pyramids

$$V = \sum_i V_i. \quad (2.38)$$

The moments of inertia also can be calculated as the integral. The expressions given in Garboczi (2002) is

$$I_{11} = \frac{m}{5V} \int_0^{2\pi} \int_0^{\pi} r^5 \sin \theta (1 - \sin^2 \theta \cos^2 \varphi) d\theta d\varphi, \quad (2.39)$$

$$I_{22} = \frac{m}{5V} \int_0^{2\pi} \int_0^{\pi} r^5 \sin \theta (1 - \sin^2 \theta \sin^2 \varphi) d\theta d\varphi, \quad (2.40)$$

$$I_{33} = \frac{m}{5V} \int_0^{2\pi} \int_0^{\pi} r^5 \sin^3 \theta d\theta d\varphi. \quad (2.41)$$

Here can be used the same scheme of numerical integration as discussed for the cases of surface area and volume.

2.6. Calculation of Curvature

The use of continuous representation functions, or simply continuous representation, of particle surface is the most promising way to implement spherical harmonics model into discrete element method. It will be shown below that the full description of the surface was not limited to only a merely point-by-point description but also to a characterisation of gradients, principal directions, curvatures, and so on, expressed in surface derivatives.

Important characteristics of particle geometry contributing particles contact are particle curvatures. A general method for obtaining expressions for curvatures in terms of surface derivatives is provided in differential geometry while detailed description of curvature expressions for ellipsoid is given by Harris (2006) and Poelaert *et al.* (2011).

As spherical harmonics are smooth functions they can be differentiated analytically. Therefore, a mathematically consistent description involves not surface values but also their derivatives. The description of the sequence of an entire process using spherical harmonics is given in studies by Feinauer *et al.* (2015); Garboczi (2002).

The main difficulty is that spherical harmonics approximations of particle surfaces are described in spherical coordinates and particle surface $F(x, y, z)$ in discrete element method has to be described using Cartesian coordinates. Normally, a spherical harmonics approximation $A(\theta, \phi)$ as presented in Eq. (2.8) is

given as a function in spherical coordinates, here $A(\theta, \phi)$ means the radius of the modelled surface, therefore $A(\theta, \phi) \equiv R(\theta, \phi)$. Knowing the relation between the Cartesian and spherical coordinates, $R(\theta, \phi)$ can be easily converted into Cartesian coordinates giving the vector of parametric functions of the surface $\mathbf{X}(\theta, \phi) \equiv \{x(\theta, \phi), y(\theta, \phi), z(\theta, \phi)\}^T$:

$$\mathbf{X} = \begin{bmatrix} x \\ y \\ z \end{bmatrix} = \begin{bmatrix} \sum_{l=0}^N \sum_{m=-l}^l a_l^m Y_l^m(\theta, \phi) \cos \phi \sin \theta \\ \sum_{l=0}^N \sum_{m=-l}^l a_l^m Y_l^m(\theta, \phi) \sin \phi \sin \theta \\ \sum_{l=0}^N \sum_{m=-l}^l a_l^m Y_l^m(\theta, \phi) \cos \theta \end{bmatrix}. \quad (2.42)$$

First and second order surface derivatives can be expressed explicitly as

$$\mathbf{X}_\theta = \frac{\partial \mathbf{X}(\theta, \phi)}{\partial \theta}, \mathbf{X}_\phi = \frac{\partial \mathbf{X}(\theta, \phi)}{\partial \phi} \quad (2.43)$$

and

$$\mathbf{X}_{\theta\theta} = \frac{\partial^2 \mathbf{X}(\theta, \phi)}{\partial \theta^2}, \mathbf{X}_{\theta\phi} = \frac{\partial^2 \mathbf{X}(\theta, \phi)}{\partial \theta \partial \phi}, \mathbf{X}_{\phi\phi} = \frac{\partial^2 \mathbf{X}(\theta, \phi)}{\partial \phi^2}, \quad (2.44)$$

then the normal to the surface is calculated using linear algebra as vector product:

$$n = \frac{\mathbf{X}_\theta \times \mathbf{X}_\phi}{|\mathbf{X}_\theta \times \mathbf{X}_\phi|}. \quad (2.45)$$

Canonical surface constants are expressed as

$$\begin{aligned} E &= \mathbf{X}_\theta \times \mathbf{X}_\theta, L = \mathbf{X}_{\theta\theta} \times n, \\ F &= \mathbf{X}_\theta \times \mathbf{X}_\phi, M = \mathbf{X}_{\theta\phi} \times n, \\ G &= \mathbf{X}_\phi \times \mathbf{X}_\phi, N = \mathbf{X}_{\phi\phi} \times n, \end{aligned} \quad (2.46)$$

and the mean curvature H – as

$$H = H(\theta, \phi) = \frac{EN + GL - 2FM}{2(EG - F^2)}. \quad (2.47)$$

It should be noticed that the above presented approach reflects only a formal side of the continuous representation. Also it is useful to mention that the contact evaluation is the most time consuming algorithmic step. Omitting conceptual discussion on detection of contact point for non-spherical particles, which was comprehensively described in the review papers of Lu *et al.* (2015) and Zhong *et al.* (2016), calculating of the contact forces will be discussed.

Analytical treatment of normal contacts for continuous solid contact partners i and j is based on the elastic contact theory of Hertz (Johnson 1987). The state of the contact behaviour between ellipsoidal particles is reviewed and discussed by Zheng *et al.* (2013). It was stated that regardless of the specific particle shape, two particles loaded in the normal direction touch and deform each other over an elliptical area. Consequently, considering of contacts between non-spherical particles, the normal contact force can be expressed by modifying the conventional Hertz force $F_{ijHn} = F_{Hn}$ which is related to the inter-particle overlap or displacement u as follows

$$F_{Hn} = \frac{4}{3} c_{cor}(\rho_{i1}, \rho_{i2}, \rho_{j1}, \rho_{j2}) E_{eff} \sqrt{\rho_{eff}} u^{3/2}. \quad (2.48)$$

Here, the effective elastic modulus is expressed in terms of Poisson's ratios ν_i and ν_j and elasticity moduli E_i and E_j of contacting partners by relation

$$\frac{1}{E_{eff}} = \frac{(1 - \nu_i^2)}{E_i} + \frac{(1 - \nu_j^2)}{E_j}. \quad (2.49)$$

Both of two other parameters – the effective radius of curvature

$$\rho_{eff}(\rho_{i1}, \rho_{i2}, \rho_{j1}, \rho_{j2}) = \sqrt{A(\rho_{i1}, \rho_{i2}, \rho_{j1}, \rho_{j2}) \cdot B(\rho_{i1}, \rho_{i2}, \rho_{j1}, \rho_{j2})/2} \quad (2.50)$$

and non-dimensional correction factor

$$c_{cor}(\rho_{i1}, \rho_{i2}, \rho_{j1}, \rho_{j2}) = \left(1 - \left[\left(\frac{B(\rho_{i1}, \rho_{i2}, \rho_{j1}, \rho_{j2})}{A(\rho_{i1}, \rho_{i2}, \rho_{j1}, \rho_{j2})} \right)^{0.0684} - 1 \right]^{1.531} \right)^{-\frac{3}{2}}, \quad (2.51)$$

where A and B are new variables determined from the local geometry.

Positive values of parameters variables A and B are determined by solving set of coupled equations (Johnson 1987):

$$\begin{cases} A + B = \frac{1}{2} \left(\frac{1}{\rho_{i1}} + \frac{1}{\rho_{i2}} + \frac{1}{\rho_{j1}} + \frac{1}{\rho_{j2}} \right) \\ B - A = \frac{1}{2} \left\{ \left(\frac{1}{\rho_{i1}} - \frac{1}{\rho_{i2}} \right)^2 + \left(\frac{1}{\rho_{j1}} - \frac{1}{\rho_{j2}} \right)^2 \right. \\ \quad \left. + 2 \left(\frac{1}{\rho_{i1}} - \frac{1}{\rho_{i2}} \right) \left(\frac{1}{\rho_{j1}} - \frac{1}{\rho_{j2}} \cos 2\alpha \right) \right\}^{1/2} \end{cases} \quad (2.52)$$

where α is inclination angle between principal axis of two bodies.

2.7. Conclusions of Chapter 2

1. The modelling concept presented in this chapter is universal. The initial data required for the modelling is the sampling points describing the surface of a particle. These points can be in Cartesian or in spherical coordinates. The known relation between Cartesian and spherical coordinates allows easily to switch from one to other systems and vice versa.
2. The semi-analytical model of a particle shape is created using the spherical harmonics. The aim is to be able to model the simplest symmetric particles. A characteristic exclusiveness of this model is the least squares method and pseudo-inverse matrix procedure used for the determination of the coefficients.
3. To evaluate the quality of developed spherical harmonics expansion various positioning strategies of the sampling points were suggested and tested numerically. As well as various descriptors of the shape was calculated to determine the approximation quality. The integration technique was applied for evaluation of the most important integral characteristics such as particle volume, surface area and inertia moments. Calculation of the second order derivatives is applied for curvature radii required in calculation of contacts.

Spherical Harmonics Application to Simple Particles

This chapter presents the modelling results. The chosen standard, but non-spherical shapes (ellipsoid, cylinder and rectangular parallelepiped) suits the best for testing the suitability of the low-resolution spherical harmonics. Not only these shapes were modelled using different expansion degree, but the effect of positioning the sampling points was also investigated. These spherical harmonics models were also used in the calculation of the curvature.

Parts of this chapter are published in Radvilaitė (2014), Radvilaitė *et al.* (2015) and Radvilaitė *et al.* (2017).

3.1. Modelling of Ellipsoid Particle

This section presents the modelling results for the ellipsoid. It is divided into several subsections: firstly, the original shape is presented, then the modelling results are shown and at last, some conclusions are made.

3.1.1. Description of the Ellipsoidal Surface

The ellipsoid of revolution is the most simple but the most studied non-spherical analytical shape considered in framework of discrete element method (Johnson and Williams 2009; Ouadfel and Rothenburg 1999; Wellmann *et al.* 2008; Zheng

et al. 2013). Illustration of ellipsoid may be motivated because of methodological reasons. Ellipsoid of revolution is classified to specific category of axi-symmetric shapes (Fig. 3.1) having smooth surface. The surface for an ellipsoid is centered in the origin of Cartesian frame. Symmetry axis of the ellipsoid is aligned with Cartesian axis Oz . Ellipsoid is formed by rotating a plane elliptical curve around the central axis. Due to rotationally symmetry, circular cross-section of the ellipsoid is characterised by a single size parameter a , semi-principal axes, since perpendicular semi-axes $b = a$. A bounding box of the ellipsoid's geometry is defined by two parameters, $2a$ and $2c$, where c stands for the length of semi-axis.

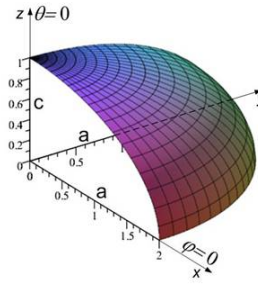


Fig. 3.1. The shape of an ellipsoid when $c = 1$ and $a = 2$

An ellipsoid is defined by a general continuous smooth function $S_{ell}(x, y, z)$, Eq. (E1). In spherical coordinates the ellipsoid is described by one-dimensional function $S_{R,ell}(\varphi, \theta) \equiv S_{R,ell}(\theta)$ (Eq. (E2)), see Garboczi (2002). The volume V_{ell} is defined by simple formula Eq. (E3), while the surface area S_{ell} by Eq. (E4) under condition that relation $c/a < 1$, see Ritchie and Kemp (1999). On the other hand, ellipsoid is the most suitable sample to illustrate performance of spherical harmonics. Various aspects of spherical harmonics approximation are shown by Garboczi (2002); Ritchie and Kemp (1999).

3.1.2. Modelling of the Ellipsoid

Detailed comparison of all the qk reference models are selected in Table 3.1. Results obtained by applying the threshold model are also presented for the sake of comparison. The threshold model for ellipsoid was obtained by generation of a regular rectangular grid along z axis. Fig. 3.2 presents the positioning of the points when the scheme contains 8×16 cells. The evaluation is made considering the division using $N_\theta = 128$ and $N_\varphi = 128$. The total number of the points in the threshold model is calculated as $N = (N_\theta - 1) \cdot N_\varphi + 2 = 16258$.

The global quality of spherical harmonics approximation is essentially evaluated by the normalized Euclidean norm $\|E_{jgk}\|^2$ obtained by Eq. (2.24). The relative deviations $\delta_{LS,jgk}$ are obtained with respect to threshold error value $\|E_{thr}\|^2 = 3.9519$. Additionally, the values of average deviations, calculated as $\|E_{jgk}\|_{av} = \|E_{jgk}\|^2 / N_{thr}$, are given in order to evaluate approximation magnitude.

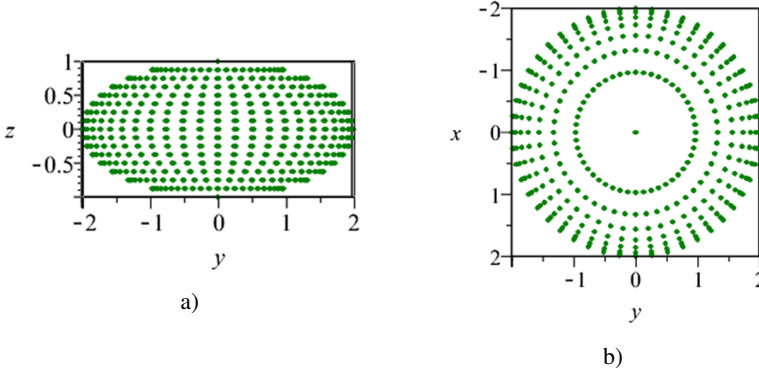


Fig. 3.2. The threshold model of the ellipsoid: a) zy plane; b) xy plane

To grasp the entire view, the three-dimensional images of particle surface $S_R(\theta, \varphi)$ are presented graphically in Fig. 3.3 as contour plots over two-dimensional angular $\theta - \varphi$ domain. Here, the exact surface is shown in Fig. 3.3a, the model of the spherical harmonics model obtained by the strategy $q = 2$ is shown in Fig. 3.3b, where small, visually hardly detectable deviations of these lines on $\varphi = 0$ indicate numerical errors. Detailed map of deviations corresponding to definition of descriptor Eq. (2.21) is presented in Fig. 3.3c.

3.1.3. Analysis of the Ellipsoid Results

The given results in Table 3.1 show that spherical harmonics expansion degree $L = 1$ is sufficient to describe the ellipsoid accurately. As each strategy was applied for the same four reference models, the best model can be determined for each strategy and overall the best approximation.

For the first strategy $q = 1$ the best reference model according to the smallest least square error is the third model $k = 3$. Here, the error is equal to 10.7% while the surface area and volume differs from the analytical value by 1.5% and 0.4%, respectively. Determining the best reference model comparing the deviation of the surface area for each model the better one would be $k = 2$ where the error is 3 times smaller than of the model $k = 3$. The deviation of the volume has the tendency to decrease for each reference model.

Table 3.1. Results of spherical harmonics description of the ellipsoid when expansion degree is $L = 1$

Strat.	Refer. model	Grid cells	Points number	LS error		Average deviation	Max. error	Surface area		Volume	
q	k	$n_\theta \times n_\varphi$	N_k	$\ \bar{E}_{jqk}\ ^2$	$\delta_{LS,jgk}$	$\ E_{jqk}\ _{av}$	$\ \bar{E}_{jqk}\ _{max}$	S_{jqk}	δ_S	V_{jqk}	δ_V
1	1	4×16	69	8.9520	1.2652	0.000551	0.00617	33.950	0.0222	16.076	0.0405
	2	8×16	137	4.6410	0.1744	0.000286	0.00602	34.894	0.0050	16.536	0.0131
	3	16×16	273	4.3758	0.1075	0.000269	0.01000	35.235	0.0148	16.685	0.0042
	4	32×16	545	4.4152	0.1724	0.000272	0.01123	35.329	0.0175	16.725	0.0018
2	1	4×16	69	6.1600	0.5587	0.000379	0.00520	34.398	0.0093	16.304	0.0027
	2	8×16	137	4.1670	0.0545	0.000256	0.00617	35.046	0.0094	16.624	0.0078
	3	16×16	273	4.1740	0.0562	0.000256	0.00931	35.267	0.0157	16.717	0.0023
	4	32×16	545	4.2348	0.0716	0.000261	0.01030	35.327	0.0175	16.741	0.0008
3	1	4×16	69	4.8220	0.2202	0.000297	0.00787	34.775	0.0016	16.464	0.0174
	2	8×16	137	3.9419	0.0025	0.000243	0.00633	35.125	0.0116	16.669	0.0051
	3	16×16	273	3.9210	0.0078	0.000241	0.00639	35.175	0.0131	16.714	0.0025
	4	32×16	545	3.9910	0.0099	0.000246	0.00623	35.166	0.0128	16.729	0.0016
4	1	4×16	69	7.3001	0.8472	0.000449	0.00377	34.230	0.0141	16.213	0.0323
	2	8×16	137	7.3027	0.8479	0.000449	0.00366	34.279	0.0127	16.274	0.0287
	3	16×16	273	6.5234	0.6507	0.000401	0.00343	34.432	0.0083	16.342	0.0246
	4	32×16	545	6.0505	0.5309	0.000372	0.00349	34.537	0.0053	16.388	0.0219
Threshold model				3.9519			Analytical	34.721		16.755	

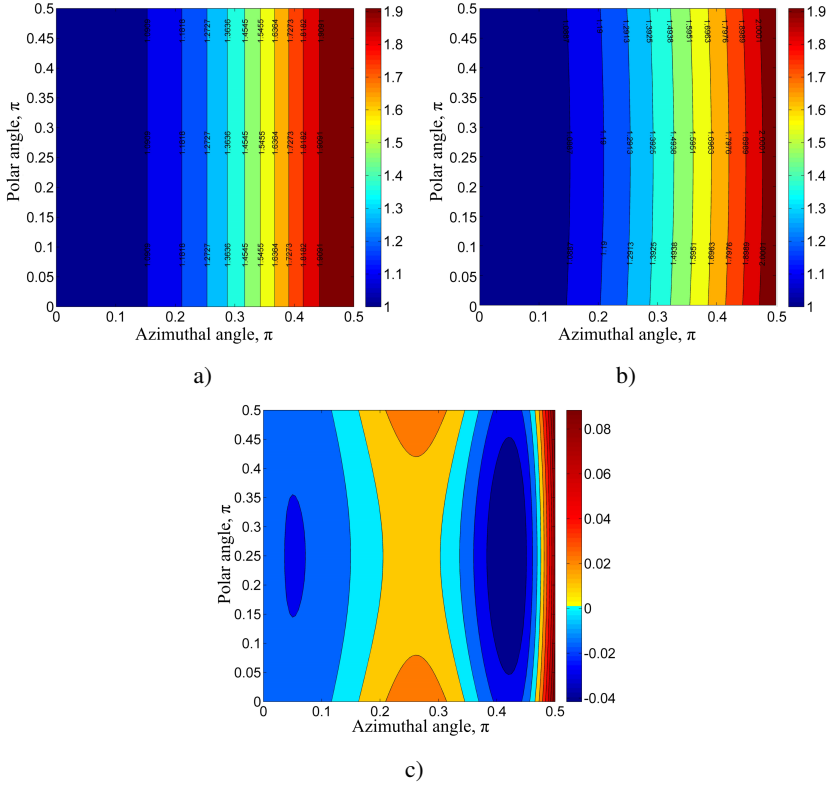


Fig. 3.3. Contour plots of the surface: a) exact analytical surface of the ellipsoid (Eq. (E2)); b) spherical harmonics approximation ($L = 2$); c) difference D_2 between the exact and approximated surface. The color bar above the figure a) and b) indicates the radius, while in c) – the value of the descriptor D_2

The second strategy $q = 2$ shows the better results for each reference model k . The least square error and the deviation of the surface area is the smallest for the reference model $k = 2$ –5.4% and 0.9%, respectively. The deviation of the volume for this model is 0.8%. The better approximation of the volume is obtained using the reference model $k = 4$, but the least square error increases by 2% and the deviation of the surface – 2 times.

The third strategy $q = 3$ overall is the best strategy. The smallest least square error is obtained by the reference model $k = 2$ and is equal to 0.2%. The deviation of the surface area for this model is 1.1% and the deviation of the volume – 0.5%.

The last strategy $q = 4$, where the Gaussian points are used, gives the highest errors of all results.

3.2. Modelling of Cylinder Particle

This section presents the modelling result for the circular cylinder. It is divided into several subsections: firstly, defining of the original shape is discussed, then the modelling results are given and some conclusions are drawn.

3.2.1. Description of the Cylinder Surface

The circular cylinder is classified to a specific category of particle shapes used in discrete element method (Kodam *et al.* 2010). The central axis of the cylinder is aligned with Cartesian axis Oz . The cylindrical surface is formed by rotating straight line parallel to the axis. If the distance between these two lines is constant and equal a , the circular cylinder is obtained (Fig. 3.4). The cylinder body is formed by two perpendicular cut-off planes, and the inter-plane distance forms the height of the cylinder equal to $2c$.

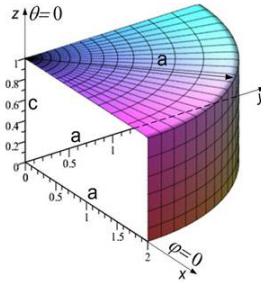


Fig. 3.4. The shape of a circular cylinder, when $c = 1$ and $a = 2$

The original surface of the cylinder is characterised by a presence of a sharp circular edge of the plane-cylinder intersection plane $z = c$. In Cartesian coordinates it is described by the continuous non-smooth function $S_{cyl}(\mathbf{x})$ expressed by Eq. (C1). Using transformation, Eq. (2.2), it may be transformed to spherical coordinates, and an alternative expression $S_{R,cyl}(\theta, \varphi)$, described by Eq. (C2), is obtained. It is obvious that this equation is a one-dimensional non-smooth equation with the singularity at a line $\theta = \theta_{cyl,ed}$. The value of the singular azimuthal angle is

$$\theta_{cyl,ed} = \tan^{-1} \left(\frac{a}{c} \right). \quad (3.1)$$

In this case, Eq. (3.1) acquires the value $\theta_{cyl,ed} = \tan^{-1}(2) = 0.3524\pi$.

Cylinder presents axi-symmetric surface $S_{R,cyl}(\varphi, \theta) \equiv S_{R,cyl}(\theta)$, therefore, only one-dimensional positioning of sampling points along azimuthal angle θ is

examined. It should be remarked, however, that polar constant surface when approximated by spherical harmonics is transformed to varying surface containing local deviations. To minimise this effect, the angular modelling subdomain φ – θ is divided into n_φ equiangular polar sectors, and constant value $n_\varphi = 16$ will be held for all modelling strategies.

3.2.2. Modelling of Cylinder

Two samples of sequential refining strategies were firstly tested. Numerical testing is aimed to find the best approximation by considering two low-resolution spherical harmonics of order $L = 3$ and $L = 2$ denoted by subscripts $j = 3$ and $j = 2$, respectively. Totally, $q \times k = 16$ reference models comprising four discrete grids with $(k = 1, \dots, 4)$ sets of sampling points generated by $(q = 1, \dots, 4)$ strategies were examined, and sixteen sets of harmonic coefficients \mathbf{a}_{jqk} were obtained using Eqs. (2.19)–(2.20) for each model j . Different strategies for the cylinder surface is given in Fig. 3.5.

The reference threshold model denoted by thr is also considered as the most accurate numerical model, which was obtained by generation of a regular rectangular grid covering the angular θ – φ plane. The threshold model is characterised by total number of $N_{thr} = 16250$ of sampling points.

Detailed comparison of all the above described qk reference models are selected in Table 3.2. Results obtained by applying the threshold model are also presented for the sake of comparison. Two types of descriptors in terms of numerically calculated values and relative deviations denoted by $\delta_{LS,jgk}$ are listed in the table. The global quality of spherical harmonics approximation is essentially evaluated by the normalized Euclidean norm $\|E_{jqk}\|^2$ obtained by Eq. (2.24). The relative deviations $\delta_{LS,jgk}$ are obtained with respect to threshold error value $\|E_{thr}\|^2 = 0.9539$. Additionally, the values of average deviations $\|E_{jqk}\|_{av} = \|E_{jqk}\|^2/N_{thr}$ are given in order to evaluate approximation magnitude. The most suitable values reflecting minimal least square errors are underlined.

To grasp the entire view, the three-dimensional images of particle surface $S_R(\theta, \varphi)$ are presented graphically in Fig. 3.8 as contour plots over two-dimensional angular θ – φ domain. Here, the exact surface is shown in Fig. 3.8a, the model of the spherical harmonics model obtained by the strategy $q = 3$ is shown in Fig. 3.8b. The values of the radius at boundaries are equal cylinder sizes $c = 1$ and $a = 2$, while the maximal value $\sqrt{5} = 2.24$ indicates location of the sharp edge $\theta_{cyl,ed} = 0.3524\pi$ obtained according to Eq. (3.1). The combined visual analytical study is focussed towards the local effects. Axial symmetry is reflected by constant angular variation $S_R(\varphi) = \text{const}$ along the entire sector $0 \leq \varphi \leq \pi/2$. Small, vi-

sually hardly detectable deviations of these lines on $\varphi = 0$ in Fig. 3.8b indicate numerical errors. Detailed map of deviations corresponding to the descriptor Eq. (2.21) is presented in Fig. 3.8c.

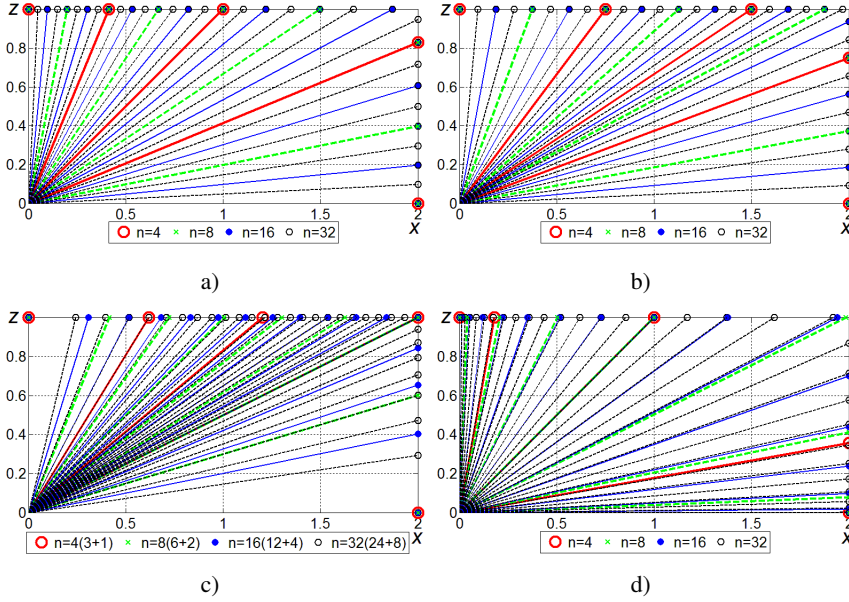


Fig. 3.5. Illustration of reference models showing locations of sampling points for cylinder generated with different modelling discretization models k having radially varying number of cells n and various modelling strategies: a) strategy $q = 1$, regular equiangular grid refinement; b) strategy $q = 2$, regular equidistant grid refinement, c) strategy $q = 3$, adaptive local grid refinement; d) strategy $q = 4$, application of Gauss points

Graphical information is also added in Fig. 3.6 to explain numerical results. Here, numerically calculated cross-sectional profiles in terms of $r(\theta)$ curves being plotted at polar angle $\varphi = 0$ are presented. Exact analytically described profiles are also shown. Performance of various strategies is illustrated in Fig. 3.6a, where the best profiles extracted from the results for each strategy are shown. Contribution of the refinement is illustrated in Fig. 3.6b, where four profiles obtained by adaptive grid refinement strategy ($q = 3$) with different numbers of positioning nodes are shown.

The global quality of approximation is also evaluated by calculating of the surface area S and the body volume V . Thereby, the theoretical value of the surface area of cylinder S_{cyl} is obtained analytically according to Eq. (C4), while V_{cyl} according to Eq. (C3). The relative deviations $\delta_{S,jqk} = |S_{cyl} - S_{jqk}|/S_{cyl}$ and

$\delta_{V,jqk} = |V_{cyl} - V_{jqk}|/V_{cyl}$ are evaluated by comparing both types of theoretical and numerical values.

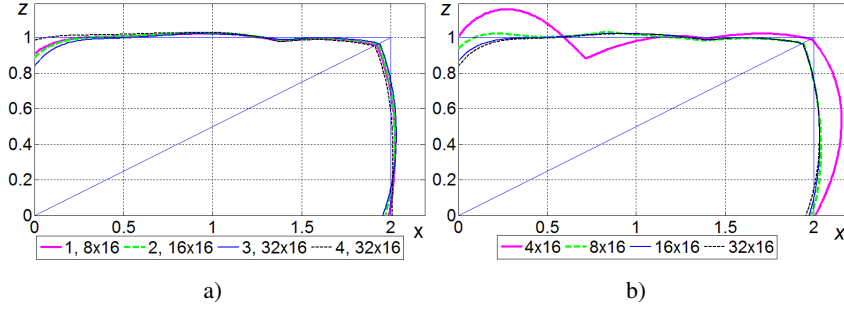


Fig. 3.6. Cross-sectional profiles obtained using various strategies and different grids: a) profiles corresponding to minimal least square error norms for different modelling strategies; b) profiles obtained by adaptive refinement strategy ($q = 3$)

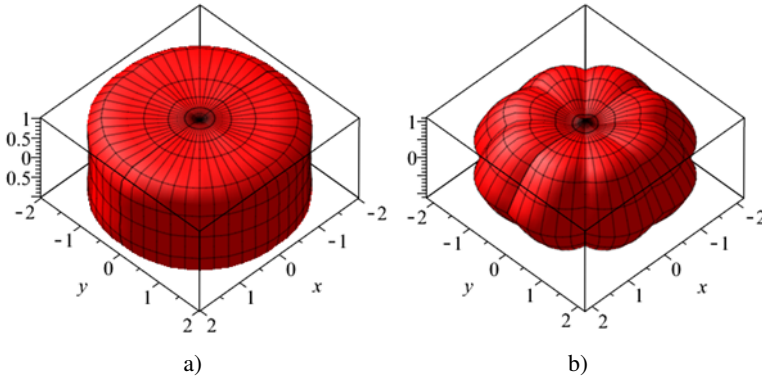


Fig. 3.7. Spherical harmonics approximation of the cylinder: a) 3D view when expansion degree $L = 3$; b) 3D view when expansion degree $L = 2$

The same testing was performed by applying expansion degree $L = 2$. Selected results obtained by applying the most successful refinement are also presented for all strategies. The values of the descriptors are given in Table 3.3. As shown in the table, the relative deviations $\delta_{LS,jgk}$ are big, but the surface area and volume is calculated with accuracy of 3% and 1%, respectively.

Illustration of differences could be clearly distinguish by comparing final three-dimensional shapes shown in Fig. 3.7. This confirms the conclusions that expansion degree $L = 2$ is not sufficient for accurate approximation of the cylinder.

Table 3.2. Results of spherical harmonics description of the cylinder when expansion degree is $L = 3$

Strat.	Refer. model	Grid cells	Points number	LS error	Average deviation	Max. error	Min. error	Surface area	Volume	
q	k	$n_\theta \times n_\varphi$	N_k	$\ E_{jqk}\ ^2$	$\ E_{jqk}\ _{av}$	$\ E_{jqk}\ _{max}$	$\ E_{jqk}\ _{min}$	S_{jqk}	V_{jqk}	δ_V
1	1	4×16	69	5.7706	5.0495	0.0003551	-0.1787	50.015	0.0050	26.245
	2	8×16	137	1.0874	0.1399	0.0000669	-0.0910	49.295	0.0193	25.129
	3	16×16	273	1.1076	0.1611	0.0000682	-0.0942	49.207	0.0210	25.087
	4	32×16	545	1.1410	0.1961	0.0000702	-0.0951	49.247	0.0203	25.100
2	1	4×16	69	3.5192	2.6893	0.0002166	-0.1326	48.240	0.0403	25.742
	2	8×16	137	1.0223	0.0717	0.0000629	-0.0847	49.360	0.0180	25.091
	3	16×16	273	1.0005	0.0488	0.0000616	-0.1128	49.389	0.0174	25.110
	4	32×16	545	1.0083	0.0570	0.0000621	-0.0851	49.408	0.0170	25.119
3	1	4×16	69	4.4318	3.6460	0.0002727	-0.1582	53.705	0.0684	27.506
	2	8×16	137	1.1247	0.1790	0.0000692	-0.0672	50.020	0.0049	25.233
	3	16×16	273	0.9855	0.0331	0.0000606	-0.1304	49.590	0.0134	25.158
	4	32×16	545	0.9755	0.0226	0.0000600	-0.1623	49.595	0.0133	25.132
4	1	4×16	69	6.2356	5.5370	0.0003837	-0.1817	47.468	0.0556	24.782
	2	8×16	137	1.3721	0.4384	0.0000844	-0.0703	50.078	0.0037	25.260
	3	16×16	273	1.2980	0.3607	0.0000799	-0.0902	49.413	0.0170	25.238
	4	32×16	545	1.2483	0.3086	0.0000768	-0.1022	49.138	0.0224	25.108
Threshold model				16250	0.9539		Analytical	50.265		25.133

Table 3.3. Results of spherical harmonics description of the cylinder when expansion degree is $L = 2$

Strat.	Refer. model	Grid cells	Points number	LS error	Average error	Max. error	Min. error	Surface area	Volume
q	k	$n_\theta \times n_\varphi$	N_k	$\ E_{jqk}\ ^2$	$\ \bar{E}_{jqk}\ _{av}$	$\ \bar{E}_{jqk}\ _{max}$	$\ \bar{E}_{jqk}\ _{min}$	S_{jqk}	V_{jqk}
1	4	32×16	545	9.8033	9.2771	0.2697	-0.4529	45.697	24.572
2	4	32×16	545	9.8033	9.2771	0.2807	-0.4270	46.731	25.362
3	3	16×16	273	9.5810	9.0440	0.3687	-0.3969	48.842	26.855
4	4	32×16	545	10.674	10.190	0.1994	-0.479	43.734	23.376
Threshold model			16250	0.9539	0.000059		Analytical	50.265	25.133
								δ_S	δ_V

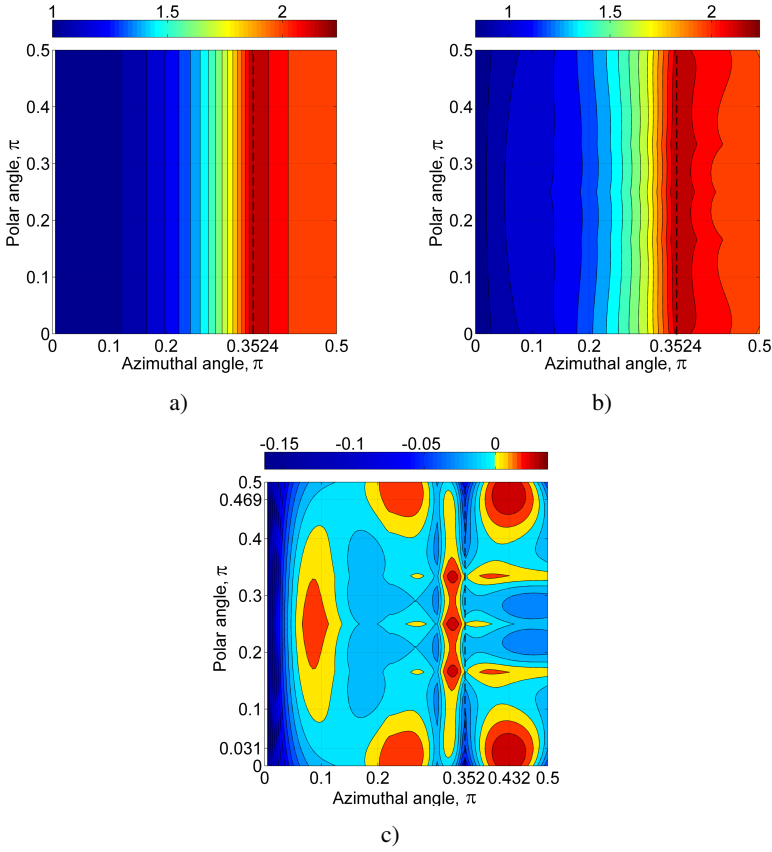


Fig. 3.8. Contour plots of the surface: a) exact cylinder analytical surface (Eq. (C2)); b) spherical harmonics approximation ($L = 3$); c) descriptor D_3 . The color bar above the figure a) and b) indicates the radius, while in c) – the value of the descriptor D_3

3.2.3. Analysis of the Cylinder Results

Comparing profiles (Fig. 3.6) obtained with expansion degree $L = 3$ and different strategies, it could be stated that regular equidistance refinement ($q = 2$) yielding nearly logarithmic angular variation adaptive refinement of the grid in vicinity of the corner prevails over equidistance one ($q = 1$). Concerning other two schemes, the locally introduced adaptive refinements (strategy $q = 3$) yields clearly the minimal global deviations characterised by quite low error about 2%. The Gauss point strategy ($q = 4$) yields however very high errors in the range of 30%.

Comparing these graphs and error norms in Table 3.2, it was found that the coarse scheme with 4 cells yields inaccurate results but sufficient accuracy is achieved practically by the second scheme with 8 cells, independently on modelling strategy. Further refinement demonstrates a reduction of global error in certain cases.

Results show that volumes are calculated with the very high accuracy with error lying below 0.01%. The accuracy of the surface area is lower: in optimal case the surface area is obtained with 1.3% accuracy.

The values of local descriptors illustrate that finding of optimal refinement is difficult because finer refinement not necessary improves approximation quality. The graphs in Fig. 3.6b demonstrate that minimal error δ_{LS} obtained by the adaptive strategy minimises the local errors in the vicinity of the singular corner but increases deviation on the edges and especially on the symmetry planes. It is obvious, that the choice of the best strategy is not straightforward, while the smallest error $\delta_{LS} = 2.3\%$ was obtained on finer grid. It could be remarked that minimal norm $\|E_{3qk}\|_{min} = 16.23\%$ (Table 3.2) is much higher compared to minimal value that equals to 6.72%.

Analising the result for the spherical harmonics expansion degree $L = 2$, the best strategy cannot be determined, because the least square error for each strategy equals to 9%–10%. The best strategy with respect to the deviation of the surface area is strategy $q = 3$, where the errors is around 3%. Here, the deviation of the volume is equal to almost 7%. The smaller deviation for the volume is obtained with the second strategy – 0.9%.

As the least square error for degree $L = 2$ shows low accuracy the higher expansion degree is needed. The 3D views of modelled particles for visual evaluation is given in Fig. 3.7. The best approximation is obtained with expansion degree $L = 3$ and using the strategy $q = 3$ and reference model $k = 4$.

3.3. Modelling of Rectangular Parallelepiped

This section presents the modelling result for the rectangular parallelepiped. Firstly, the description of the original shape is presented, then the modelling results are given and some conclusions are made.

3.3.1. Description of the Parallelepiped Surface

The rectangular parallelepiped (Fig. 3.9), presents the large type of polyhedral shapes (Boon *et al.* 2013; Höhner *et al.* 2013; Lu *et al.* 2015; Nezami *et al.*

ment – Fig. 3.10b. The equidistance rectangular threshold model (Fig. 3.10c) with the total number $N_{thr} = 16380$ of points is generated in order to avoid coincidence of positioning points.

Combination of polar and azimuthal refinement allows to construct four new two-dimensional strategies denoted further as $q = 5, 6, 7, 8$, i.e. strategy $q = 5$ means that for azimuthal refinement was used strategy $q = 2$ and for polar – strategy $q = 1$. In this manner, all four combinations $(q = 2, q = 1)$, $(q = 3, q = 1)$, $(q = 2, q = 3)$ and $(q = 3, q = 3)$ get their number $q = 5, q = 6, q = 7$ and $q = 8$.

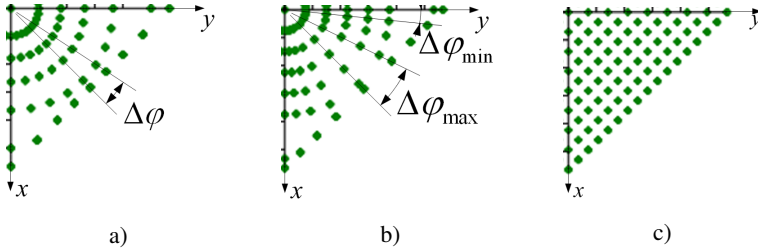


Fig. 3.10. Positioning of sampling points on the face: a) equiangular azimuthal refinement strategy; b) adaptive azimuthal refinement strategy; c) threshold refinement

Numerical testing is aimed to find the best approximation by considering low-resolution spherical harmonics. Totally, $q \times k = 20$ reference models comprising five discrete grids with $(k = 3, 5, \dots, 8)$, i.e. 8×8 , 12×12 , 16×16 , 24×24 and 32×32 , sets of sampling points generated by $(q = 5, \dots, 8)$ strategies were examined.

3.3.2. Modelling of Rectangular Parallelepiped

Detailed comparison of all the above described qk reference models are selected in Table 3.4. Results obtained by applying the threshold model are also presented for the comparison. The relative deviations δ_{LS} are obtained with respect to threshold error value $\|E_{thr}\|^2 = 4.6622$. The most suitable values reflecting minimal least square errors are underlined.

The global quality of approximation is also evaluated by calculating of the surface area S and the body volume V . Thereby, the theoretical value of the surface area of parallelepiped S_{par} is obtained analytically according to Eq. (P4), while V_{par} according to Eq. (P3). The relative deviations $\delta_{S,jqk} = |S_{par} - S_{jqk}|/S_{par}$ and $\delta_{V,jqk} = |V_{par} - V_{jqk}|/V_{par}$ are evaluated by comparing both types of theoretical and numerical values.

Graphical information is aided to evaluate numerical results. Cross-sectional profiles in terms of $r(\theta)$ curves being plotted at polar angle $\varphi = 0$ and $\varphi = \frac{\pi}{4}$ are presented graphically in Fig. 3.11.

To grasp the entire view, the three-dimensional images of particle surface $S_R(\theta, \varphi)$ are presented graphically in Fig. 3.12 as contour plots over two-dimensional angular $\theta - \varphi$ domain. Here, the exact surface is shown in Fig. 3.12a, the model of the spherical harmonics model obtained by the strategy $q = 6$ is shown in Fig. 3.12b. Detailed map of deviations corresponding to definition of descriptor Eq. (2.21) is presented in Fig. 3.12c.

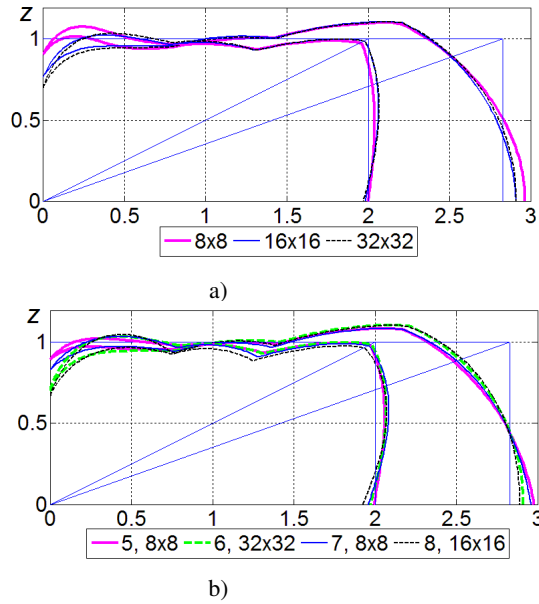


Fig. 3.11. Illustration of parallelepiped spherical harmonics approximation by degree $L = 3$: a) cross-sectional profiles obtained using strategy $q = 6$ for different refinements; b) profiles corresponding to the best reference models of each strategy

The same testing was performed by applying expansion degree $L = 2$. Selected results obtained by applying the most successful refinement are also presented for all strategies. The values of descriptors are given in Table 3.5.

The results for expansion degree $L = 2$ show that surface area and volume is calculated with accuracy of 8–9% and less than 1%, respectively. However, the least square errors are high, almost 3 times bigger than the value of threshold model.

Table 3.4. Results of spherical harmonics description of the rectangular parallelepiped when expansion degree is $L = 3$

Strat.	Refer. model	Grid cells	Points number	LS error	Average deviation	Max. error	Min. error	Surface area	Volume		
q	k	$n_\theta \times n_\varphi$	N_k	$\ E_{jqk}\ ^2$	δ_e	$\ \bar{E}_{jqk}\ _{av}$	$\ \bar{E}_{jqk}\ _{min}$	A_{jqk}	δ_A	V_{jqk}	δ_V
5	5	8×8	73	5.0326	0.0794	0.0003071	0.1812	60.613	0.0529	31.845	0.0048
	6	12×12	157	5.3140	0.1398	0.0003243	0.1534	59.744	0.0665	31.519	0.0150
	3	16×16	273	5.0638	0.0861	0.0003090	0.1659	60.316	0.0577	31.725	0.0086
	7	24×24	601	5.2141	0.1184	0.0003182	0.1428	59.861	0.0647	31.603	0.0124
	8	32×32	1057	5.1169	0.0975	0.0003123	0.1550	60.114	0.0607	31.704	0.0093
6	5	8×8	73	5.0326	0.0794	0.0003071	0.2144	61.688	0.0361	32.251	0.0078
	6	12×12	157	4.8681	0.0442	0.0002971	0.2117	60.572	0.0536	31.776	0.0070
	3	16×16	273	4.8182	0.0335	0.0002940	0.2277	61.194	0.0438	31.898	0.0032
	7	24×24	601	4.7736	0.0239	0.0002913	0.2252	61.126	0.0449	31.815	0.0058
	8	32×32	1057	<u>4.7566</u>	<u>0.0202</u>	0.0002903	0.2244	61.505	0.0390	31.874	0.0039
7	5	8×8	73	4.8530	0.0409	0.0002962	0.1799	61.205	0.0437	31.856	0.0045
	6	12×12	157	5.1190	0.0980	0.0003124	0.1400	60.917	0.0482	31.779	0.0069
	3	16×16	273	4.8914	0.0492	0.0002985	0.1610	61.027	0.0465	31.737	0.0082
	7	24×24	601	5.0977	0.0934	0.0003111	<u>0.1359</u>	60.983	0.0471	31.757	0.0076
	8	32×32	1057	5.0086	0.0743	0.0003057	0.1464	61.223	0.0434	31.797	0.0063
8	5	8×8	73	4.8369	0.0375	0.0002952	0.2071	61.559	0.0381	<u>31.942</u>	<u>0.0018</u>
	6	12×12	157	4.8056	0.0308	0.0002933	0.2227	61.641	0.0369	31.756	0.0076
	3	16×16	273	4.8041	0.0304	0.0002932	0.2186	61.884	0.0331	31.694	0.0096
	7	24×24	601	4.8805	0.0468	0.0002978	0.2231	61.963	0.0318	31.802	0.0062
	8	32×32	1057	4.9478	0.0613	0.0003020	0.2129	<u>62.485</u>	<u>0.0237</u>	31.657	0.0107
Threshold model			16380	4.6622		0.0000285	Analytical	64.00		32.00	

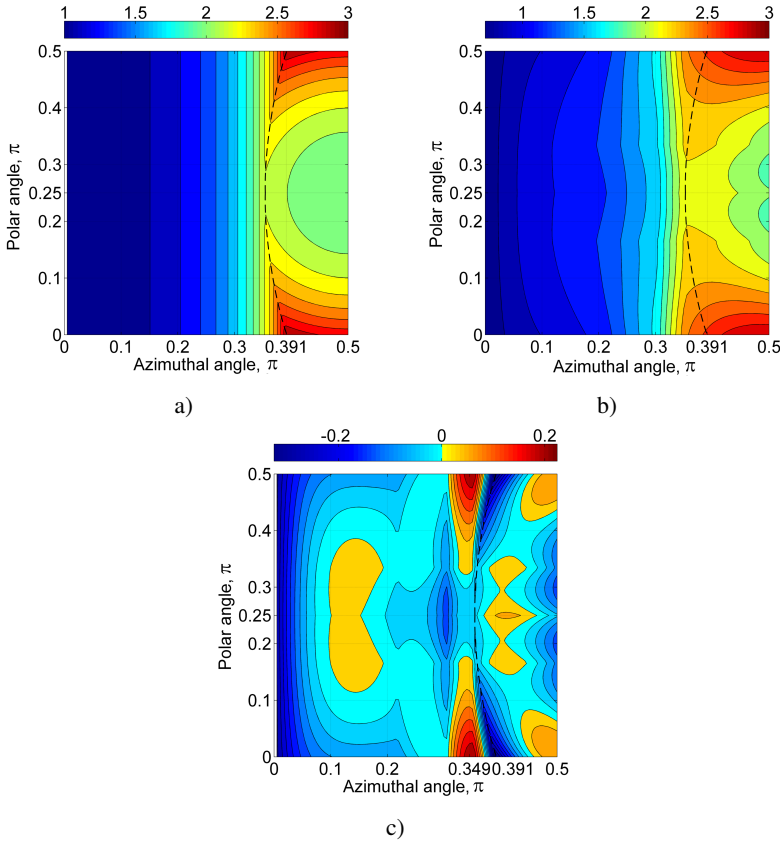


Fig. 3.12. Contour plots of the surface: a) exact analytical surface; b) spherical harmonics approximation by degree $L=3$; c) the descriptor D_3

The three-dimensional models with degree $L = 3$ and $L = 2$ are plotted in Fig. 3.13a and Fig. 3.13b, respectively.

Similar to cylinder, expansion degree $L = 2$ does not approximate the rectangular parallelepiped with satisfactory errors. Obtained 3D views verifies that spherical harmonics model with expansion degree $L = 3$ gives more accurate approximation.

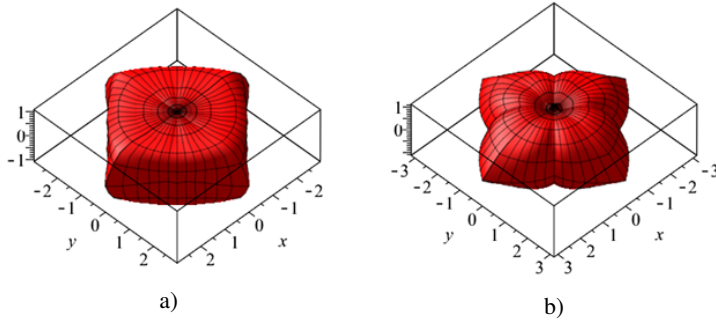


Fig. 3.13. Spherical harmonics approximation of rectangular parallelepiped:
a) 3D view when expansion degree $L = 3$; b) 3D view when expansion degree $L = 2$

3.4. The Curvature and Other Factors for Contact Calculation

For numerical illustration of the contact behaviour, the sample of rotational oblate ellipsoid defined by size parameters $a = b = 2$ and $c = 1$ will be investigated. Recent sample includes evaluation of curvatures and calculation of normal contact force. Potentially, analytical instead of numerical treatment of the contact would be preferable while numerical finite element method analysis will be used for verification purposes.

Regarding axial symmetry geometry of the particle is defined by the surface profile in longitudinal section. The perfect analytically described ellipsoid and quasi-ellipsoids obtained by low-resolution spherical harmonics approximation is considered for representation of this shape. Various profiles of particle surface plotted in the Cartesian Oxz plain are shown in Fig. 3.14a.

In order to restore full picture of particle properties, these profiles are also alternatively considered in spherical coordinates. Here, profiles of the quasi-ellipsoid are considered at fixed polar angle $\varphi = 0$, and they are described by relationship $r(\theta)$. Thereby, azimuthal angle θ is counted from Cartesian axis Oz restricting to maximal value $\pi/2$ ($0 \leq \theta \leq \pi/2$) in central cross-sectional plane.

Profiles of quasi-ellipsoids are originally calculated by low-resolution spherical harmonics approximation and depicted in Fig. 3.14b. Here, perfect ellipsoid is illustrated by thin solid line while spherical harmonics models – by dashed lines.

Comparing character of perfect and spherical harmonics profiles, three characteristic regions could be detected. Here, the conditional boundaries $\theta_1 = 0.16\pi$ and $\theta_2 = 0.052\pi$ in Fig. 3.14 reflect character of approximated profile corresponding to $L = 1$. They indicate middle region where approximated profile quite

closely mimics analytical one. The first region ($0 \leq \theta \leq \theta_1$) restricted by angle θ_1 indicates occurrence of wavy profile in vicinity of the cross-section centre $x = 0, y = 0$. The third region ($\theta_2 \leq \theta \leq \pi/2$) restricted by angle θ_2 indicates that spherical harmonics produces asperity with sharp angle in the central section $z = 0$.

If consideration of the non-smooth and concave surface is not satisfactory, the smooth quasi-quadric surface could be constructed. In this case, both the first and the third regions are replaced by circles having common tangent, or common external normal, in intersection points θ_1 and θ_2 . In the first region, the center of the approximating circle is located in the central axis Oz , while its radius r_1 is larger than semi-axis c , i.e. $r_1 > c$. Increasing of approximation order reduces the boundary angle θ_1 , and, consequently, the size of region. In three dimensions, this region presents spherical cup with radius r_1 .

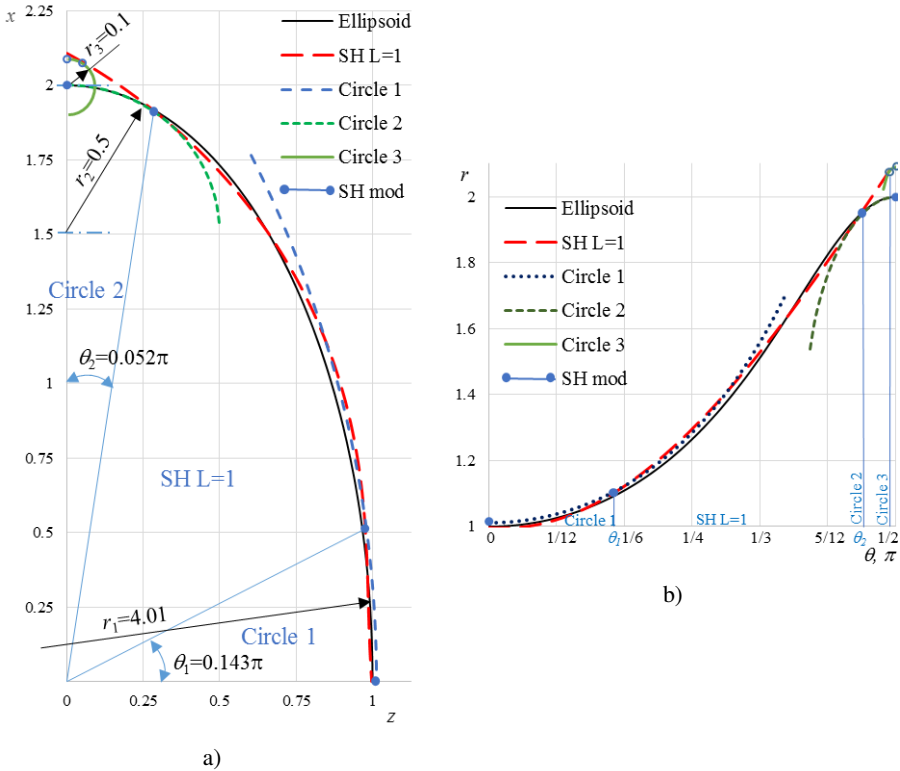


Fig. 3.14. Profiles and curvatures of quasi-quadric surfaces (quasi-ellipsoids):
a) in Cartesian coordinates; b) in spherical coordinates

In the third region, approximating sphere is inscribed sphere the center of

which is located in the central plane Oxy . Reducing initial radius $r_2 = 0.5$ and approaching it to the almost zero, a set of surfaces with radii $r_{2i} \rightarrow \min$, approximating quasi-quadric shape with different degree of accuracy may be generated. Increase of expansion reduces the above mentioned central almost circularly varying sharpness and improves the global indicators, thereby, approaching to perfect shape. The spheres in Fig. 3.14 are denoted by dotted lines, while resultant smooth quasi-quadric surface by bold dashed line.

In three dimensions, this region presents toroid, or spherical ring, with cross-sectional radius R_2 and external radius a . Three-dimensional views of particles are illustrated in Fig. 3.15, where quasi-ellipsoid with sharp edge is shown in Fig. 3.15a and resultant quasi-quadric composite bodies are shown in Fig. 3.15b and Fig. 3.15c, respectively.

It could be noted that approximation of complex curve by circular arches is common practice used in discrete element method. The equivalent contact sphere method for approximation of ellipsoids by four arches is elaborated in Johnson *et al.* (2004). Approximation of rotational prolate ellipsoid by the spherical end cup combined with the multi-sphere technique in the reminder body is presented in Markauskas *et al.* (2010).

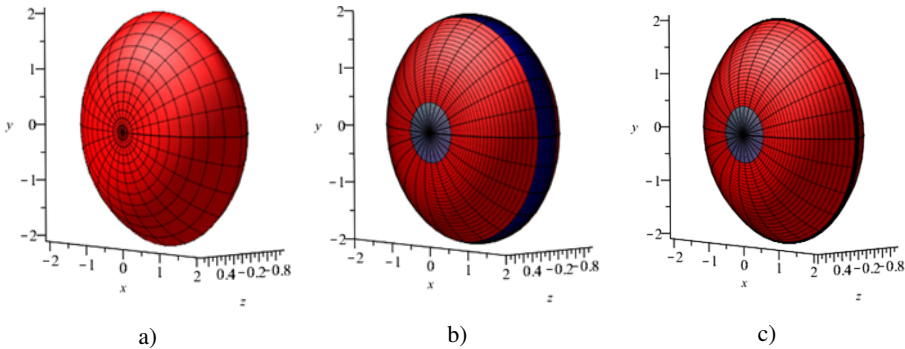


Fig. 3.15. Three-dimensional views of particles: a) quasi-ellipsoid with sharp edge; b) resultant quasi-quadric composed various bodies ($r_2 = 0.5$); c) resultant quasi-quadric composed various bodies ($r_1 = 0.1$)

Variations of curvature radii are shown in Fig. 3.16. The obtained curvatures are used further for calculation of normal contact force.

Contribution of the local particle shape occurred due to low-resolution spherical harmonics description is demonstrated by solving normal contact of the above oblate ellipsoid with plane plate. The case of contact of a perfectly elastic ellipsoid onto a semi-infinite plane surface was also considered in study by Wynn (2009). Computational set up of the normal particle-plane contact is illustrated in Fig. 3.17.

Here, normal axial orientation of particle with plane perpendicular to central axis Oz is shown. Particle center was subjected by normal displacement u , while contact force F_n is a resultant reaction. Potentially, analytical instead of numerical treatment of the contact is preferable because, analytical results may be used for multi-particle computations.

Analytical treatment of the above discussed contact is performed by applying Eqs. (2.48)–(2.52). Parameters of the body i are identified to ellipsoid and denoted by subscript ell , while second body j is identified as plane and denoted with the subscript pl .

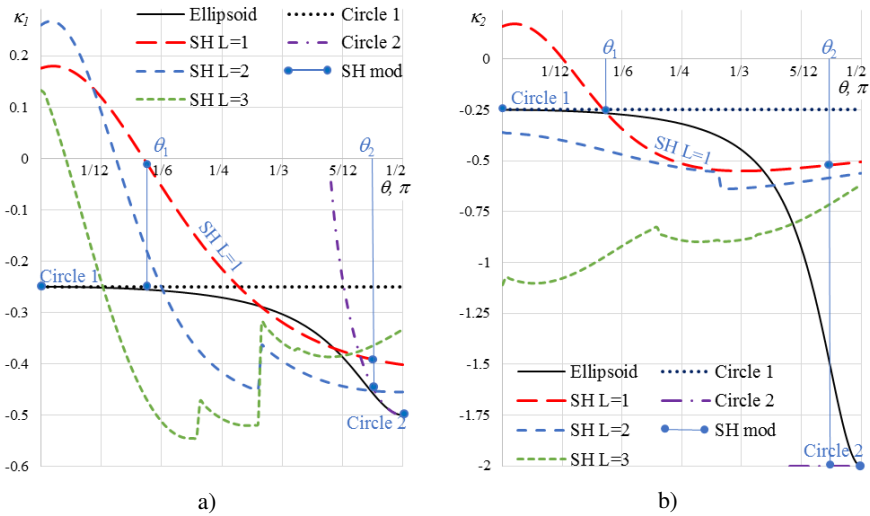


Fig. 3.16. Variation of curvature radii in longitudinal section presented in spherical coordinates: a) curvatures along section profile; b) perpendicular to cross-section profile

In this problem, the inclination angle is $\alpha = 0$, and for plane the curvature radii is $\rho_{pl1} = \rho_{pl2} = \infty$, consequently, parameters $A \equiv A(\rho_{i1})$ and $B \equiv B(\rho_{i2})$ take a form:

$$A(\rho_{ell1}) = \frac{1}{2\rho_{ell1}} \quad \text{and} \quad B(\rho_{ell2}) = \frac{1}{2\rho_{ell2}}. \quad (3.3)$$

It is easy to detect that these parameters are curvatures parameters $A = \kappa_{ell1}/2$ and $B = \kappa_{ell2}/2$.

Comparison of various approaches is done in non-dimensional form and computational experiment is organised in the following manner. All length variables are scaled to parameter R and defined by a set of non-dimensional parameters.

Therefore, defining the indentation displacement by $u_{rel} = u/R$ and effective radius (Eq. (2.50)) by $\rho_{effrel} = \rho_{eff}R$, the normal force in Eq. (2.48) may be also expressed in non-dimensional form as

$$F_{Hn} = \overline{F_{Hn}} E_{eff} R^2, \quad (3.4)$$

where contact force is defined by non-dimensional factor

$$\overline{F_{Hn}} \frac{4}{3} c_{cor} \sqrt{\rho_{eff}} (u_{rel})^{3/2}. \quad (3.5)$$

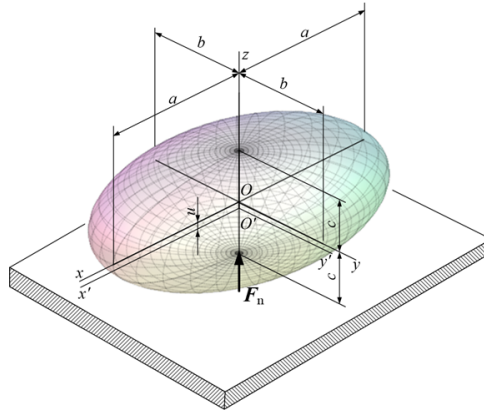


Fig. 3.17. Computational set up of the normal particle-plane contact

Contact analysis was conducted by assuming dimensional length parameter $R = b$ and relative indentation $u_{rel} = 0.01$. Four characteristic samples were solved analytically, and sample data and solution results are given in Table 3.6. Each of the samples are denoted by identifier containing orientation of the contacting particle, contact type and solution method.

The first two samples denoted as RAD_ELL_ANL and RAD_SH_ANL illustrate results of radially oriented perfect ellipsoid and spherical harmonics model with circular round off of artificial asperity, respectively. The next two samples denoted as NORM_ELL_ANL and NORM_SH_ANL illustrate results of normally oriented perfect ellipsoid and spherical harmonics model with spherical cup, respectively.

In order to verify applicability of analytical models, the problem of normal elastic particle-plane contact was solved numerically, using Finite Element Method.

Table 3.6. Summary of contact analysis results

No.	Model identification	Orientation	Curvature radii		Non-dimensional factors		Relative forces
			$\overline{\rho_n} = \rho_n/\rho$	$\overline{\rho_t} = \rho_t/\rho$	c_{cor}	$\overline{\rho_e}$	$F_{rel}/F_{rel,max}$
Analytical solutions							
1	RAD_ELL_ANL Ellipsoidal	$\frac{\pi}{2}$	0.25	1.0	1.0455	0.5	$0.9857 \cdot 10^{-3}$ 0.5221
2	RAD_MOD_ANL Ellipsoidal	$\frac{\pi}{2}$	0.05	1.0	1.1782	0.2236	$0.7429 \cdot 10^{-3}$ 0.3935
3	NORM_ELL_ANL Ellipsoidal (Spherical)	0	2.0	2.0	1.0	2.0	$1.885 \cdot 10^{-3}$ 0.9984
4	NORM_MOD_ANL Ellipsoidal (Spherical)	0	2.005	2.005	1.0	2.005	$1.888 \cdot 10^{-3}$ 1.0
Numerical (Finite element method) solutions							
5	RAD_ELL_FEM Ellipsoidal	$\frac{\pi}{2}$	0.25	1.0	–	–	$0.707 \cdot 10^{-3}$ 0.3744
6	RAD_SH_FEM Sharp angle	$\frac{\pi}{2}$	–	2.0	–	–	$0.1936 \cdot 10^{-3}$ 0.1025
7	NORM_ELL_FEM Ellipsoidal (Spherical)	0	2.0	2.0	–	–	$1.879 \cdot 10^{-3}$ 0.9952

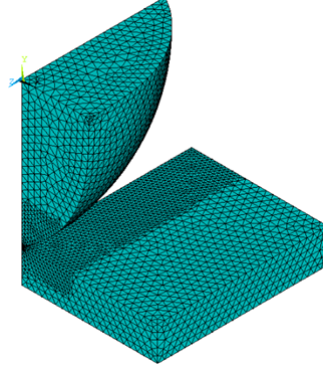


Fig. 3.18. The meshed finite element model (quater)

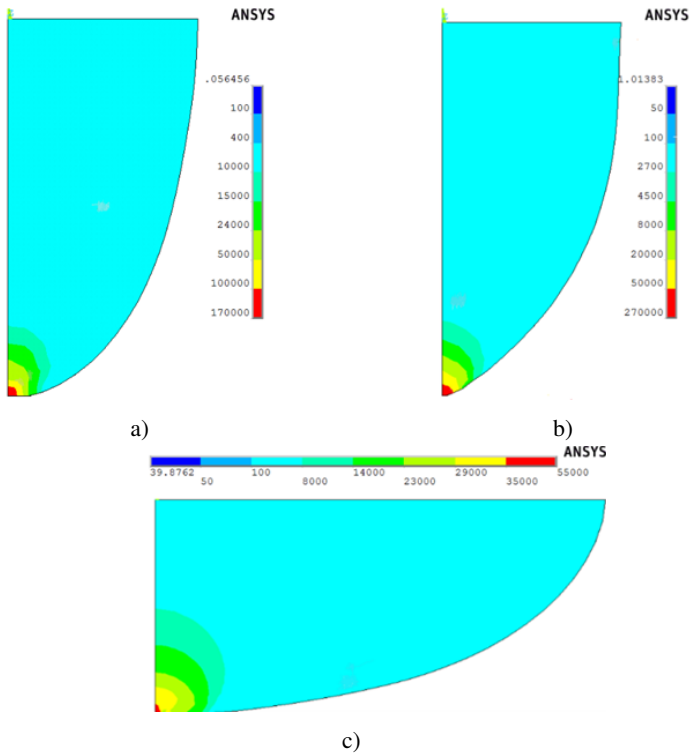


Fig. 3.19. Variation of von Mises stresses in contact zone of particle at relative indentation $u_{rel} = 0.01$: a) radially oriented perfect ellipsoid; b) radially oriented spherical harmonics model, $L = 1$; c) normally oriented perfect ellipsoid

The non-adhesive perfectly stick contact is assumed, therefore, tangential sliding is not allowed. The surfaces of contacting bodies in contact zone are assumed to be smooth. The problem is three-dimensional, and computational domain comprises a quarter of bodies because of plane symmetry. Contacting bodies are discretised by the volume brick-type elements defined by 8 nodes. The multipurpose commercial available finite element analysis package ANSYS was used for these purpose. The finite element models are shown in Fig. 3.18.

Three characteristic samples were solved numerically. Two samples of radially oriented ellipsoid, denoted as RAD_ELL_FEM and RAD_SH_FEM, involves computations of radially oriented perfect ellipsoid and spherical harmonics model with sharp edge, respectively. The third sample, denoted as NORM_ELL_FEM, involves normally oriented ellipsoid. Illustration of computational results is presented in Fig. 3.19. Here, numerically obtained distributions of the von Mises stresses are shown.

3.5. Comparison Study of Low-Resolution Harmonics for Various Shapes

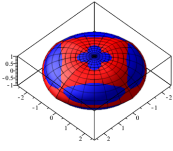
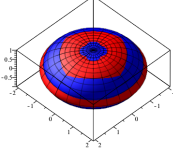
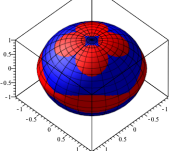
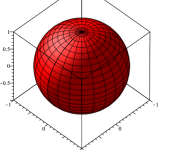
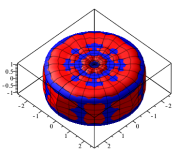
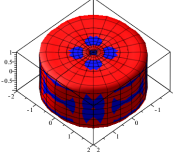
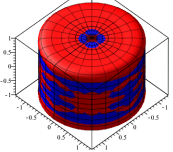
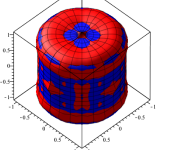
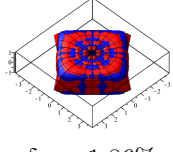
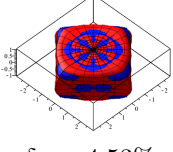
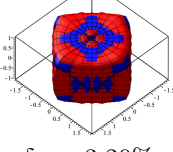
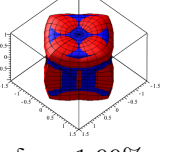
In previous sections, some characteristic features of the spherical harmonics models were demonstrated by considering ellipsoid, cylinder and parallelepiped, limited, however, to single set of two size parameters, the length $c = 1$ and cross-sectional size, or thickness, $a = 2$. In order to compare various values of a and c , they are expressed in terms of dimensional size parameter R and non-dimensional factors $\bar{a} = a/R$ and $\bar{c} = c/R$, respectively. Generally, characterisation of the shape is done in terms of non-dimensional quantities, see Blott and Pye (2008). If parameter c is considered as length parameter, and perpendicular sizes $b = a$ as cross-sectional perpendicular parameters, the ratio c/a means elongation degree $k_{elon} = c/a$. For symmetric section, this quantity is also flatness degree (Blott and Pye 2008). In many situations, the value of the degree of elongation k_{elon} is used for classification of particle shapes. Traditional terminology characterizes particles having $k_{elon} = 1.0$ – 0.8 as non-elongated but drop of the degree up to 0.2 changes characterization from slightly elongated up to extremely elongated.

Suitability of lower resolution harmonics to description of particles is studied by considering flattening of initially selected shapes for specified values of the elongation degree decreasing from 1.0 up to 0.4 was examined. Despite a similarity of considered elongation of the shape, different shapes exhibit remarkable differences. It could be shown that the oblate ellipsoid characterised by parameters

$c < a$ can be imagined as flattened sphere having elongation ratio $k_{elon} < 1$. A limit case of a flattened ellipsoid is characterised by equal semi-axes $c = a$ and elongation factor $k_{elon} = 1.0$, which transforms ellipsoid to sphere, see Eq. (S1) and (S2). Concerning approximation accuracy of spherical harmonics, expansion degree $L = 2$ is expected to be sufficient for accurate description (Ritchie and Kemp 1999). Consequently, simulation of ellipsoid was conducted limiting to first order expansion with $L = 1$ with $M = 4$ harmonic terms.

Concerning cylinder and parallelepiped, thereby, previously discussed results obtained for cylinder and parallelepiped with elongation $k_{elon} = 0.5$ are used as template for further investigations. The new set characterized by different k_{elon} is calculated by applying the most suitable reference model yielding the minimal least square error. This set of coefficients is then used for the characterisation of particles.

Table 3.7. Pictorial summary and relative errors of different shapes

	0.4	0.5	0.75	1
Ellipsoid	 $\delta_S = 2.11\%$ $\delta_V = 1.02\%$ $\delta_{LS} = 1.70\%$	 $\delta_S = 1.43\%$ $\delta_V = 0.06\%$ $\delta_{LS} = 2.26\%$	 $\delta_S = 0.56\%$ $\delta_V = 0.52\%$ $\delta_{LS} = 0.69\%$	 $\delta_S = 1.29\%$ $\delta_V = 1.08\%$ $\delta_{LS} = 1.51\%$
Cylinder	 $\delta_S = 2.11\%$ $\delta_V = 1.02\%$ $\delta_{LS} = 1.70\%$	 $\delta_S = 1.43\%$ $\delta_V = 0.06\%$ $\delta_{LS} = 2.26\%$	 $\delta_S = 0.56\%$ $\delta_V = 0.52\%$ $\delta_{LS} = 0.69\%$	 $\delta_S = 1.29\%$ $\delta_V = 1.08\%$ $\delta_{LS} = 1.51\%$
Parallelepiped	 $\delta_S = 1.86\%$ $\delta_V = 0.79\%$ $\delta_{LS} = 6.72\%$	 $\delta_S = 4.53\%$ $\delta_V = 0.32\%$ $\delta_{LS} = 2.02\%$	 $\delta_S = 3.20\%$ $\delta_V = 1.13\%$ $\delta_{LS} = 4.49\%$	 $\delta_S = 1.99\%$ $\delta_V = 0.51\%$ $\delta_{LS} = 5.08\%$

Pictorial summary of models of all shapes is shown and the relative errors for each case are given in Table 3.7. Here three-dimensional views of approximated particle shapes are presented, where red surface shows the spherical harmonics model of the shape and blue one is original surface. Three-dimensional views show that approximated models retain basic features of original shapes while local deviations near the axis are observed. Additionally, sharp edges are transformed into locally smooth surfaces. Quantitatively shapes are characterised by different error indicators. The best accuracy is achieved in approximation of particle volumes while accuracy of surface area correlates with least square error. It could be stated that generally the cylinder is approximated by spherical harmonics with higher accuracy yielding average errors of 2%. The parallelepiped is approximated with the error in the range of 5%. Scattering of results could be explained by considering the shape of spherical harmonics involved, i. e. each particular figure is approximated by different harmonics, and no regularity is detected. Since the results were obtained by limited number of positioning the higher accuracy could be found by detailed optimization analysis.

Also several selected shapes that can be classified as axi-symmetric and plane-symmetric are illustrated. The pictorial summary of axi-symmetric shapes spherical harmonics images are shown in Table 3.8. Presentation is restricted by two, $L = 1$ and $L = 3$, images. First columns in these tables shows the point clouds of the original surfaces.

Table 3.8. Pictorial summary of axi-symmetric shapes

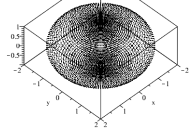
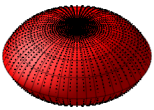
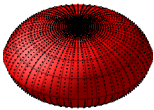
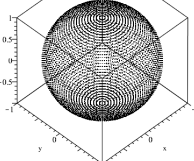
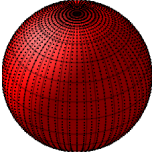
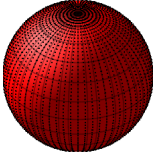
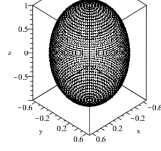
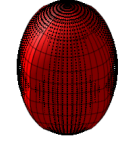
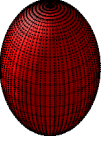
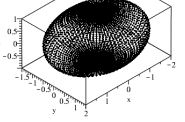
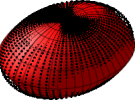
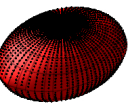
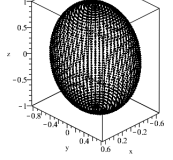
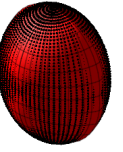
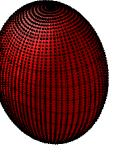
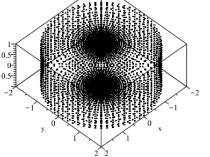
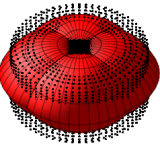
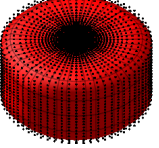
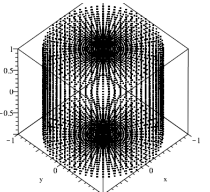
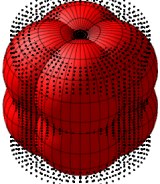
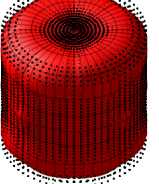
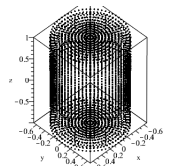
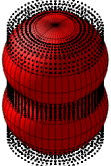
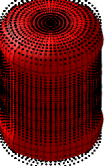
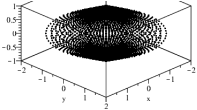
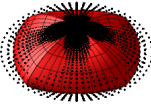
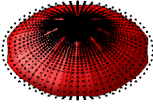
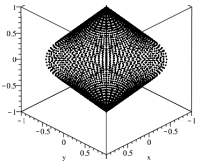
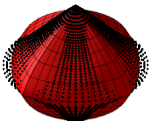
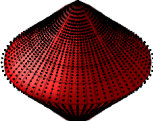
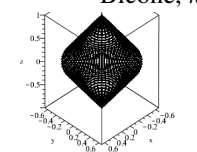
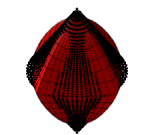
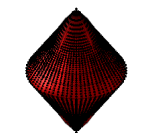
No.	Original shape	Approximated shapes	
		$L = 1$	$L = 3$
1.	Axisymmetric ellipsoid, $k_{elon} = 0.5$, oblate ellipsoid 		
2.	Axisymmetric ellipsoid, $k_{elon} = 1.0$, sphere 		

Table 3.8 continued

No.	Original shape	Approximated shapes	
		$L = 1$	$L = 3$
3.	Axisymmetric ellipsoid, $k_{elon} = 1.5$, prolate ellipsoid 		
4.	Tri-axial ellipsoid, $k_{elon} = 0.5$, $c < b < a$ 		
5.	Tri-axial ellipsoid, $k_{elon} = 1.5$, $c > b > a$ 		
6.	Circular cylinder, $k_{elon} = 0.5$, oblate cylinder 		
7.	Circular cylinder, $k_{elon} = 1.0$, regular cylinder 		
8.	Circular cylinder, $k_{elon} = 1.5$, prolate cylinder 		

End of Table 3.8

No.	Original shape	Approximated shapes	
		$L = 1$	$L = 3$
9.	Bicone, $k_{elon} = 0.5$, oblate bicone 		
10.	Bicone, $k_{elon} = 1, 0$, regular bicone 		
11.	Bicone, $k_{elon} = 1.5$, prolate bicone 		

The pictorial summary of another class of symmetric shapes that have plane symmetry are shown in Table 3.9. Here, the numbering of the shape is continued because these numbers later are used as a reference.

Table 3.9. Pictorial summary of plane-symmetric shapes

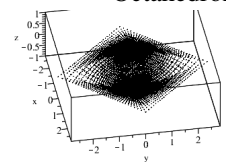
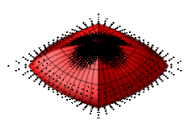
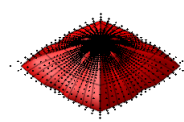
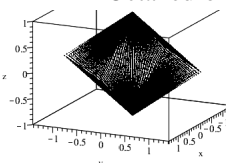
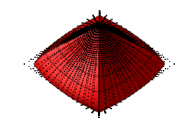
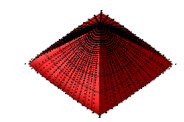
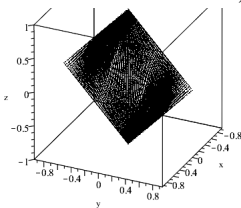
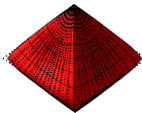
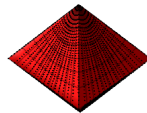
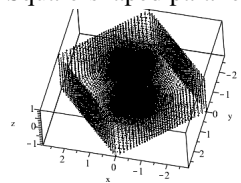
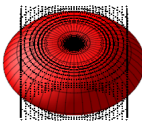
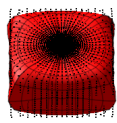
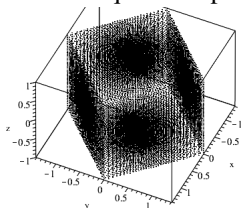
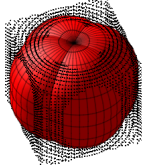
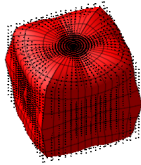
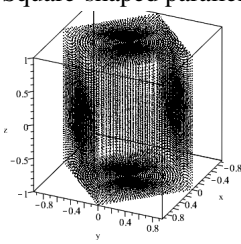
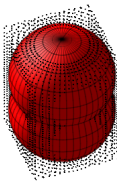
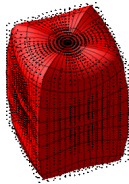
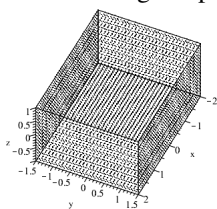
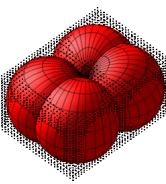
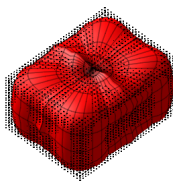
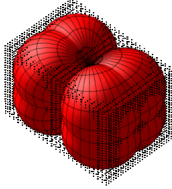
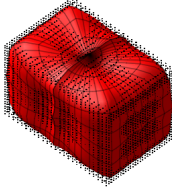
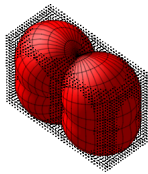
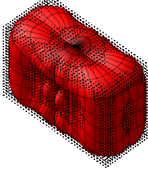
No.	Original shape	Approximated shapes	
		$L = 1$	$L = 3$
12.	Octahedron, $k_{elon} = 0.5$, oblate octahedron 		
13.	Octahedron, $k_{elon} = 1.0$, regular octahedron 		

Table 3.9 continued

No.	Original shape	Approximated shapes		
		$L = 1$	$L = 3$	
14.	Octahedron, $k_{elon} = 1.5$, prolate octahedron			
15.	Square-shaped parallelepiped, $k_{elon} = 0.5$, oblate parallelepiped			
16.	Square-shaped parallelepiped, $k_{elon} = 1.0$, cube			
17.	Square-shaped parallelepiped, $k_{elon} = 1.5$, prolate parallelepiped			
18.	Rectangular parallelepiped, ($c/a = 0.5$, $c/b = 2/3$)			

End of Table 3.9

No.	Original shape	Approximated shapes	
		$L = 1$	$L = 3$
19.	Rectangular parallelepiped, ($c/a = 1.0, c/b = 2/3$)		
20.	Rectangular parallelepiped, ($c/a = 1.5, c/b = 2/3$)		

Several reasons could be mentioned to support the choice of shapes. Ellipsoid, especially ellipsoid of revolution, is the most simple but the most studied non-spherical smooth analytical shape. Extending this problem to non-perfect ellipsoids, these shapes have practical importance in geotechnical engineering. Naturally, the rounded particles of gravel fluvial origin are classified as ellipsoids. Considering non-smooth surfaces characterized by presence of sharp edges and additionally corners on polyhedral particles the issue is still open. It is only guess that potentially increases polynomials order is expected. Deeper analysis given by (Zhou *et al.* 2015) supports this guess informing that degree $L \leq 3$ gives major contribution to capture formation of the shape.

Approximation quality is illustrated in Table C.1, given in Annex C, where geometric parameters such as the body volume V , surface area S , least square error E and sphericity Ψ , are compared. Spherical harmonics models are characterized by absolute values and relative errors obtained with respect to exact analytical values. The least squared error is calculated using two times finer grid than used for modeling – total 16258 points. Important particle characteristic, sphericity of particle Ψ , is also included. It is defined as the ratio of the surface area of the volume-equivalent sphere divided by the surface area of the particle.

Results show that expansion degree $L = 1$ is sufficient for equal-sized and extended particles, where approximation error is below 2%, while increase of expansion degree L up to 3 is not decisive. In particular, for octahedrals approxima-

tion error dropped from 1.8% up to 0.30%. Similar 1% difference is observed for ellipsoid-shaped particles. For the above discussed particles, the surface area is the most approximation sensible parameter leading to highest errors. Also moments of inertia was calculated and given in Table C.2.

Different behaviors were observed for two- and three-plane symmetry hexahedrons (rectangular parallelepipeds). Here, expansion degree $L = 1$ leads unacceptable shapes, see Table 3.9, and high error varying in the range of 15–24%. Using of the higher degree $L = 3$ substantially improves the approximation quality reducing error up to 5%. To conclude the discussion, it could be stated that low-resolution harmonics is proper tool for approximation of particle shape on the scale of entire particle.

3.6. Conclusions of Chapter 3

1. The ellipsoid of revolution is the most simple but the most studied non-spherical analytical shape considered in framework of discrete element method. This shape is the most suitable sample to illustrate performance of spherical harmonics. Four strategies are used for the surface description: the equiangular refining strategy ($q = 1$), regular equidistance refining strategy ($q = 2$), the global adaptive refining combined with the local refinement ($q = 3$) and the Gauss points strategy ($q = 4$). Detailed results show, that the sufficient spherical harmonics expansion degree to model the ellipsoid is $L = 1$. The best results are obtained using the adaptive refinement strategy ($q = 3$), where the deviation of the model is 0.78%. The surface area and volume are calculated with the error equal to 0.15% and 0.08%, respectively.
2. The circular cylinder is classified to a specific category of particle shapes used in discrete element method. Cylinder presents axis-symmetric surface, therefore, only one-dimensional positioning of sampling points along azimuthal angle θ is examined. The same four strategies are used as in the case of ellipsoid. The expansion degree is used $L = 2$ and $L = 3$. Using the spherical harmonics expansion degree $L = 3$ the cylinder is modelled with the error equal to 2%, the deviation of surface area and volume is 3.7% and 0.004%, respectively. The lower expansion degree $L = 2$ gives higher global errors, although surface area and volume are modelled with error equal to 2.8% and 0.9%, respectively. These results show that ex-

pansion degree $L = 2$ is not sufficient for accurate approximation of the cylinder.

3. The rectangular parallelepiped presents the large type of polyhedral shapes. The two strategies yielding the best results for the cylinder is used for two-dimensional positioning of the samplings points. Combination of polar and azimuthal refinement allows to construct four new two-dimensional strategies, thus, they are tested in the same manner as the previous samples. Obtained modelling results show that the best spherical harmonics model of the rectangular parallelepiped is obtained with expansion degree $L = 3$. The accuracy of such model is 2%. The surface area and volume is obtained with the accuracy of 2.4% and 0.18%, respectively. The use of spherical harmonics expansion degree $L = 2$ yields to increase of the approximation error. The deviation of surface area is 8%, volume – 0.35%. As for the cylinder, expansion degree $L = 2$ is not sufficient for accurate approximation of the rectangular parallelepiped.

Spherical Harmonics Application to Complex Particles

Spherical harmonics model can be applied to the complex shapes of the particle, for example, used in the food industry. There are several reasons why an accurate description of the shape of agricultural grains is desirable. Identification methods for variety classification or quality inspection (i. e., crushed, damaged, diseased, immature, or overmature) require an accurate description of the grain geometry. This is the main reason for applying spherical harmonics model to the grains (bean, chickpea and maize) presented in this chapter.

Parts of this chapter are published in Kačianauskas *et al.* (2015) and Radvilaitė *et al.* (2016).

4.1. Modification of the Modelling Technique

Spherical harmonics functions are a valuable technique for the representation of particles. Using this technique, the exact shape of a particle is represented as a spherical harmonic function of increasing accuracy (Feinauer *et al.* 2015). Usually, the limitation of this technique is that particles need to be star-like shaped to be described. Agricultural grains usually meet this requirement.

To obtain the spherical function that describes the shape of a grain, some initial geometric information is needed, i.e. the coordinates of a set of points on the surface of the grain that geometrically define the real shape and its characteris-

tics. These can be obtained by 3D scanning techniques. More recently, a technique based on X-ray micro-computed tomography has allowed the quantification and reconstruction of the 3D characteristics of particles and grains (Fonseca *et al.* 2012, 2013; Uday *et al.* 2013). However, this technique is highly sophisticated and requires a specialized operator; the cost is also an issue. Other 3D scanning techniques, still unexplored for this purpose, are becoming increasingly popular, easy-to-use, and low-cost, depending on the resolution of the scanning process. The most affordable and commonly used technologies to obtain 3D volumes are based on structured light and achieve resolutions of about 0.01 mm. Less accurate techniques include non-contact passive approaches such as stereoscopy, photometrics, and silhouettes. Passive 3D imaging solutions do not emit any kind of radiation themselves, but instead rely on detecting reflected ambient radiation. Most solutions of this type detect visible light, because it is a readily available ambient radiation. Other types of radiation, such as infrared, could also be used. Passive methods can be economical, because they generally do not need specialized hardware besides a simple digital camera. Using these techniques and computer-aided design programs, a set of points (commonly named a cloud) and their positions within a specific coordinate system are obtained. These clouds can be directly used for measurement and visualization.

The modelling technique for agricultural grains are almost the same as discussed in Chapter 2. However, here the division of the surface is introduced. Some changes in the mathematical approach is added. The whole surface S is divided into several parts, and each part is treated separately. Thus, the formula in Eq. (2.8) can be adjusted to read

$$A_i(\theta, \phi) \cong \begin{cases} \sum_{l=0}^L \sum_{m=-l}^l a_l^m Y_l^m(\varphi, \theta), & \text{when } (\theta, \phi) \in W_i, \\ 0, & \text{otherwise.} \end{cases} \quad (4.1)$$

The subscript i in Eq. (4.1) denotes the i^{th} part of the surface. The final analytical function of the surface is obtained by adding the separate functions for each part as

$$A(\theta, \phi) = \sum_{W_i \in W} \sum_{l=0}^L \sum_{m=-l}^l a_l^m Y_l^m(\varphi, \theta). \quad (4.2)$$

The surface is divided into smaller parts as follows. The initial points of the surface in Cartesian coordinates are transformed into spherical coordinates. All points are then within a range of $[0, 2\pi) \times [0, \pi]$. These two intervals are divided

into smaller parts containing different segments of the surface to be modelled. For example, if the number of segments is chosen to be 2 in each interval, the first interval $[0, 2\pi)$ is divided into $[0, \pi)$ and $[\pi, 2\pi)$. The same goes for the second: $[0, \frac{\pi}{2})$ and $[\frac{\pi}{2}, \pi]$. Therefore, the whole surface is divided into four segments: I $-[0, \pi) \times [0, \frac{\pi}{2})$, II $-[0, \pi) \times [\frac{\pi}{2}, \pi)$, III $-[\pi, 2\pi) \times [0, \frac{\pi}{2})$, and IV $-[\pi, 2\pi) \times [\frac{\pi}{2}, \pi]$. Different segments are shown in different colours in Fig. 4.1.

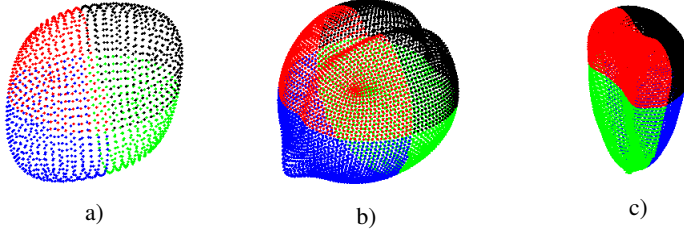


Fig. 4.1. The surface of particles divided into four segments: a) bean; b) chickpea; c) maize

4.2. Modelling of Bean Particle

Several particle shapes were described using the spherical harmonics technique. The first shape described was a type of bean with a smooth and convex shape, which is the simplest of the three models presented in this chapter. The initial dataset contained 1538 unique points. The example of the real particle and the surface points are given in Fig. 4.2a.



Fig. 4.2. Bean particle: a) the real shape; b) point cloud of the surface

For this model, the number of functions and segments were selected on a trial-and-error basis. The modelling process started using one function and one segment.

As the focus is on low-resolution spherical harmonics, the bean was modelled using four expansion degrees: $L = 0$, $L = 1$, $L = 2$ and $L = 3$. For each expansion degree the modelling process was started using the whole surface without any

division and increasing the number of segments yielded to more accurate approximation. The best model for each expansion degree is given in Fig. 4.3.

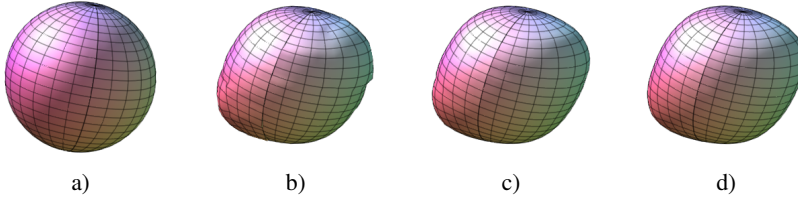
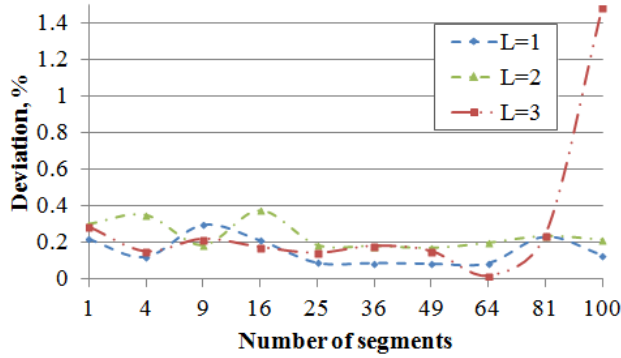
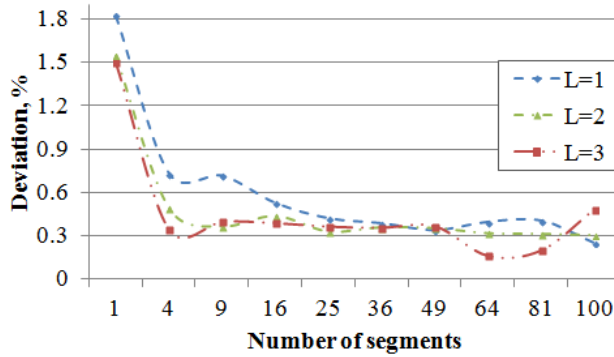


Fig. 4.3. The best spherical harmonics model of bean grain for each expansion expansion degrees: a) $L = 0, n_s = 1$; b) $L = 1, n_s = 49$; c) $L = 2, n_s = 25$; d) $L = 3, n_s = 16$



a)



b)

Fig. 4.4. Deviation of bean-like grain characteristics for different expansion degree with respect to number of segments: a) surface area; b) volume

To illustrate the modelling process, the results have been compared to the measured values from the initial geometrical data. The deviation of surface area (Eq. (2.27)) and volume (Eq. (2.34)) is illustrated by the graphs in Fig. 4.4. Here, the graphs are given for the number of segments till $n_s = 100$. The deviation of the surface area of the model with the expansion degree $L = 1$ and number of the segment $n_s = 49$ is equal to 0.08%, the deviation of the volume – 0.34%.

The deviation of the surface area of the model obtained with the expansion degree $L = 3$ and number of the segment $n_s = 16$ is equal to 0.18%, the deviation of the volume – 0.39%. Although the model with $n_s = 64$ segments shows better numerical performance, see Fig. 4.4, visually these two models looks the same. Taken into account, the more segment increase the complexity of the model, the simpler model having smaller number of segments is preferable.

4.3. Modelling of Chickpea Particle

The second shape to be described was the chickpea (Fig. 4.5a), which is more complex. This shape is concave and has a part with a special geometry that is characteristic of many agricultural grains, the tip cap.



Fig. 4.5. Chickpea particle: a) the real shape; b) point cloud of the surface

As the shape is more complex, the number of initial points (Fig. 4.5b) is bigger – 6146. Using the same modelling technique as for the bean particle, the surface is modelled by increasing the number of spherical harmonics and the surface sections.

As for the bean particle, the best spherical harmonics models of chickpea grain with different expansion degrees is presented in Fig. 4.6. The modelling is started with the sphere (Fig. 4.6a).

The quality of the models can be evaluate by the graphical figures, but it is quite subjective. The more accurate assessment can be obtained by comparing geometrical parameters. The deviations of the surface area and volume enabled numerical evaluation of the model.

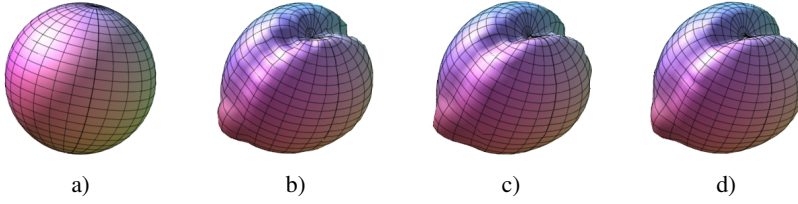
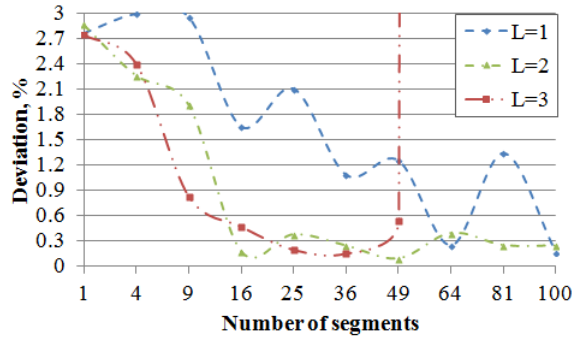
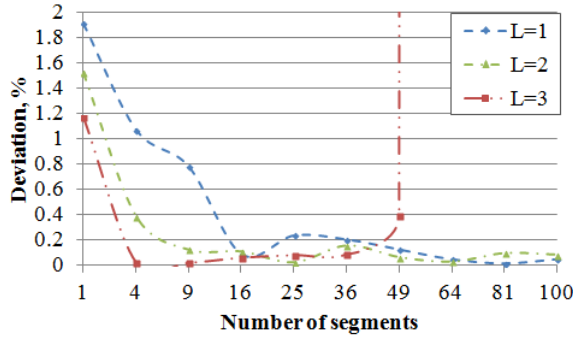


Fig. 4.6. Spherical harmonics reconstruction of chickpea grain with different expansion degrees: a) $L = 0$, $n_s = 1$; b) $L = 1$, $n_s = 100$; c) $L = 2$, $n_s = 49$; d) $L = 3$, $n_s = 25$



a)



b)

Fig. 4.7. Deviation of chickpea grain characteristics for different expansion degree with respect to number of segments: a) surface area; b) volume

The deviation of surface area and volume for different grain models is illustrated by the graphs in Fig. 4.7. The deviation of the surface area of the model with the expansion degree $L = 1$ and number of the segment $n_s = 100$ is equal to 0.16%, the deviation of the volume – 0.05%. The deviation of the surface area and

the volume of the model with the expansion degree $L = 3$ and number of the segment $n_s = 25$ is equal to 0.19% and 0.08%, respectively. Although the numerical evaluation for expansion degree $L = 3$ shows a little bit higher errors, visually the model looks more smooth (see, Fig. 4.6b and Fig. 4.6d).

4.4. Modelling of Maize Particle

The third shape selected was the shape of a grain of maize (Fig. 4.8a). This was the most complex of the three shapes, also having the tip cap as the shape of the chickpea.

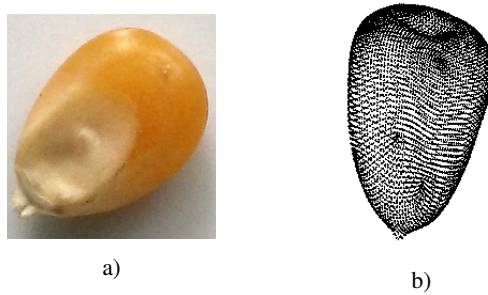


Fig. 4.8. Maize grain particle: a) the real shape; b) point cloud of the surface

The number of initial points was 6146. Applying the same modelling technique as for the two previous examples, the surface was modelled by selecting the appropriate number of spherical harmonics and surface segments.

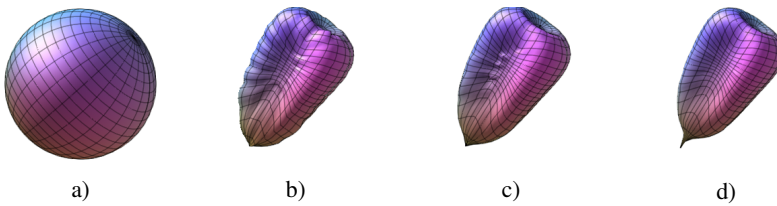
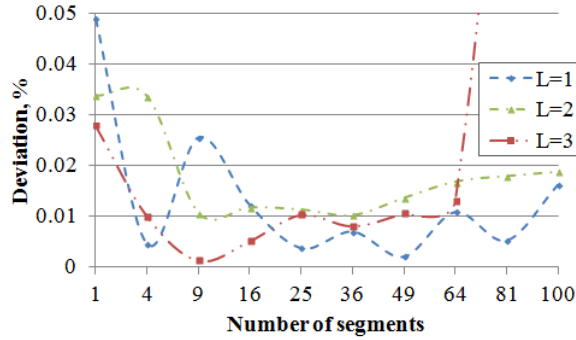


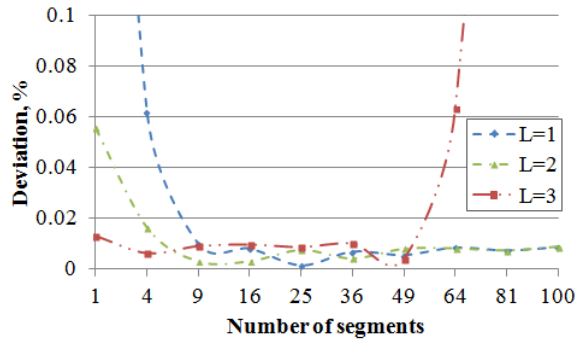
Fig. 4.9. Spherical harmonics reconstruction of maize grain with different expansion degrees: a) $L = 0$, $n_s = 1$; b) $L = 1$, $n_s = 81$; c) $L = 2$, $n_s = 49$; d) $L = 3$, $n_s = 36$

The spherical harmonics models of maize grain with different expansion degrees is presented in Fig. 4.9. The starting surface of modelling is sphere (Fig. 4.9a), same as for bean and chickpea.

The best maize grain model for each expansion degree was obtained. The deviation of the surface area and volume is given in Fig. 4.10.



a)



b)

Fig. 4.10. Deviation of maize grain characteristics for different expansion degree with respect to number of segments: a) surface area; b) volume

The deviation of the surface area and volume for each expansion degree is very similar – approximately 0.01% and 0.007%. Basically, the evaluation is done only visually, determining which model gives continuous and smoother surface.

4.5. Comparative Analysis of the Results

Although the complex shapes presented in this chapter was modelled using the division of the surface, it is interesting to see the results without the division. Such technique treats the surface as whole and do not divide it into smaller segments.

The modelling of the simple shapes (ellipsoid, cylinder or rectangular parallelepiped) without the division of the surface low-resolution spherical harmonics was suitable for the accurate approximation – ellipsoid was modelled with expan-

sion degree $L = 1$, cylinder and rectangular parallelepiped with $L = 3$. This low expansion degree can be used for modelling shapes as bean, chickpea or maize grain, but the division of the surface is needed. The results of the modelling without the division of the surface yielding to almost the same accuracy as modelling with the division of the surface is given in Table 4.1.

The given evaluation shows, that modelling of the bean particle without the division of the surface requires high resolution spherical harmonics, i.e. expansion degree $L = 7$, but with the division can be used $L = 3$ and the accuracy depends on the number of segments. The first case has total 64 coefficients and the second, when the division of the surface is used – 16 coefficients for each segment of the surface. Because the surface is divided into 9 segments, the total number of coefficients is $16 \cdot 9 = 144$. Comparing only the number of coefficients, it is obvious that the number of coefficients is smaller in the models without the division. However, considering such a model to be adapted into discrete element method simulation, the divisions of the surface could have some advantages.

Table 4.1. Comparison of the result with the division of the surface and without it

	Without division	Deviation, %	With division	Deviation, %
Bean	$L = 7$ (total 64 coeff.)	$\delta_S = 0.26$ $\delta_V = 0.37$	$L = 3$ (each 16 coeff.) $n_s = 9$	$\delta_S = 0.22$ $\delta_V = 0.40$
Chickpea	$L = 15$ (total 256 coeff.)	$\delta_S = 0.25$ $\delta_V = 0.09$	$L = 3$ (each 16 coeff.) $n_s = 25$	$\delta_S = 0.19$ $\delta_V = 0.08$
Maize	$L = 20$ (total 441 coeff.)	$\delta_S = 0.016$ $\delta_V = 0.05$	$L = 3$ (each 16 coeff.) $n_s = 36$	$\delta_S = 0.008$ $\delta_V = 0.01$

Modelling the contact with the discrete element method requires the search for the contact point and using the appropriate algorithm the contact area could be distinguished. So for the calculations all 64 coefficients would be needed if the model has been created without the division of the surface. Thus using the division of the surface and having the contact area, the number of coefficients can be decreased. For the calculation could be needed only the coefficients of the one or two segments. In such a manner the calculation of contact could be improved, especially for the cases of complex shapes as chickpea or maize grain.

4.6. Conclusions of Chapter 4

1. This chapter presented the result of modelling the complex shapes. The chosen shapes differed in complexity: the first shape was the simplest of all grains in the chapter. The shape of bean is smooth and convex. The modelling technique was used with the division of the surface. In order to get the most accurate model, the segments of the surface were increased hierarchically for each expansion degree. The numerical evaluation of the model was based on the deviation of the surface area and volume. The best model was obtained with the expansion degree $L = 3$ and the number of segments 9. Thus, the deviation of the surface area and volume was 0.22% and 0.4%, respectively.
2. The chickpea shape is concave and has a part with a special geometry that is characteristic of many agricultural grains, the tip cap. As the shape is more complex, the number of initial point is bigger as well. Thus it was used more segments, that divided the whole surface into smaller parts. The best model was obtained with the expansion degree $L = 3$ and the number of segments 25. The deviation of the surface area was 0.19%, the deviation of the volume – 0.08%. Considered only the deviation of the volume the model of the chickpea could be better with lower expansion degree. The surface area in that case is quite big, so the evaluation of the model is composed of two parts – numerical and graphical analysis.
3. The shape of a maize grain was the most complex of the three shapes having the concave shape and tip cap similar to chickpea. The modelling technique was the same as in the previous cases. The best model was obtained with expansion degree $L = 3$ and the number of segments – 36. The deviation of this model was small: the difference of the surface area – 0.008%, the volume – 0.01%.
4. The results when modelling with the division of the surface and without, allows to compare two modelling approaches. The high expansion degree when modelling complex shapes, such as bean, chickpea and maize grain, is required in order to get the accurate approximation of the particle. The division of the surface can decrease the expansion degree, thus the number of spherical harmonics used. Such modelling technique with the division into smaller segments could be the advantage in the discrete element method calculations of the contact.

General Conclusions

1. Performed review on particle shapes and their description methods revealed that there is not yet developed a versatile analytical description method for non-spherical particles. Known semi-analytical method of spherical harmonics is potentially suitable method for solving this problem. The performance of this approach should be based, however, on research results.
2. The semi-analytical model of particle shape is elaborated on the basis of real part of complex spherical harmonics series. The aim is to model the simplest symmetric star-shaped (radially convex) particles. A characteristic exclusiveness of this model – determination of coefficients by the least squares method and the pseudo-inverse computational procedure.
3. To evaluate the quality of developed spherical harmonics expansion various positioning strategies of the sampling points were suggested and tested numerically. It was found that a rational compromise between the numerical accuracy and computational expenses is achieved by applying locally adaptive strategies.
4. The developed spherical harmonics expressions are enhanced by integration and differentiation techniques. They are applied for evaluation of the most important integral characteristics such as particle volume, surface

area and inertia moments. Calculation of the second order derivatives is applied for curvature radii required in calculation of contacts. The values are compared with the results of finite element method – the difference is 0.3%.

5. A general spherical harmonics model was explored for development of particular low-resolution harmonics model. A unified version limited with the expansion degree $L \leq 3$ was further applied for construction of primitive but widespread oblate industrial shapes such as ellipsoid of revolution, circular cylinder and rectangular parallelepiped. The suitability of the low-resolution harmonics was demonstrated. This method is very sensitive to positioning of sampling points, and, approximation quality is increased by applying locally adaptive positioning strategies.
6. On the basis of numerical results obtained, several tendencies have been observed. Comprehensive study was performed by considering prolate shapes with elongation ratio equal to 0.5. Numerical results showed that a good approximation of an ellipsoid is obtained with expansion degree $L = 1$ while the cylinder and parallelepiped requires $L = 3$. The volume of ellipsoid is described with 0.8%, cylinder with 0.004% and parallelepiped with 0.18% error. The surface area of ellipsoid is described with 0.15%, cylinder with 0.37% and parallelepiped with 2.4% error. The least square error norm for ellipsoid is achieved with 0.25% accuracy while cylinder and parallelepiped are characterized with 2.2% and 2.0% accuracy.
7. It was found, however, that refinement of the density of sampling points has a tendency to improve the values of the global descriptors but increasing the error of local deviations. On the other hand, it was shown that the increase of local error may have insignificant or, in opposite, positive consequences. Local internal deviations yielding non-convex indentations may be not taken into accounts, while smooth approximation of sharp edges plays positive role giving the idea how to eliminate unrealistic effects of the local concentrators.
8. The modelling technique was used for modelling the complex shaped agricultural grains such as bean, characterised by smooth and convex shape, the chickpea, which is more complex concave, and the maize grain having the concave shape and tip cap similar to chickpea. The best model of a bean was obtained with the expansion degree $L = 3$ and the number of segments 9. Thus, the deviation of the surface area and volume was 0.22%

and 0.4%, respectively. The best results for modelling a chickpea was obtained with the expansion degree $L = 3$ and the number of segments 25. The deviation of the surface area was 0.19%, the deviation of the volume – 0.08%. The maize model was obtained with expansion degree $L = 3$ and the number of segments – 36, where the difference of the surface area is 0.008% and the volume – 0.01%.

References

- Abbaspour-Fard, M. H. 2004. Theoretical validation of a multi-sphere, discrete element model suitable for biomaterials handling simulation, *Biosystems Engineering* 88(2), 153–161.
- Abdallah, A. B.; Ghorbel, F.; Chatti, K.; Essabbah, H.; Bedoui, M. H. 2010. A new uniform parametrization and invariant 3D spherical harmonic shape descriptors for shape analysis of the heart's left ventricle – a pilot study, *Pattern Recognition Letters* 31(13): 1981–1990.
- Agnolin, I.; Roux, J.-N. 2008. On the elastic moduli of three-dimensional assemblies of spheres: Characterization and modeling of fluctuations in the particle displacement and rotation, *International Journal of Solids and Structures* 45(3–4): 1101–1123.
- Alonso-Marroquín, F.; Ramírez-Gómez, Á.; González-Montellano, C.; Balaam, N.; Hanaor, D.A.H.; Flores-Johnson, E.A.; Gan, Y.; Chen, S.; Shen, L. 2013. Experimental and numerical determination of mechanical properties of polygonal wood particles and their flow analysis in silos, *Granular Matter* 15(6): 811–826.
- Amaratunga, K.; Castrillon-Candas, J. E. 2001. Surface wavelets: A multiresolution signal processing tool for 3D computational modelling, *International Journal for Numerical Methods in Engineering*, 52: 239–271.
- Arasan, S.; Akbulut, S.; Hasiloglu, A. S. 2011. The relationship between the fractal dimension and shape properties of particles, *KSCE Journal of Civil Engineering*, 15(7): 1219–1225.

- Balevičius, R.; Kačianauskas, R.; Mróz, Z.; Sielamowicz, I. 2011. Analysis and DEM simulation of granular material flow patterns in hopper models of different shapes, *Advanced Powder Technology*, 22(2): 226–235.
- Blott, S. J.; Pye, K. 2008. Particle shape: a review and new methods of characterization and classification, *Sedimentology*, 55: 31–63.
- Boon, C. W.; Houlsby, G. T.; Utili, S. 2012. A new algorithm for contact detection between convex polygonal and polyhedral particles in the discrete element method, *Computers and Geotechnics*, 44: 73–82.
- Boon, C. W.; Houlsby, G. T.; Utili, S. 2013. A new contact detection algorithm for three-dimensional non-spherical particles, *Powder Technology*, 248: 94–102.
- Bräuer, K.; Pfitzner, M.; Krimer, D. O.; Mayer, M.; Jiang, Y.; Liu, M. 2006. Granular elasticity: Stress distributions in silos and under point loads, *Physical Review E*, 74(6): 061311.
- Bullard, J. W.; Garboczi, E. J. 2013. Defining shape measures for 3D star-shaped particles: sphericity, roundness and dimensions, *Powder Technology*, 249: 241–252.
- Chen, J.; Schinner, A.; Matuttis, H. 2011. Discrete element simulation for polyhedral granular particles, *Theoretical and Applied Mechanics Japan*, 59: 335–346.
- Cleary, P.W. 2008. The effect of particle shape on simple shear flows. *Powder Technology*, 179(3):144–163.
- Courrieu, P. 2008. Fast Computation of Moore-Penrose Inverse Matrices, *Neural Information Processing – Letters and Reviews*, 8(2): 25–29.
- Cundall, P. A. 1988. Formulation of a three-dimensional distinct element model – part 1. A scheme to detect and represent contacts in a system composed of many polyhedral blocks, *International Journal of Rock Mechanics and Mining Sciences*, 25(3): 107–116.
- Džiugys, A.; Peters, B. 2001. An approach to simulate the motion of spherical and non-spherical fuel particles in combustion chambers, *Granular matter* 3 (4): 231–265.
- Feinauer, J.; Spettl, A.; Manke, I.; Strege, S.; Kwade, A.; Pott, A.; Schmidt, V. 2015. Structural characterization of particle systems using spherical harmonics, *Materials Characterization*, 106: 123–133.
- Fonseca, J.; O’Sullivan, C.; Coop, M. R.; Lee, P. D. 2012. Non-invasive characterization of particle morphology of natural sands, *Soils and Foundations* 52(4): 712–722.
- Fonseca, J.; Bésuelle, P.; Viggiani, G. 2013. Micromechanisms of inelastic deformation in sandstones: an insight using x-ray micro-tomography, *Géotechnique Letters* 3 (2): 78–83.
- Galindo-Torres, S. A.; Alonso-Marroquín, F.; Wang, Y. C.; Pedroso, D.; Muñoz Castaño, J. D. 2009. Molecular dynamics simulation of complex particles in three dimensions and the study of friction due to nonconvexity, *Physical Review E*, 79(6): 060301.

- Galindo-Torres, S. A.; Muñoz, J. D.; Alonso-Marroquín, F. 2010. Minkowski-Voronoi diagrams as a method to generate random packings of spheropolygons for the simulation of soils, *Physical Review E*, 82(5): 056713.
- Galindo-Torres, S. A.; Pedroso, D. M. 2010. Molecular dynamics simulations of complex-shaped particles using Voronoi-based spheropolyhedra, *Physical Review E*, 81(6 Pt 1): 1–9.
- Galindo-Torres, S. A.; Pedroso, D. M. 2012. Breaking processes in three-dimensional bonded granular materials with general shapes. *Computer Physics Communications*, 183(2): 266–277.
- Garboczi, E. J. 2002. Three-dimensional mathematical analysis of particle shape using X-ray tomography and spherical harmonics: Application to aggregates used in concrete, *Cement and Concrete Research*, 32(10): 1621–1638.
- Garboczi, E. J. 2011. Three dimensional shape analysis of JSC-1A simulated lunar regolith particles, *Powder Technology*, 207(1–3): 96–103.
- González-Montellano, C.; Fuentes, J. M.; Ayuga-Téllez, E.; Ayuga, F. 2012. Determination of the mechanical properties of maize grains and olives required for use in DEM simulations, *Journal of Food Engineering*, 111 (4): 553–562.
- Harkness, J. 2009. Potential particles for the modeling of interlocking media in three dimensions, *International Journal for Numerical Methods in Engineering*, 80(12): 1573–1594.
- Harris, W. F. 2006. Curvature of ellipsoids and other surfaces, *Ophthalmic and Physiological Optics*, 26(5): 497–501.
- Höhner, D.; Wirtz, S.; Kruggel-Emden, H.; Scherer, V. 2011. Comparison of the multi-sphere and polyhedral approach to simulate non-spherical particles within the discrete element method: influence on temporal force evolution for multiple contacts, *Powder Technology*, 208(3): 643–656.
- Höhner, D.; Wirtz, S.; Scherer, V. 2012. A numerical study on the influence of particle shape on hopper discharge within the polyhedral and multi-sphere discrete element method, *Powder Technology*, 226: 16–28.
- Höhner, D.; Wirtz, S.; Scherer, V. 2013. Experimental and numerical investigation on the influence of particle shape and shape approximation on hopper discharge using the discrete element method, *Powder Technology*, 235: 614–627.
- Höhner, D.; Wirtz, S.; Scherer, V. 2014. A study on the influence of particle shape and shape approximation on particle mechanics in a rotating drum using the discrete element method *Powder Technology*, 253: 256–265.
- Horabik, J.; Parafiniuk, P.; Molenda, M. 2016. Experiments and discrete element method simulations of distribution of static load of grain bedding at bottom of shallow model silo, *Biosystems Engineering*, 149: 60–71.

- Houlsby, G. T. 2009. Potential particles: a method for modeling non-circular particles in DEM, *Computers and geotechnics*, 36(6): 953–959.
- Jalaal, M.; Ganji, D. D.; Ahmadi, G. 2012. An analytical study on settling of non-spherical particles, *Asia-Pacific Journal of Chemical Engineering*, 7(1): 63–72.
- Jha, A. K.; Gill, J. S.; Puri, V. M. 2008. Percolation segregation in binary size mixtures of spherical and angular-shaped particles of different densities, *Particulate Science and Technology*, 26(5): 482–493.
- Jiang, Y.; Liu, M. 2007. A brief review of “granular elasticity” – Why and how far is sand elastic?, *The European Physical Journal E*, 22 (3): 255–260.
- Jiang, Y.; Liu, M. 2008. Incremental stress-strain relation from granular elasticity: Comparison to experiments, *Physical Review E*, 77 (2): 021306.
- Jiang, Y.; Liu, M. 2009. Granular solid hydrodynamics, *Granular Matter*, 11 (3): 139–156.
- Jin, F.; Xin, H.; Zhang, C.; Sun, Q. 2011. Probability-based contact algorithm for non-spherical particles in DEM, *Powder Technology*, 212(1): 134–144.
- Johnson, K. L. 1987. *Contact mechanics*. Cambridge University Press. First edition. 452 p.
- Johnson, S.; Williams, J. R.; Cook, B. 2004. Contact resolution algorithm for an ellipsoid approximation for discrete element modeling, *Engineering Computations*, 21(2/3/4): 215–234.
- Johnson, S. M.; Williams, J. R. 2009. Sub-discretized surface model with application to contact mechanics in multi-body simulation, *Powder Technology*, 193(3): 319–331.
- Kačianauskas, R.; Tumonis, L.; Džiugys, A. 2014. Simulation of the normal impact of randomly shaped quasi-spherical particles, *Granular Matter*, 16(3): 339–247.
- Keys, A. S.; Iacovella, C. R.; Glotzer, S. C. 2011. Characterizing complex particle morphologies through shape matching: Descriptors, applications and algorithms, *Journal of Computational Physics*, 230(17): 6438–6463.
- Kock, I.; Huhn, K. 2007. Influence of particle shape on the frictional strength of sediments – A numerical case study. *Sedimentary Geology*, 196(1–4): 217–233.
- Kodam, M.; Bharadwaj, R.; Curtis, J.; Hancock, B.; Wassgren, C. 2009. Force model considerations for glued-sphere discrete element method simulations, *Chemical Engineering Science*, 64(15): 3466–3475.
- Kodam, M.; Bharadwaj, R.; Curtis, J.; Hancock, B.; Wassgren, C. 2010. Cylindrical object contact detection for use in discrete element method simulations. Part I – Contact detection algorithms, *Chemical Engineering Science*, 65(22): 5852–5862.

- Krimer, D. O.; Pfitzner, M.; Bräuer, K.; Jiang, Y.; Liu, M. 2006. Granular elasticity: General considerations and the stress dip in sand piles, *Physical Review E*, 74(6): 061310.
- Kruggel-Emden, H.; Simsek, E.; Rickelt, S.; Wirtz, S.; Scherer, V. 2007. Review and extension of normal force models for the Discrete Element Method, *Powder Technology*, 171(3): 157–173.
- Kruggel-Emden, H.; Rickelt, S.; Wirtz, S.; Scherer, V. 2008. A study on the validity of the multi-sphere Discrete Element Method, *Powder Technology*, 188(2): 153–165.
- Laplace, P. S.; Bowditch, N. 1829 *Mécanique Céleste*. Boston: The Press of Isaac R. Butts. English edition. 748 p.
- Liu, X.; Garboczi, E. J.; Grigoriu, M.; Lu, Y.; Erdogan, S. T. 2011. Spherical harmonic-based random fields based on real particle 3D data: Improved numerical algorithm and quantitative comparison to real particles, *Powder Technology*, 207 (1–3): 78–86.
- Lu, G.; Third, J. R.; Muller, C. R. 2015. Discrete element models for non-spherical particle systems: From theoretical developments to applications, *Chemical Engineering Science*, 127: 425–465.
- Mallat, S. G. 1989. A Theory for Multiresolution Signal Decomposition: The Wavelet Representation, *IEEE Transactions on Pattern Analysis and Machine Intelligence*, 11: 674–693.
- Markauskas, D.; Kačianauskas, R.; Džiugys, A.; Navakas, R. 2010. Investigation of adequacy of multi-sphere approximation of elliptical particles for DEM simulations, *Granular Matter*, 12(1): 107–123.
- Markauskas, D.; Ramírez-Gómez, Á.; Kačianauskas, R.; Zdancevičius, E. 2015. Maize grain shape approaches for DEM modelling, *Computers and Electronics in Agriculture*, 118: 247–258.
- Masad, E.; Saadeh, S.; Al-Rousan, T.; Garboczi, E.; Little, D. 2005. Computations of particle surface characteristics using optical and X-ray CT images, *Computational Materials Science*, 34: 406–424.
- Mellmann, J.; Hoffman, T.; Füll, C. 2014. Mass flow during unloading of agricultural bulk materials from silos depending on particle form, flow properties and geometry of the discharge opening, *Powder Technology*, 253: 46–52.
- Mofrad, F. B.; Zoroofi, R. A.; Tehrani-Fard, A. A.; Akhlaghpour, S.; Sato, Y. 2014. Classification of normal and diseased liver shapes based on spherical harmonics coefficients, *Journal of Medical Systems*, 38(5): 1–9.
- Møller, P. C. F.; Bonn, D. 2007. The shear modulus of wet granular matter, *EPL (Europhysics Letters)*, 80(3): 38002.
- Mollon, G.; Zhao, J. 2012. Fourier-Voronoi-based generation of realistic samples for discrete modeling of granular materials, *Granular Matter*, 14(5): 621–638.

- Mollon, G.; Zhao, J. 2013. Generating realistic 3D sand particles using Fourier descriptors, *Granular Matter*, 15(1): 95–108.
- Mollon, G.; Zhao, J. 2014. 3D generation of realistic granular samples based on random fields theory and Fourier shape descriptors, *Computer Methods in Applied Mechanics and Engineering*, 279: 46–65.
- Morris, R. J.; Najmanovich, R. J.; Kahmaran, A.; Thorton, J. M. 2005. Real spherical harmonic expansion coefficients as 3D shape descriptors for protein binding pocket and ligand comparisons, *Bioinformatics*, 21(10): 2347–2355.
- Mouse, M.-H.; Chaine, R.; Akkouché, S.; Galin, E. 2008. Toward an efficient triangle-based spherical harmonics representation of 3D objects, *Computer aided geometric design*, 25(8): 561–575.
- Nezami, E. G.; Hashash, Y. M. A.; Zhao, D.; Ghaboussi, J. 2004. A fast contact detection algorithm for 3-D discrete element method, *Computers and Geotechnics*, 31: 575–587.
- Nouguier-Lehon, C.; Cambou, B.; Vincens, E. 2003. Influence of particle shape and angularity on the behaviour of granular materials: a numerical analysis. *International Journal for Numerical and Analytical Methods in Geomechanics*, 27(14): 1207–1226.
- Novotni, M.; Klein, R. 2004. Shape retrieval using 3D Zernike descriptors, *Computer-Aided Design*, 36(11): 1047–1062.
- Ouadfel, H.; Rothenburg, L. 1999. An algorithm for detecting inter-ellipsoid contacts, *Computers and Geotechnics*, 24(4): 245–263.
- Parafiniuk, P.; Molenda, M.; Horabik, J. 2013. Discharge of rapeseeds from a model silo: Physical testing and discrete element method simulations, *Computers and Electronics in Agriculture*, 97: 40–46.
- Parafiniuk, P.; Molenda, M.; Horabik, J. 2014. Influence of particle shape and sample width on uniaxial compression of assembly of prolate spheroids examined by discrete element method. *Physica A: Statistical Mechanics and its Applications*, 416: 279–289.
- Peña, A. A.; García-Rojo, R.; Herrmann, H. J. 2006. Influence of particle shape on sheared dense granular media, *Granular Matter*, 9(3–4): 279–291.
- Peña, A. A.; McNamara, S.; Lind, P. G.; Herrmann H. J. 2009. Avalanches in anisotropic sheared granular media. *Granular Matter*, 11(4): 243–252.
- Poelaert, D.; Schniewind, J.; Janssens, F. 2011. Surface Area and Curvature of the general Ellipsoid, arXiv:1104.5145 [math.CA].
- Razzaghi, P.; Palhang, M.; Gheissari, N. 2013. A new invariant descriptor for action recognition based on spherical harmonics, *Pattern Analysis and Applications*, 16(4): 507–518.

- Ritchie, D. W.; Kemp, G. J. L. 1999. Fast Computation, Rotation, and Comparison of Low Resolution Spherical Harmonic Molecular Surfaces, *Journal of Computational Chemistry*, 20(4): 383–395.
- Rokhlin, V.; Tygert, M. 2006. Fast algorithms for spherical harmonic expansions, *SIAM Journal on Scientific Computing*, 27(6): 1903–1928.
- Santamarina, J.; Cho, G. 2004. Soil behaviour: The role of particle shape. *Advances in Geotechnical Engineering. Proceedings of the Skempton Conference*, 1–14.
- Santhanam, A. P.; Min, Y.; Mudur, S.P.; Rastogi, A.; Ruddy, B.H.; Shah, A.; Divo, E.; Hassab, A.; Roll, J. P.; Kupelian, P. 2010. An inverse hyper-spherical harmonics-based formulation for reconstructing 3D volumetric lung deformations, *Comptes Rendus Mécanique*, 338(7–8): 461–473.
- Shen, L.; Farid, H.; McPeck, M. A. 2009. Modeling three-dimensional morphological structures using spherical harmonics, *Evolution*, 63(4): 1003–1016.
- Soga, K.; Bowman, E. T.; Drummond, W. 2005. Particle shape characterisation using Fourier descriptor analysis, *Géotechnique*, 51(6): 545–554.
- Szarf, K.; Combe, G.; Villard, P. 2011. Polygons vs. clumps of discs: a numerical study of the influence of grain shape on the mechanical behaviour of granular materials, *Powder Technology*, 208(2): 279–288.
- Tangelder, J. W. H.; Velt mp, R. C. 2008 A survey of content based 3D shape retrieval methods, *Multimedia Tools and Applications*, 39(3): 441–471.
- Thomson, W.; Tait, P. G. 1867. *Treatise on natural philosophy*. Oxford University Press 508 p.
- Uday, K. V.; Padmakumar, G. P.; Singh, D. N. 2013. Some studies on morphology of the coarse-grained soils, *Engineering Geology*, 152(1): 48–55.
- Wellmann, C.; Lillie, C.; Wriggers, P. 2008. A contact detection algorithm for superellipsoids based on the common-normal concept, *International Journal for Computer-Aided Engineering and Software*, 25(5): 432–442.
- Wynn, E. J. W. 2009. Simulations of rebound of an elastic ellipsoid colliding with a plane, *Powder Technology*, 196(1): 62–73.
- Zhang, D.; Lu, G. 2004. Review of shape representation and description techniques, *Pattern Recognition*, 37(1): 1–19.
- Zhang, L.; da Fonseca, M. J.; Ferreira, A. 2007. Survey on 3D shape descriptors, Technical Report, DecorAR (FCT POSC/EIA/59938/2004).
- Zheng, Q. J.; Zhou, Z. Y.; Yu, A. B. 2013. Contact forces between viscoelastic ellipsoidal particles, *Powder Technology*, 248: 25–33.

Zhong, W.; Yu, A.; Liu, X.; Tong, Z.; Zhang, H. 2016. DEM/CFD-DEM Modelling of Non-spherical Particulate Systems: Theoretical Developments and Applications, *Powder Technology*, 302: 108–152.

Zhou, B.; Wang, J.; Zhao, B. 2015. Micromorphology characterization and reconstruction of sand particles using micro X-ray tomography and spherical harmonics, *Engineering Geology*, 184: 126–137.

List of Publications by the Author on the Topic of the Dissertation

Papers in the Reviewed Scientific Journals

Radvilaitė, U. 2014. Sferinių harmoninių funkcijų taikymas kubo formos dalelei aprašyti. *Mokslas – Lietuvos ateitis = Science – future of Lithuania: Mechanika, medžiagų inžinerija, pramonės inžinerija ir vadyba = Mechanics, material science, industrial engineering and management*. Vilnius: Technika. ISSN 2029-2341. T. 6, nr. 6, p. 682–685.

Radvilaitė, U.; Ramírez-Gómez, Á.; Kačianauskas, R. 2016. Determining the shape of agricultural materials using spherical harmonics. *Computers and Electronics in Agriculture*. Oxford: Elsevier. ISSN 0168-1699. Vol. 128, p. 160–171 (ISI Web of Science).

Radvilaitė, U.; Kačianauskas, R.; Rusakevičius, D. 2017. Investigation of symmetric non-spherical particle shapes by applying low-resolution spherical harmonics Nonlinear Analysis: Modelling and Control. ISSN 1392-5113. Vol. 22, no. 1, p. 155–133 (ISI Web of Science).

Other Papers

Kačianauskas, R.; Ramírez-Gómez, Á.; Radvilaitė, U. 2015. Semi-analytical model for non-spherical particles. *Proceedings of international conference on numerical analysis and applied mathematics 2014 (ICNAAM-2014), Rhodes, Greece, 22–28 September 2014*. Melville: AIP Publishing. ISSN 0094-243X, ISBN 9780735412873. Vol. 1648, p. 1–4.

Radvilaitė, U.; Kačianauskas, R.; Rusakevičius, D. 2015. Application of spherical harmonics to description of non-spherical particles. *OAS 2015: proceedings of the 3rd international conference Optimization and Analysis of Structures, August 23–25, 2015 Tartu, Estonia*. Editors: J. Lellep, E. Puman. Tartu: University of Tartu. ISSN 2461-2677. p. 98–103.

Summary in Lithuanian

Įvadas

Problemos formulavimas

Nemažai reiškinių, vykstančių gamtoje ar modeliuojamų pramonėje, aprašomi kaip birios medžiagos ar dalelių sistemos, kurios sudarytos iš daugelio atskirų dalelių. Kai kurias medžiagas, sudarytas iš nedidelio skaičiaus dalelių, galima tirti atliekant eksperimentus, tačiau dauguma atvejų eksperimentus vykdyti yra brangu. Medžiagų, sudarytų iš daugybės dalelių, modeliavimui pasitelkiami skaitiniai metodai, kuriuose labai svarbu kuo tiksliau aproksimuoti dalelių formą.

Birios medžiagos yra svarbios beveik visose mokslo ir technologijų srityse, todėl jos sudaro didžiulę medžiagų klasę, plačiai taikomų chemijos, farmacijos, maisto ir kt. pramonės srityse. Nesvarbu kur ir kaip jos taikomos (birių medžiagų transportavimas ar įvairūs technologiniai procesai), jose esančių dalelių dydis ir forma įtakoja modeliavimo ir skaičiavimo rezultatus.

Dalelės forma labai svarbi mechaninei birių medžiagų elgsenai, įtakojanti įvairius medžiagos rodiklius. Dalelės tūris ir forma yra svarbūs rodikliai sprendžiant pakavimo uždavinius, o lokalūs kampuotumai turi įtakos kontakto taško paieškai ir kontakto jėgų skaičiavimui. Bendruoju atveju, teisingas dalelių formos aprašymas lemia sprendžiamo mechanikos uždavinio rezultatų tikslumą.

Darbo aktualumas

Dauguma realių dalelių yra nesferinės, o metodų tokioms formos aprašyti nėra daug. Išskiriami du pagrindiniai būdai nesferinių formų dalelėms aprašyti: monomerinis ir kompozitinis. Glotnių tolydžių formų (elipsoidų, super-elipsoidų ar super-kubų) naudojimas apsunkina kontakto rodiklių skaičiavimus, nes kontakto taško paieškai tenka keletą kartų spręsti netiesinių lygčių sistemą. Kompozitinis būdas gali būti naudojamas bet kokios formos netaisyklingos geometrijos kūnui, tačiau šiuo atveju kontaktui aprašyti reikalingi specialūs metodai.

Kadangi nėra jokio vieningo metodo tiek dalelių formų aprašymui, tiek kontakto taško paieškos ir rodiklių skaičiavimui, šiame darbe nagrinėjamas metodas, naudojantis sferines harmonikas, kurių naudojant galima suvienodinti dalelės formos aprašymo metodiką bet kokiai formai.

Tyrimo objektas

Darbo tyrimų objektas yra nesferinės formos dalelės ir jų kuo tikslesnis aprašymas taikant sferines harmonikas.

Darbo tikslas

Šio darbo tikslas – sukurti sferinių harmonikų modelį, aprašantį nesferinės formos daleles, ir ištirti žemo laipsnio sferinių harmonikų tinkamumą įvairių nesferinės formos dalelių aprašymui.

Darbo uždaviniai

Darbo tikslui pasiekti reikia spręsti šiuos uždavinius:

1. Atlikti literatūros analizę dalelių formos aprašymui taikomų metodų ir sferinių harmonikų tematika.
2. Sudaryti matematinį modelį, naudojant žemo laipsnio ($L \leq 3$) sferines harmonikas.
3. Ištirti modelio tinkamumą taikant sferinių harmonikų modelį paprastoms simetrinėms (elipsoidinėms, cilindrinėms ir daugiasienėms) dalelėms.
4. Pritaikyti sferinių harmonikų modelį sudėtingos formos dalelių aprašymui.

Tyrimų metodika

Darbe taikomi matematinio ir skaitinio modeliavimo metodai.

Mokslinis naujumas

Rengiant disertaciją buvo gauti šie mechanikos inžinerijos mokslui nauji rezultatai:

1. Pasiūlytas pusiau analitinis sferinių harmonikų modelis dalelės formai aprašyti. Modelio koeficientams apskaičiuoti naudojamas mažiausių kvadratų metodas, ir pseudo-atvirkštinės matricos skaičiuojamoji procedūra.
2. Koeficientams rasti pritaikytos įvairios taškų pozicionavimo strategijos, įvertinančios paviršiaus kampuotumą.
3. Šio metodo tinkamumas ištirtas taikant jį paprastoms simetrinėms dalelėms ir skaičiuojant paviršiaus ploto ir tūrio įverčius. Šiame darbe pateikti rezultatai parodo, kad žemo laipsnio sferinių harmonikų skleidinys (iki $L = 3$) gerai aproksimuoja nesferinės formos daleles.
4. Modelis pritaikytas sudėtingoms neiškilios formos dalelėms. Sudėtingesnėms formoms modeliuoti įvedamas paviršiaus dalijimas į smulkesnes dalis, leidžiantis sumažinti skleidinio laipsnį.

Darbo rezultatų praktinė reikšmė

Pasiūlytas sferinių harmonikų metodas gali būti taikomas bet kokių formų dalelėms aproksimuoti. Tokiu būdu aproksimuotos dalelės aprašomos viena analitine funkcija, kurią vėliau galima naudoti įvairiems rodikliams skaičiuoti (integruojant gaunami paviršiaus plotas, tūris ar inercijos momentai, diferencijuojant – normalė ir kreivis) ar taikyti kontakto jėgų skaičiavimuose.

Ginamieji teiginiai

1. Žemo laipsnio sferinės harmonikos yra tinkamas įrankis aprašyti apvalių ir kampuotų vienodų matmenų dalelių formai, kurio tikslumas mažėja keičiantis dalelės matmenų santykiui.
2. Mažiausių kvadratų metodo kartu su adaptyviomis strategijomis taikymas iki dvejų kartų padidina sferinių harmonikų metodo tikslumą.

3. Sudėtingų formų dalelių taikymams sferinių harmonikų modelis naudojamas kartu su paviršiaus dalijimu leidžia taikyti žemo laipsnio harmonikas.

Darbo rezultatų aprobavimas

Disertacijos tema paskelbti 5 straipsniai: du – mokslo žurnaluose, įtraukuose į Thomson ISI sąrašą (Radvilaitė *emphet al.* 2016, 2017), vienas – konferencijų medžiagoje, referuotose Thomson ISI Proceedings duomenų bazėje (Kačianauskas *et al.* 2015), vienas – kitų tarptautinių duomenų bazių cituojamame žurnale (Radvilaitė *et al.* 2014), vienas – recenzuojamoje tarptautinės konferencijos medžiagoje (Radvilaitė *et al.* 2015).

Disertacijoje atliktų tyrimų rezultatai buvo paskelbti aštuoniose mokslinėse konferencijose Lietuvoje ir užsienyje:

- Jaunųjų mokslininkų konferencijoje „Fizinių ir technologijos mokslų tarpdalykiniai tyrimai“, 2014 m. vasario 11 d., Vilniuje;
- XXII-ajame Lietuvos skaičiuojamos mechanikos asociacijos seminare, 2014 m. balandžio 25 d., Vilniuje;
- Tarptautinėje konferencijoje „Numerical Analysis and Applied Mathematics (ICNAAM)“, 2014 m. rugsėjo 22–28 d., Rode, Graikijoje;
- XXIII Lietuvos skaičiuojamosios matematikos seminare, 2015 m. balandžio 24 d., Vilniuje;
- Tarptautinėje konferencijoje „Optimization and Analysis of Structures (OAS 2015)“, 2015 m. rugpjūčio 23–25 d., Tartu, Estijoje;
- Tarptautinėje konferencijoje „3rd Polish Congress of Mechanics and 21st Computer Methods in Mechanics (PCM-CMM 2015)“, 2015 m. rugsėjo 8–11 d., Gdanske, Lenkijoje;
- XXIV Lietuvos skaičiuojamosios matematikos seminare, 2016 m. balandžio 20 d., Vilniuje;
- Tarptautinėje konferencijoje „Modern Building Materials, Structures and Techniques (MBMST 2016)“, 2016 m. gegužės 26–27 d., Vilniuje.

Disertacijos struktūra

Disertaciją sudaro įvadas, keturi skyriai ir bendrosios išvados. Taip pat yra penki priedai. Darbo apimtis yra 126 puslapiai, neskaitant priedų, tekste panaudotos 62

numeruotos formulės, 31 paveikslas ir 11 lentelių. Rašant disertaciją buvo panaudoti 94 literatūros šaltiniai.

1. Literatūros šaltinių apie daleles ir jų formas analizė

Birios medžiagos yra svarbios beveik visose mokslo ir technologijų srityse, jos sudaro didžiulę medžiagų klasę, plačiai taikomų chemijos, farmacijos, maisto ir kt. pramonės srityse. Tai paprastos sistemos, susidedančios iš daugelio įvairių dydžių ir formos dalelių. Priklausomai nuo fizinės aplinkos, dalelių skaičius medžiagoje gali labai skirtis. Dalelės biriose medžiagose slysta ir rieda, taip pat jos gali būti suspaudžiamos ar šliejamos. Todėl labai svarbu gerai suprasti ir žinoti birių medžiagų elgseną. Nors tai atrodo gan paprasta, birių medžiagų savybės ir reiškiniai nėra visiškai iki galo suprantami, nes eksperimentus atlikinėti yra gan brangu, o labai gerų kompiuterinio modeliavimo metodų birioms medžiagoms beveik nėra.

Kadangi dalelės forma yra svarbi ypatybė įtakojanti atskirų grūdų sąveiką, yra atliekama daugybė tyrimų siekiant patobulinti supratimą apie formos vaidmenį birių medžiagų elgsenoje. Iš pradžių diskrečių elementų programos modeliavo sąveikas tarp apvalių diskų ar sferinių dalelių, nes tokios dalelės lengvai implementuojamos į programas ir dėl paprastumo skaičiavimai yra trumpi. Elipsinės dalelės yra labiausiai naudojamos nesferinėms glotnioms dalelėms aprašyti diskrečių elementų metodo skaičiavimuose. Elipsės (2D) arba elipsoido (3D) naudojimas sumažina sferinėms dalelėms būdingą sukimosi tendenciją, kuri laikoma viena svarbiausia diskrečių elementų metodo neatitikimo nuo realių dalelių elgsenos priežastimi. Kontakto taško paieškai tarp elipsinių ir elipsoidinių dalelių dažniausiai reikalingas iteracinis daugianarių šaknų skaičiavimas, o tai gali apimti daug laiko priklausomai nuo pasirinkto skaitinio algoritmo ir pradinės iteracijų reikšmės.

Kitas modelis aprašantis sudėtingesnes daleles naudoja daugiasienių kūnų formas. Daugiasienių formų naudojimo privalumas tas, kad jos gali būti taikomos įvairioms sudėtingų formų dalelėms modeliuoti gaunant tikslesnius rezultatus diskrečių elementų metodo skaičiavimuose. Tačiau aštrių viršūnių buvimas komplikuoja dalelių kontakto skaičiavimus ir klausimas kaip kontakto jėgos tarp dviejų susiduriančių kūnų yra skaičiuojamos dar nėra pilnai atsakyta. Siekiant supaprastinti kontakto skaičiavimus, tačiau išlaikyti modeliavimo tikslumą, buvo sukurtas kompozitinis arba multi-sferų modelis. Čia viena dalelė yra aprašoma sujungiant kelias sferas, kurios gali skirtis dydžiu ir netgi persidengti viena su kita. Toks formos aprašymo algoritmas gali būti lengvai implementuojamas ir apima efektyvią

kontakto paiešką, nes jis naudoja sferos su sfera kontakto paieškos algoritmą netaisyklingos formos objektams.

Formai aprašyti taip pat yra taikomi ir įvairūs matematiniai modeliai: nuo pačių paprasčiausių, kai paviršiai aprašomi taškų ar tūrinių objektų aibėmis, iki sudėtingesnių – Minkovskio operatorių ar Zernike daugianarių. Tarp tokių matematinių modelių pastaraisiais metais vis labiau nagrinėjamas metodas, kuris naudoja sferines harmonikas.

2. Dalelių formos matematinis modelis

Dalelė yra laikoma tolydžiu „žvaigždinio tipo“ trimačiu kūnu, turinčiu bent vieną simetrijos ašį. Kūnas apibrėžiamas lokaliaje sistemoje, kurios pradžia yra kūno svorio centre. Aprašymui gali būti naudojamos dvi koordinačių sistemos – Dekarto $Oxyz$ ir sferinė $Or\varphi\theta$.

Bet koks paviršius A , aproksimuojamas pusiau-analitiniu sferinių harmonikų metodu, išreiškiamas baigtine M narių eilute

$$A(\varphi, \theta) = \mathbf{f}(\varphi, \theta)^T \cdot \mathbf{a}, \quad (\text{S2.1})$$

čia, nežinomi koeficientai sudaro vektorių $\mathbf{a} = \{a_1, \dots, a_2, \dots, a_M\}^T$, o daugianariai – $\mathbf{f}(\varphi, \theta)$. Aproksimacijos sudėtingumas (S2.1) formulėje apibrėžiamas daugianarių skaičiumi M .

Tokio modelio aproksimacijos paklaida išreiškiama kaip skirtumas tarp originalaus ir aproksimuoto paviršių

$$E_j(\varphi, \theta) = A_j(\varphi, \theta) - S_R(\varphi, \theta). \quad (\text{S2.2})$$

Akivaizdu, kad didesnis naudojamų daugianarių skaičius modelyje $j \rightarrow \infty$ sumažina aproksimacijos paklaidą iki nulio ir garantuoja konvergavimą $E_{j=L, L < \infty}(\varphi, \theta) \rightarrow 0$.

Modelyje naudojamos sferinės harmonikos $Y_l^m(\theta, \varphi)$. Tai vienareikšmės, glodžios, t. y. diferencijuojamos be galę kartų, kompleksinės dviejų kintamųjų θ ir φ funkcijos, žymimos dviem indeksais l ir m . Sferinės harmonikos $\{Y_l^m(\theta, \varphi) : |m| \leq l \in N_0\}$ konstruojamos ant vienetinės sferos S^2 su dviem parametrais (θ, φ) sferinėse koordinatėse. Nors šios harmonikos formaliai apibrėžiamos kaip kompleksinės funkcijos, dažniausiai uždaviniuose naudojamos realių reikšmių funkcijos

$$Y_l^m(\theta, \varphi) = \begin{cases} \sqrt{2} N_l^m \cos(m\phi) P_l^m(\cos \varphi), & \text{kai } m > 0, \\ N_l^0 P_l^0(\cos \varphi), & \text{kai } m = 0, \\ \sqrt{2} N_l^{|m|} \sin(|m|\varphi) P_l^{|m|}(\cos \varphi), & \text{kai } m < 0, \end{cases} \quad (\text{S2.3})$$

čia apatinis indeksas $l \in N_0$ parodo skleidinio laipsnį, viršutinis indeksas $-l \leq m \leq l$ parodo sferinių harmonikų eilę, N_l^m ir $P_l^m(\cos \varphi)$ – atitinkamai normalizacijos konstanta ir jungtinis Ležandro daugianaris.

Paviršiaus aprašymui taikant sferines harmonikas ((S2.1) formulė) pirmiausiai reikia rasti koeficientus a_l^m . Skleidinio koeficientų skaičiavimas gali būti nagrinėjamas kaip skirtumas tarp realaus paviršiaus ir aproksimuoto sferinėmis harmonikomis. Ši sąryšį galima užrašyti matriciniu pavidalu:

$$[\mathbf{Y}_j(\varphi_{qk}, \theta_{qk})] \mathbf{a}_{jqk} = \mathbf{r}_{qk}(\varphi_{qk}, \theta_{qk}). \quad (\text{S2.4})$$

Čia, $[\mathbf{Y}_j]$ stačiakampė transformacijos matrica, kuri susieja nežinomus koeficientus \mathbf{a}_{jqk} su diskrečiomis reikšmėmis $\mathbf{r}_{qk}(\varphi_{qk}, \theta_{qk})$.

Naudojant matricinę algebrą, sprendinys tokiam uždaviniui gaunamas taikant pseudo-atvirkštinės matricos procedūrą:

$$\mathbf{a}_{jqk} = [\mathbf{Y}_{jqk}]^+ S_{R,qk}(\varphi_{qk}, \theta_{qk}), \quad (\text{S2.5})$$

čia pseudo-atvirkštinės matricos apibrėžimas yra

$$[\mathbf{Y}_{jqk}]^+ = [\mathbf{Y}_{jqk}]^T ([\mathbf{Y}_{jqk}][\mathbf{Y}_{jqk}]^T)^{-1}. \quad (\text{S2.6})$$

Gavus dalelės formos modelį sferinėmis harmonikomis, galima skaičiuoti įvairius formos rodiklius. Dalelės paviršiaus plotas yra skaičiuojamas pagal formulę

$$S = \int_0^{2\pi} \int_0^\pi A (A_\varphi^2 + A_\theta^2 \sin^2 \theta + A^2 \sin^2 \theta)^{1/2} d\theta d\varphi, \quad (\text{S2.7})$$

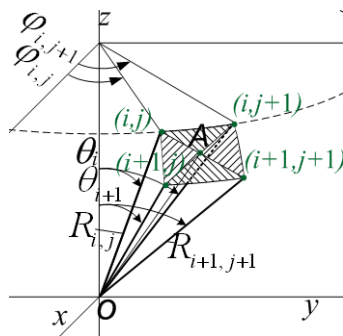
čia A yra sferinių harmonikų skleidinys, A_φ ir A_θ yra funkcijos $A(\theta, \varphi)$ išvestinės atitinkamai pagal φ ir θ . Tūris apibrėžiamas tokiu integralu

$$V = \frac{1}{3} \int_0^{2\pi} \int_0^\pi A^3 \sin \theta d\theta d\varphi. \quad (\text{S2.8})$$

Nors A funkcija yra analitinė, skaičiuoti integralus analitiškai gali būti brangu ir ilgu, todėl integravimas (S2.8) ir (S2.7) formulėse pakeičiamas sumavimu. Paviršius dalijamas į stačiakampius elementus, kurie aprašomi keturiais taškais

(i, j) , $(i + 1, j)$, $(i, j + 1)$ ir $(i + 1, j + 1)$. Tokia sumavimo schema pateikiama S2.1 paveiksle.

Vienas i -asis elementas suskaidomas į keturis trikampus ir atskirai skaičiuojamas kiekvieno trikampio plotas. Todėl vieno elemento plotas yra keturių trikampių plotų suma, o viso dalelės paviršiaus plotas yra lygus visų tokių elementų plotų sumai. Panašiu principu skaičiuojamas ir dalelės tūris. Šiuo atveju naudojami tie patys elementai, kurie sudaro piramides, ir sumuojami jų tūriai.



S2.1 pav. Skaitinio integravimo schema

Tokių sferinių harmonikų modelį galima ne tik integruoti, bet ir diferencijuoti. Funkcijos išvestinės naudojamos kreivumo spindulių skaičiavimui.

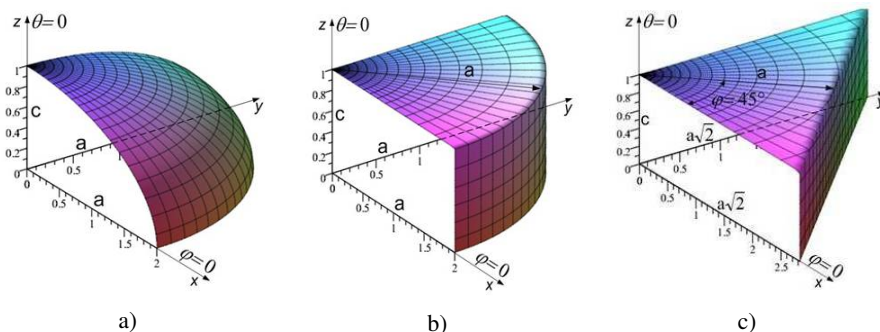
3. Sferinių harmonikų taikymas monomerinėms dalelėms

Modelis pritaikytas trims standartinės ir simetrinės formos dalelėms: elipsoidui, cilindrai ir stačiakampiui gretasieniui. Elipsoidas (S3.1a paveikslas) yra paprasčiausia dalelė, turinti ašinę simetriją ir glotnų paviršių.

Cilindras yra priskiriamas specialiai dalelių formos grupei diskrečių elementų metodo taikymuose. Cilindrinė forma yra gaunama sukant tiesią, lygiagrečią z ašiai liniją. Jei atstumas tarp šių dviejų linijų yra konstanta ir lygi a , gaunamas apskritas cilindras (S3.1b paveikslas). Cilindro paviršius ribojamas dviem plokštumomis, tarp kurių atstumas ir sudaro cilindro aukštį lygų $2c$.

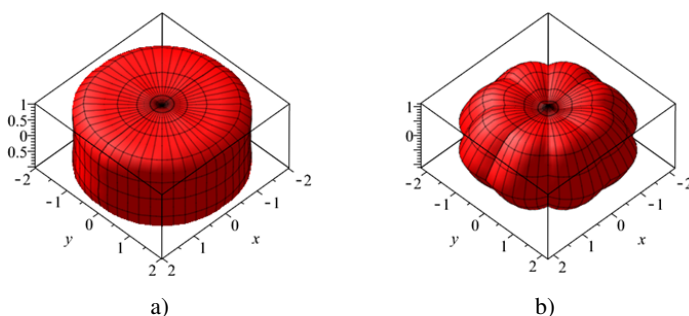
Stačiakampė gretasienė dalelė (S3.1c paveikslas) priklauso didžiulei daugiasienių dalelių grupei. Daugiasienės dalelės yra sudėtingos formos, turinčios tris poras lygiagrečių sienų, kurios susijungdamos sudaro aštrias briaunas ir kampus.

Paviršiaus aprašymui taikomos keturios strategijos: lygiakampė dalijimo strategija $q = 1$, kai kampinis posritis padengiamas reguliaru tinkleliu; reguliarius vienodo atstumo dalijimas $q = 2$, kai naudojamas reguliarius vienodo atstumo paviršiaus dalijimas, tačiau nėra pastovus azimutinio kampo dalijimas; trečioji strategija $q = 3$ yra parinkta derinant globaliai adaptyvų smulkinimą su lokaliu smulkinimu; paskutinė strategija $q = 4$ taiko Gauso taškus.



S3.1 pav. Paprastos simetrinės nesferinės formos: a) elipsoidas; b) cilindras; c) stačiakampis gretasienis

Taip pat naudojamas bazinis modelis, žymimas thr , kuris laikomas tiksliausiu skaitiniu modeliu. Toks modelis gaunamas generuojant reguliarių stačiakampį tinklą, degiantį $\theta-\varphi$ sritį. Elipsoido atveju šis modelis turi $N_{thr} = 16258$ taškų, cilindro – $N_{thr} = 16250$ modeliavimo taškų, stačiakampio gretasienio – $N_{thr} = 16380$ taškų.

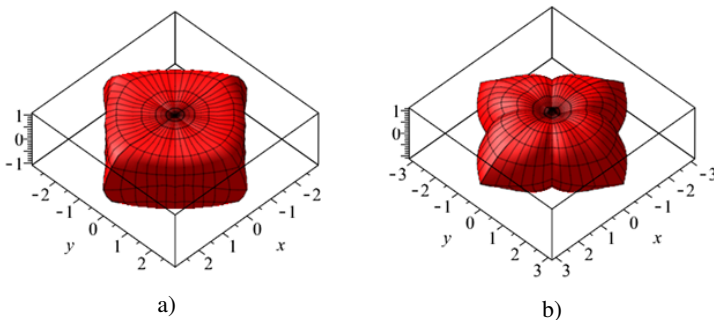


S3.2 pav. Cilindro aproksimacija naudojant sferines harmonikas: a) trimatis vaizdas, kai skleidinio laipsnis yra $L = 3$; b) trimatis vaizdas, kai skleidinio laipsnis $L = 2$

Paklaidų įverčiai rodo, kad elipsoidui modeliuoti užtenka pirmojo skleidinio laipsnio $L = 1$ ir geriausiai elipsoidas yra modeliuojamas naudojant adaptyvią

strategiją ($q = 3$), kur modelio paklaida yra lygi 0,78 %. Paviršiaus plotas ir tūris gaunami atitinkamai su 0,15 % ir 0,08 % paklaida.

Cilindro paviršiaus taškų dalijimui taikomos tos pačios strategijos kaip ir elipsoidui, tačiau skleidinio laipsnis parenkamas aukštesnis – $L = 2$ ir $L = 3$. Cilindro aproksimacijos trimačiai vaizdai pateikiami S3.2 paveiksle. Aukštesniu skleidinio laipsniu ($L = 3$) cilindras modeliuojamas su 2 % paklaida, kai paviršiaus plotas ir tūris gaunamas atitinkamai 3,7 % ir 0,004 % tikslumu. Žemesniam laipsniui ($L = 2$) globalios paklaidos labai išauga, nors paviršiaus ploto ir tūrio paklaidos išlieka nedidelės – atitinkamai 2,8 % ir 0,9 %. Pagal gautus rezultatus matyti, kad skleidinio laipsnis $L = 2$ nėra pakankamas geram cilindrinės formos aprašymui.



S3.3 pav. Stačiakampio gretasienio sferinių harmonikų aproksimacijos trimačiai vaizdai: a) $L = 3$; b) $L = 2$

Priešingai negu elipsoido ar cilindro formos dalelės, stačiakampio gretasienio atveju sukimo simetrijos nėra ir naudojamas dvimatis srities diskretizavimas abiejomis kampų kryptimis. Remiantis cilindro modeliavimo rezultatais, dvi azimutinės krypties dalijimo strategijos (lygiakampio dalijimo strategija $q = 2$ ir adaptvyvi strategija $q = 3$), kuriomis gautos minimalios aproksimavimo paklaidos, yra naudojamas tolesniems tyrimams. Šios dvi strategijos buvo naudojamos tiek azimutinio kampo, tiek polinio kampo dalijimams. Šių dviejų strategijų kombinacijos leidžia sudaryti keturias naujas strategijas, kurios taikytos dviem skleidinio laipsniams – $L = 2$ ir $L = 3$ (S3.3 paveikslas). Gauti modeliavimo rezultatai rodo, kad stačiakampio gretasienio sferinių harmonikų modelis, kai skleidinio laipsnis yra $L = 3$, yra gaunamas 2 % tikslumu, o paviršiaus plotas ir tūris – atitinkamai 2,4 % ir 0,18 %. Kai skleidinio laipsnis yra $L = 2$, paklaidos išauga gana stipriai. Paviršiaus plotas gaunamas su 8 % paklaida, o tūris – su 0,35 % paklaida. Kaip ir cilindro atveju, skleidinio laipsnis $L = 2$ nėra pakankamas tiksliam stačiakampės formos dalelei modeliavimui.

4. Sferinių harmonikų taikymas sudėtingoms dalelėms

Sferinių harmonikų modeli galima pritaikyti ir sudėtingų formų dalelėms aprašyti, pavyzdžiui, naudojamoms maisto pramonėje. Identifikuojant grūdų kokybę (nustatant, ar jis pažeistas, ligotas, nesubrendęs ar per daug subrendęs) taip pat kaip ir klasifikuojant juos, reikalingas tikslus grūdo geometrijos aprašymas. Būtent dėl tokių priežasčių sukurta metodologija pritaikyta šiame skyriuje pateikiamiems grūdų (pupelės, avinžirnio bei kukurūzo grūdo) pavyzdžiams modeliuoti.

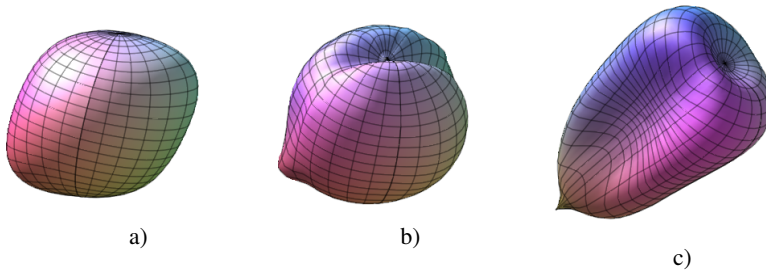
Modeliavimo idėja tokia pati kaip ir paprastoms dalelėms, tačiau esant sudėtingai formai, reikia naudoti daugiau sferinių harmonikų. Dėl to gali išaugti skaičiavimų apimtis ir sudėtingumas, todėl įvedamas paviršiaus dalijimas į smulkesnius segmentus. Pradiniai dalelės paviršiaus taškai yra aprašomi sferinėmis koordinatėmis, kurios yra išsidėsčiusios intervale $\varphi \times \theta = [0, 2\pi) \times [0, \pi]$. Šie du intervalai yra dalijami į smulkesnius, taip apimdami skirtingas paviršiaus dalis, kurių kiekviena gali būti modeliuojama nepriklausomai nuo kitų.

Pirmoji iš pasirinktų modeliuoti grūdų formų buvo pupelės forma, kuri išgaubta ir lygaus paviršiaus, sąlyginai paprasčiausia iš visų grūdų formų. Pradinis taškų skaičius, aprašantis šios formos paviršių, buvo 1538.

Kadangi sferinės harmonikos suteikia galimybę hierarchiškai aproksimuoti paviršių, tai pradinis metodo etapas – sfera, kurios spindulys yra vidutinis viso modeliuojamo paviršiaus spindulys. Pridedant daugiau sferinių harmonikų ir/arba dalijant paviršių į daugiau segmentų yra gaunamas tikslesnis pupelės formos modelis.

Geriausias rezultatas buvo pasiektas, kai visas dalelės paviršius buvo suskaidytas į 9 segmentus ir kiekvienas iš jų buvo modeliuojamas atskirai. Atlikus skaičiavimus gaunamos 9 atskiros funkcijos, aprašančios kiekvieną iš segmentų, kurios yra sumuojamos kartu norint gauti visą formos paviršių. Geriausias pupelės formos modelis pateiktas S4.1a paveiksle. Tūrio ir paviršiaus ploto įverčiai yra atitinkamai 0,22 % ir 0,40 %.

Antroji pasirinkta forma yra šiek tiek sudėtingesnė – tai avinžirnio forma. Tokia forma yra įgaubta ir turi specifinės geometrijos dalį – smailų galiuką – būdingą daugeliui grūdinių kultūrų. Kadangi forma yra sudėtingesnė, jos paviršių aprašančių pradinių taškų skaičius irgi yra didesnis – 6146. Naudojant tą pačią strategiją kaip pupelės atveju, paviršius modeliuojamas parenkant sferinių harmonikų bei segmentų skaičių. Geriausi rezultatai gauti, kai sferinių harmonikų skleidinio laipsnis yra $L = 3$, o segmentų skaičius – 25. Tokio modelio (S4.1b paveikslas) paviršiaus ploto ir tūrio paklaidos atitinkamai lygios 0,19 % ir 0,08 %.



S4.1 pav. Skirtingų grūdų sferinių harmonikų modeliai: a) pupelės; b) avinžirnio; c) kukurūzo

Trečioji pasirinkta forma buvo kukurūzo grūdo dalelės. Tai pati sudėtingiausia forma iš visų trijų nagrinėtų, turinti taip pat įgaubtą paviršių bei smailų galiuką. Pradinių paviršiaus taškų skaičius buvo 6146. Naudojant tą pačią modeliavimo strategiją kaip ir pirmiems dviem pavyzdžiams, paviršius buvo modeliuojamas parenkant sferinių harmonikų bei segmentų skaičių.

Geriausias kukurūzo grūdo modelis (S4.1c paveikslas) buvo gautas, kai paviršius buvo sudalytas į 36 dalis, o sferinių harmonikų skleidinio laipsnis $L = 3$. Tokio modelio paviršiaus ploto ir tūrio paklaidos atitinkamai yra 0,008 % ir 0,01 %.

Bendrosios išvados

1. Atlikta dalelių formos ir jos aprašymo metodų literatūros šaltinių analizė atskleidė, kad sunku rasti universalų analizinį formos aprašymo metodą nesferinės formos dalelėms, o žinomas pusiau analizinis sferinių harmonikų metodas yra potencialiai tinkamas bet kokios formos dalelėms aprašyti, kurio veikimas turi būti pagrįstas tyrimų rezultatais.
2. Nesferinės formos dalelėms aprašyti sudarytas sferinių harmonikų modelis, skirtas žvaigždės pavidalo (radialiai iškilųjų) dalelių formai aprašyti. Būdingas šio modelio išskirtinumas – koeficientų nustatymas taikant mažiausių kvadratų metodą ir pseudo-atvirkštinės matricos skaičiuojamąją procedūrą. Atskirų formų tyrimas atskleidė, kad mažiausių kvadratų metodas leidžia tiksliau aprašyti lokalius formos pokyčius.
3. Sferinių harmonikų skleidinio koeficientų skaičiavimo kokybei įvertinti sudarytos ir ištirtos įvairios kontrolinių taškų pozicionavimo strategijos. Nustatyta, kad racionalus tikslumo ir skaičiavimų apimties kompromisas pasiekiamas naudojant lokaliai prisitaikančias strategijas.

4. Sferinių harmonikų modeliui pritaikyti integravimas ir diferencijavimas. Integravimas taikomas skaičiuojant integralines charakteristikas, pvz., paviršiaus plotą, tūrį ir inercijos momentus, kurios parodo sukurto modelio tikslumą. Antrosios eilės išvestinės naudojamos skaičiuojant kreivumo spindulį ir kontakto jėgas, kuriojs lyginamos su baigtinių elementų metodu išspręstu uždaviniu – rezultatai skiriasi 0,3 %.
5. Sukurtas sferinių harmonikų modelis ištirtas naudojant žemo laipsnio sferines harmonikas. Universalus skleidinys, kurio laipsnis ribojamas iki $L \leq 3$, buvo pritaikytas modeliuojant paprastas ir dažnai taikomų formų daleles, tokias kaip elipsoidas, cilindras ir stačiakampis gretasienis. Atlikti skaičiavimai leidžia tvirtinti, kad mažiausios paklaidos gaunamos esant vienodų matmenų dalelėms – didėjant ar mažėjant matmenų santykiui modelio tikslumas mažėja.
6. Pailgų formų, kurių kraštinių santykis yra 0,5, gauti rezultatai parodė, kad modeliuojamo elipsoido tūris gaunamas su 0,8 % paklaida, cilindro – 0,004 %, stačiakampio gretasienio – 0,18 %. Mažiausių kvadratų paklaidos norma elipsoidui gaunama iki 0,25 % tikslumu, cilindrai ir stačiakampiui gretasieniui – atitinkamai iki 2,2 % ir 2,0 % tikslumu.
7. Pradinių taškų tankinimas iki dviejų kartų pagerina globalių įverčių tikslumą, tačiau kai kuriais atvejais išauga lokalios paklaidos. Bet tai turi nedidelę arba tam tikru požiūriu net ir teigiamą reikšmę. Lokalūs vidiniai nuokrypiai neturi įtakos skaičiavimams ir gali būti nevertinami, o aštrių kampų suapvalinimas aproksimuojant palengvina tolesnius skaičiavimus, pvz., modeliuojant kontaktą.
8. Taip pat sukurtas sferinių harmonikų modelis buvo pritaikytas sudėtingos formos grūdinės dalelėms: pupelės formos dalelėms, apibrėžiamoms glotniu ir iškiliu paviršiumi, avinžirniui, kuris yra sudėtingos įgaubtos formos, ir kukurūzo grūdai, kuris taip pat kaip ir avinžirnis turi įgaubtą formą ir smailų galiuką.

Annexes¹

Annex A. Low-Resolution Spherical Harmonics

Annex B. Analytical Descriptors of Particle Shape

Annex C. Various Characteristics of Modelled Shapes

Annex D. The Co-authors Agreements to Present Publications for the Dissertation Defence

Annex E. The Copies of Scientific Publications by the Author on the topic of the Dissertation

¹The annexes are supplied in the enclosed compact disc

Urtė RADVILAITĖ

SPHERICAL HARMONICS MODELS AND THEIR APPLICATION TO
NON-SPHERICAL SHAPE PARTICLES

Doctoral Dissertation

Technological Sciences,
Mechanical Engineering (09T)

Urtė RADVILAITĖ

SFERINIŲ HARMONIKŲ MODELIAI IR JŲ TAIKYMAS NESFERINĖS
FORMOS DALELĖMS

Daktaro disertacija

Technologijos mokslai,
mechanikos inžinerija (09T)

2016 12 09. 10,5 sp. l. Tiražas 20 egz.
Vilniaus Gedimino technikos universiteto
leidykla „Technika“,
Saulėtekio al. 11, 10223 Vilnius,
<http://leidykla.vgtu.lt>
Spausdino UAB „BMK leidykla“,
J. Jasinskio g. 16, 01112 Vilnius